

---

**Visible-Light-Responsive Nanocarbon Catalyst  
for Radical-Mediated Organic Transformations**

**March 2025**

**Md Razu Ahmed**

**Graduate School of Natural Science and  
Technology  
(Doctor's Course)**

**Okayama University (Japan)**



---

## Abstract

The development of efficient and sustainable catalytic systems is a critical focus in modern organic synthesis. This thesis explores the design and application of visible-light-responsive nanocarbon catalysts for radical-mediated organic transformations, a promising approach to achieving energy-efficient and environmentally friendly chemical processes. Nanocarbon materials, such as graphene oxide, functionalized nanocarbon, and carbon quantum dots offer unique properties, including a high surface area, tunable electronic characteristics, and exceptional photophysical behavior, making them ideal candidates for photocatalytic applications. The study investigates the synthesis, characterization, and catalytic activity of nanocarbon-based catalysts with tailored light absorption and radical-generation capabilities. Emphasis is placed on their ability to harness visible light to drive diverse organic reactions, including oxidative dehydrogenation, carbon-carbon bond formation, and carbon-nitrogen bond formation. Mechanistic insights into radical generation and reaction pathways are provided, highlighting the role of the nanocarbon materials structure and surface chemistry in modulating activity and selectivity. The research demonstrates that these catalysts not only reduce reliance on traditional metal-based systems but also enable mild reaction conditions, high efficiency, and scalability. Finally, progress towards a sustainable and green pathway for photochemical reaction optimization using nanocarbon photocatalyst. The summary of each chapter is described below.

**In chapter I**, an introductory section presents the background of this research and general consideration of the state-of-the-art in the field of carbon catalysis, focusing on light sensitivity and applications for organic reactions. The carbon-based catalysts were initially applied for functional group transformations, such as oxidation and esterification reactions. Recently, they have been used to construct C–C bonds, which are fundamental reactions in synthesizing fine chemicals, medicinal and pharmaceutical agents, agrochemicals, and organic electronics materials. Therefore, catalysts from sustainable materials such as carbon nanomaterials are specifically attractive because of their mechanical and physicochemical properties. Graphene-based materials have a

---

large surface area and a 2D morphology making accessible most of the atoms that make these materials suitable as catalysts. This is one of the reasons why there is growing interest in exploring the potential of graphene-based materials as heterogeneous catalysts. Carbon nanomaterials as a photocatalyst have not been developed due to their low reactivity. With the rapid development of the photocatalysis field, graphene oxide has received increasing attention in carbon photocatalysis. Its high surface area, tunable electronic properties, and chemical stability make it a promising photocatalyst for organic transformation.

**In chapter II**, visible-light-induced photocatalytic dehydrogenation of N-heterocycles was achieved by carbon catalyst. Herein, delineated the use of GO as a metal-free and recyclable photocatalyst for dehydrogenation under visible light irradiation. The reactions proceeded smoothly under mild reaction conditions and afforded the desired products in good to excellent yields. Unlike previously reported thermally induced GO-promoted reactions, this system generates radicals and molecular hydrogen, which are confirmed by electron spin resonance and gas chromatography. Both light and GO were proved to be essential for this reaction; no desired product was observed when the reaction was conducted in the dark and the absence of GO. A metal-free, oxidant-free, and recyclable photocatalytic reaction was achieved by a carbon-based system for the first time.

**In chapter III**, explores the radical properties of oxidized carbon materials under visible light irradiation. Oxidized carbon materials have abundant surface functional groups for generating radicals, these radicals play a crucial role in photocatalytic reactions. Unlike reactive oxygen species such as hydroxide or superoxide radicals that have been reported previously, oxidized carbon also produces stable carbon radicals under photo-irradiation. This has been confirmed through electron spin resonance. Among the various oxidized carbon materials synthesized, graphene oxide shows the largest number of carbon radicals when exposed to blue LED light. The resulting radical species are utilized for catalysis in the oxidative dehydrogenation of indoline and the oxidative coupling of benzylamine. The light absorption capacity, high surface area, and unique structural characteristics of oxidized carbon materials offer a unique function for

---

radical-mediated oxidative reactions.

**In chapter IV**, visible-light-responsive nanocarbon was systematically synthesized via a one-step hydrothermal method using citric acid and Congo Red; this nanocarbon exhibited visible-light absorption at 516 nm and photocatalytic activity for the carbon-carbon bond-forming reaction between benzylamine and ethyl cyanoacetate. Various characterization methods confirmed the structure and surface functional groups of nanocarbon. Mechanistic investigations proved that this system generates sulfur radicals from nanocarbon under irradiation of blue LED light, and the reactions proceed via radical pathways, which are confirmed by electron spin resonance. Both nanocarbon and visible light synergistically worked to control the progress of the reaction. A metal-free, mildly conditioned, and recyclable photocatalytic reaction was achieved by the visible-light-responsive nanocarbon system.

**In chapter V**, the conclusion of the research results obtained in the duration of the doctoral research has led to the following three points.

1. Visible-light-induced photocatalytic dehydrogenation of N-heterocycles promoted by radicals from graphene oxide.
2. Investigating the radical properties of oxidized carbon materials under photo irradiation and their application in catalytic reactions.
3. Synthesis of visible-light-responsive nanocarbon using citric acid and Congo Red, and application for photocatalytic carbon-carbon bond formation.

---

## List of Publications

### Journal

1. Photocatalytic Dehydrogenation of N-Heterocycles Promoted by Radicals from Graphene Oxide  
**Md Razu Ahmed** and Y. Nishina,  
*Bulletin of the Chemical Society of Japan*, 96, 6, 568–571 (2023).
2. Investigating the Radical Properties of Oxidized Carbon Materials Under Photo-Irradiation: Behavior of Carbon Radicals and Their Application in Catalytic Reactions  
**Md Razu Ahmed**, Israel Ortiz Anaya, and Yuta Nishina  
*Chemical Communication*, 60, 76, 10544-10547 (2024).
3. Synthesis of Visible-Light-Responsive Nanocarbon and Application for Photocatalytic Carbon-Carbon Bond Formation  
**Md Razu Ahmed**, Yi Kai Cheng, and Yuta Nishina,  
*Industrial & Engineering Chemistry Research*, 63, 16, 7475-7480 (2024).

### Conference

1. Graphene Oxide Catalyzed Photo-Catalytic Dehydrogenation by Radical Intermediate Process  
**Md Razu Ahmed** and Yuta Nishina  
131<sup>st</sup> Symposium on Catalysis, Catalysis Society of Japan, (Kanazawa University, 2023-03).
2. Photocatalytic Dehydrogenation of N-Heterocycles Promoted by Radicals from Graphene Oxide  
**Md Razu Ahmed** and Yuta Nishina  
42<sup>nd</sup> Symposium on Catalytic Chemistry Involving Light, Okayama University, (2023-07).
3. Synthesis of Visible Light Responsive Nanocarbon and Investigation of Radical Mechanism in the Carbon-Carbon Coupling Reaction  
**Md Razu Ahmed** and Yuta Nishina  
International Symposium on Catalysis and Fine Chemicals, Catalysis Society of Japan (Tokyo Metropolitan University, 2023-12).

---

## Table of Contents

Abstract.....	1
List of Publications.....	4

### Chapter I

1.1	General introduction to photocatalyst.....	9
1.2	Carbon and its family.....	10
1.3	History of carbon catalyst.....	13
1.4	General carbon catalysis.....	14
1.4.1	Oxidation reaction.....	14
1.4.2	Dehydrogenation of N-heterocycle.....	17
1.4.3	C-C bond formation.....	19
1.4.3.1	Oxidative coupling reaction.....	19
1.4.3.2	Aldol-type reactions.....	21
1.4.3.3	Friedel Crafts-type reactions.....	23
1.4.4	C-N coupling reaction.....	24
1.4.4.1	Oxidative coupling.....	24
1.5	Carbon photocatalysis.....	26
1.6	Conclusion.....	32
1.7	Objective and scope of this thesis.....	32
1.8	References.....	34

### Chapter II

2.1	Introduction.....	42
2.2	Result and discussion.....	43
2.2.1	Screening of the reaction.....	43
2.2.2	Radical properties analysis.....	45
2.2.3	Mechanism investigation.....	46
2.2.4	Recyclability test.....	48
2.2.5	Substrate scope.....	50
2.3	Conclusion.....	52
2.4	Experimental.....	52
2.4.1	Materials.....	52
2.4.2	General information.....	52
2.4.3	Preparation of carbon materials.....	53
2.4.4	ESR measurement technique.....	54
2.4.5	Light on/off experiment.....	54
2.4.6	The reaction with radical scavenger.....	55
2.4.7	GC analysis of air and H <sub>2</sub> .....	55
2.5	References.....	56

---

## Chapter III

3.1	Introduction.....	60
3.2	Result and discussion.....	60
3.2.1	Characterization.....	61
3.2.2	Photo-radical properties.....	63
3.2.3	Mechanistic investigation.....	64
3.2.4	Evaluation of catalytic performance.....	66
3.3	Conclusion.....	69
3.4	Experimental.....	69
3.4.1	General information.....	69
3.4.2	General procedure for synthesis of oxidized carbon materials.....	70
3.4.3	FTIR spectra of Am-GO.....	70
3.4.4	XPS Spectra of GO and Am-GO.....	70
3.4.5	EI-Mass spectra of product 4.....	71
3.5	References .....	72

## Chapter IV

4.1	Introduction.....	75
4.2	Result and discussion.....	76
4.2.1	Optimization course.....	76
4.2.2	Characterization.....	77
4.2.3	Reaction screening.....	80
4.2.4	Evaluation of catalytic activity.....	81
4.2.5	Substrate scope.....	82
4.2.6	Mechanism investigation.....	83
4.2.7	Proposed reaction mechanism.....	84
4.2.8	Recyclability test.....	86
4.3	Conclusion.....	88
4.4	Experimental.....	88
4.4.1	General information.....	88
4.4.2	Experimental procedure for the synthesis of carbo.....	89
4.4.3	UV-visible spectra.....	89
4.4.4	ESR measurement technique.....	95
4.4.5	The reaction with radical scavenger.....	95
4.4.6	Identification of benzaldehyde via imine formation.....	96
4.4.7	ICP-MS.....	97
4.4.8	GC and mass spectra of product 3a.....	100
4.4.9	NMR spectra of product 3a-f.....	101
4.5	References.....	109

---

## Chapter V

Conclusion and Future Prospectives.....	114
Acknowledgment.....	120

---

# Chapter I

## General Introduction

---

## 1.1 General introduction to photocatalyst

The word "photocatalysis" seemed to incorporate the idea of the application of zinc oxide (ZnO) illumination to the bleaching of the dark blue pigment as early as 1911.<sup>1</sup> The synthesis of formaldehyde under visible light was then investigated by Baly et al. in 1921, employing ferric hydroxides and colloidal uranium salts as catalysts.<sup>2</sup> Prussian blue bleaching by ZnO under illumination photocatalysis was first described by scientists in 1924. Subsequent studies employing ZnO as a photocatalyst for additional processes, like the reduction of  $\text{Ag}^+$  to Ag under light irradiation, have been motivated by this result.<sup>3</sup> The groundbreaking efforts of Fujishima and Honda in the 1970s increased interest in this technology.

The groundbreaking efforts of Fujishima and Honda in the 1970s increased interest in this technology. This seemingly insignificant project created a whole new range of opportunities for clean hydrogen production using inexpensive, plentiful water and sunlight.<sup>4</sup> Numerous candidates with photocatalytic activity greater than those of  $\text{TiO}_2$  have been investigated in the development of novel photocatalysts; the majority of these candidates have broad bandgaps and are only active when exposed to UV light.<sup>5</sup> In parallel, visible light-absorbing photocatalysts have been sought for increased efficiency.<sup>6,7</sup> In the meantime, scientists gained a better understanding of the fundamentals of photocatalysis.

*A photocatalyst is a substance that accelerates photoreaction by absorbing light and transferring the energy to reactants without undergoing permanent chemical change itself.* Photocatalysts are crucial in various applications, especially in environmental cleanup, energy production, and organic synthesis.<sup>8-10</sup> Photocatalysts offer several distinct advantages in organic reactions, making them increasingly popular in synthetic chemistry. The advantages of photocatalysts in organic reactions highlight their potential to revolutionize synthetic chemistry. By offering mild conditions, selectivity, energy efficiency, green chemistry benefits, innovative pathways, reusability, broad applicability, and enhanced reaction rates, photocatalysts provide powerful tools for developing more sustainable and efficient chemical processes.<sup>11,12</sup>

---

The catalyst forms electron-hole pairs to catalyze reactions in a typical photocatalytic process by absorbing photons to move from the ground state to the excited state. Photocatalytic processes can be classified as either homogeneous or heterogeneous based on the phases of the reactants and photocatalysts. Reactants and photocatalysts are present in the same phase for homogeneous photocatalysis. Stated differently, the reactants themselves become photoexcited by absorbing photons, resulting in active intermediates that can be utilized to catalyze a sequence of events.<sup>13,14</sup> Heterogeneous photocatalysis is also used extensively in addition to homogeneous photocatalysis. Heterogeneous photocatalysis relies on carbonaceous materials since the light absorber and reactants are in a different phase (often liquid or gaseous) than photocatalysts. Photogenerated electrons and holes are produced when electrons are photoexcited from their ground state to their stimulated state in a typical heterogeneous photocatalytic process. Electrons and holes can go to the photocatalyst's surface locations to take part in catalytic reduction and oxidation half-reactions, respectively. Heterogeneous photocatalysts are better suited for industrial and research applications than homogeneous ones because they are easily recyclable and can be separated from reactants and products.<sup>15,16</sup> The usage of heterogeneous photocatalysis in a variety of reactions, such as oxidation, dehydrogenation, aromatization, C-C coupling events, and C-N bond formation, has therefore increased dramatically in recent years.

## 1.2 Carbon and its family

One of the most prevalent elements in the earth's crust is carbon (**Figure 1.1**), which can form strong covalent bonds with other elements to create a variety of carbonaceous compounds that make up organic chemistry. Carbon differs from other elements due to its propensity to form strong covalent bonds with itself, which produces a variety of kinetically stable allotropes with varying sizes. A wide range of features, including fullerenes, graphite ( $sp^2$  hybridization), diamond ( $sp^3$  hybridization), carbon nanotubes (CNTs), and graphene, can be produced by the great structural diversity inherent in carbon materials (**Figure 1.2**).<sup>17,18</sup>



**Figure 1.1** Carbon

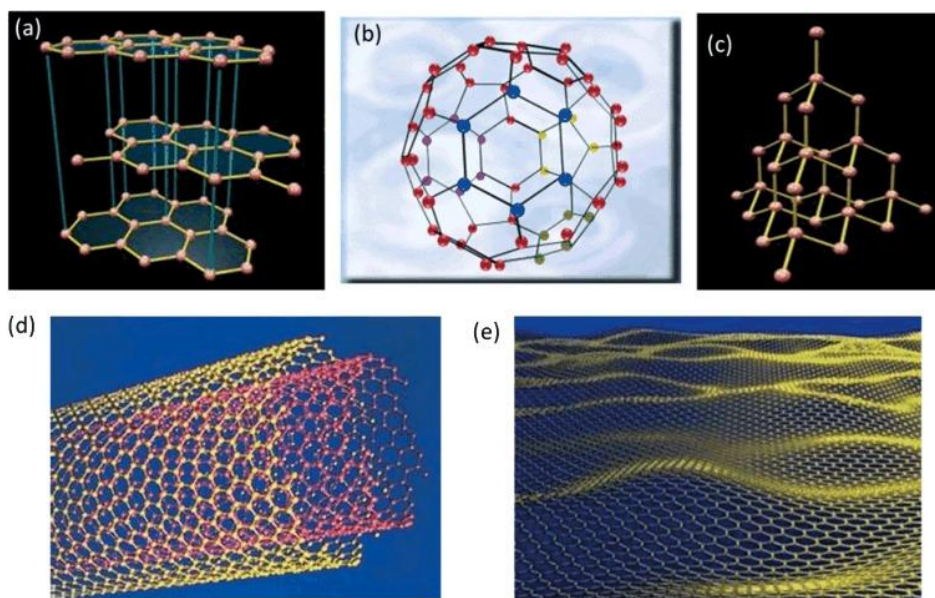
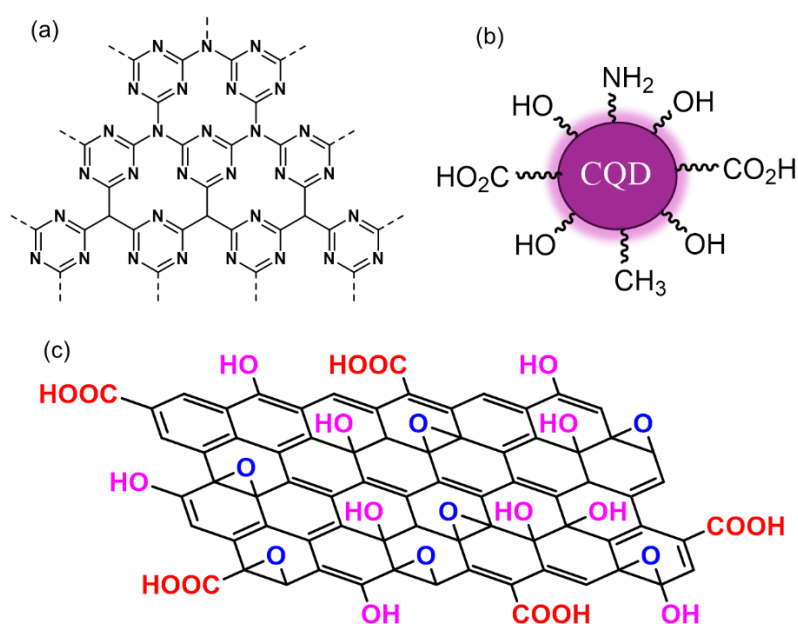


**Figure 1.2** Carbon materials (a) graphite, (b) fullerene, (c) diamond, (d) CNTs, and (e) graphene. *Reprinted with permission from referece<sup>18</sup>. Copyright 2024 Wiley.*

Fullerenes are composed of stacked graphene sheets of linked hexagonal, pentagonal, or heptagonal rings, and each carbon atom is bonded to three others, which is similar to graphite in structure.<sup>19</sup> Iijima's discovery of carbon nanotubes (CNTs) ushered in a new age of carbon chemistry. According to recent research, CNTs may improve electrochemical reactivity and encourage electron transport.<sup>20,21</sup> Since its realization in 2004, graphene a one-atom-thick planar sheet in a honeycomb lattice has gained much attention due to its special qualities, which include the ambipolar electric field effect,

ballistic conduction of charge carriers, tunable band gap, high elasticity, and quantum hall effect.<sup>22-24</sup> A new class of carbon catalyst, graphene also exhibits good ability due to its exceptional facility for a wide range of functions.<sup>25</sup>

The mechanical and physicochemical characteristics of carbon nanomaterials, such as their enormous surface area, electrical characteristics, resistance to corrosion, and thermal stability, make them particularly appealing. These qualities have led to the widespread use of carbon materials as superior catalysis agents. Numerous nanocarbon compounds, such as graphene oxide (GO), carbon quantum dots (CQD), and graphite carbonitride (g-C<sub>3</sub>N<sub>4</sub>), have been produced recently (**Figure 1.3**).<sup>26-28</sup> Graphite carbon nitride (g-C<sub>3</sub>N<sub>4</sub>) is a nonmetallic polymeric substance that has been widely used as a light-responsive photocatalyst due to its abundance of sources and ease of synthesis in the rapidly developing field of photocatalysis. According to this perspective, g-C<sub>3</sub>N<sub>4</sub> has been regarded as a promising photocatalyst because of its low cost, environmental friendliness, intriguing electronic band topologies, and photochemical stability.<sup>29-31</sup> As an intriguing family of carbon nanomaterials, carbon dots have already emerged as a hot topic in several areas of photoelectric study. Strong UV-vis optical absorption, adjustable energy-level configuration, exceptional charge transfer capability, outstanding physicochemical stability, ease of manufacturing, low toxicity, and high solubility have all attracted special attention as metal-free photocatalysts.<sup>32-33</sup>



---

**Figure 1.3** Nanocarbon materials (a) g-C<sub>3</sub>N<sub>4</sub>, (b) CQD, and (c) GO.

Because of its exceptional qualities, graphene and its derivatives have garnered a lot of attention from researchers lately in comparison to the rest of the carbon family. In contrast to the other carbon compounds in the nanostructure (100 to 1000 m<sup>2</sup>/g), graphene materials have a high surface area (2630 m<sup>2</sup>/g), as was previously mentioned. Furthermore, the large concentration of oxygen-containing functional groups on the surface of GO makes it simple to functionalize the materials in covalent, non-covalent, and ionic ways. This characteristic makes graphene materials perfect for a novel suitable heterogeneous catalytic system.

### 1.3 History of carbon catalysts

Carbon catalyst is defined as *a catalytic system that uses carbon materials as a catalyst for organic transformations*. It should be mentioned that carbon catalysts have been known since the initial discovery of carbon materials' catalytic properties decades ago.<sup>34</sup> The behavior of active charcoal as a catalyst for the low-temperature oxidation of oxalic acid was reported by Rideal and Mary in 1925.<sup>35</sup> In the absence of carbon materials, no conversion was seen.<sup>36</sup> It is clear that the production of geminal diols begins with the aerobic oxidation of carbon. The diols additionally form peroxide intermediates when exposed to ambient oxygen, which further reacts with the substrate to produce water and carbon dioxide (**Scheme 1.1**).



**Scheme 1.1** Charcoal as a catalyst for the aerobic oxidation of oxalic acid.

In 1988, the oxidative dehydrogenation process of ethylbenzene to styrene was catalyzed by activated carbon.<sup>37</sup> A redox-type reaction mechanism was proposed by the evidence of oxygenated species present in the activated carbon and their involvement in oxidative dehydrogenation. Ritter oxidized 4-chlorophenol with graphite to produce

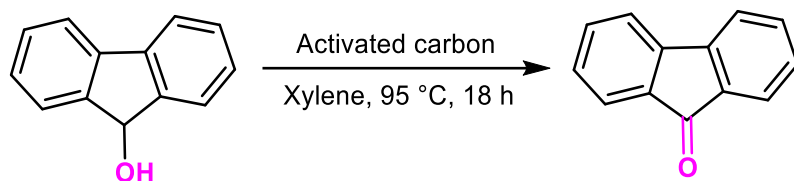
---

CO<sub>2</sub>, HCl, and H<sub>2</sub>O.<sup>38</sup> It was discovered that the graphite catalyst has the same reactivity as Fenton's reagent.<sup>39</sup> However, at that time, there was little interest in carbon-based catalysts. Although most carbon-based catalysts have limited reactivity, they can catalyze a number of processes. To address these issues researchers concentrated on oxidized carbon compounds with a large surface area.

## 1.4 General carbon catalysis

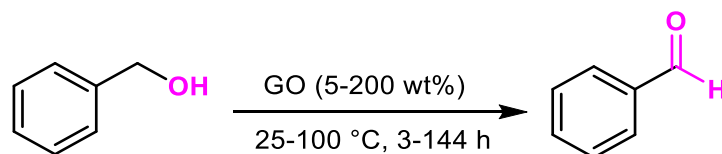
### 1.4.1 Oxidation reaction

Organic synthesis relies heavily on selective oxidation, and the chemical industry is looking for environmentally friendly, effective selective oxidation methods. In the synthesis of fine chemicals, the selective oxidation of alcohols is a crucial transformation.<sup>40</sup> Since oxygen or air are employed as the terminal oxidant to replace stoichiometric metal oxides like chromates and manganese oxides, aerobic oxidation methods have drawn more attention recently. Benzyl alcohol and its substituted derivatives can be easily oxidized by oxygen under mild reaction conditions using a novel protocol called the nitric acid-assisted carbon-catalyzed oxidation system (NACOS), which provides high conversions and good selectivity into the appropriate aldehydes.<sup>41</sup> Following acidic treatment and electrochemical oxidation, surface oxidized carbon black itself shows strong catalytic activity for the electrochemical oxidation of alcohols and water.<sup>42</sup> Dehydrogenative oxidation of cyclohexane catalyzed by active carbon proceeds via a radical mechanism to produce benzene.<sup>43</sup> The atomic hydrogen absorbed on active carbon was easily removed by oxygen, resulting in the high conversion of benzene. In the presence of activated carbon, 30% hydrogen peroxide (H<sub>2</sub>O<sub>2</sub>) was used to selectively oxidize a range of benzylic alcohols to their corresponding carbonyl compounds (**Scheme 1.2**).<sup>44</sup> Anthrone, xanthenes, and fluorenes were among the alkylarenes that were successfully oxygenated to the carbonyl molecule.



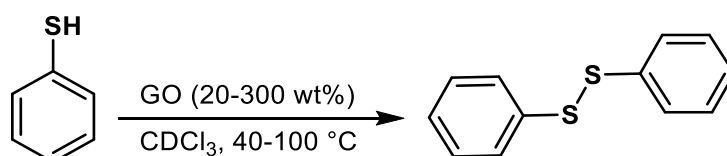
**Scheme 1.2** Activated carbon catalyzed oxidation of secondary benzyl alcohol.

According to Bielawski, GO and other readily available and reasonably priced carbon-based materials are utilized as catalysts to create aldehydes or ketones from various alcohols, alkenes, and alkynes (**Scheme 1.3**).<sup>45</sup> The target products (aldehyde, ketone, or acid) were produced in good yields by these reactions, which were discovered under comparatively mild reaction conditions. Excellent chemoselectivity and activity were nevertheless attained, but a high GO loading (200 wt%) was required.



**Scheme 1.3** GO catalyzed oxidation of benzyl alcohol.

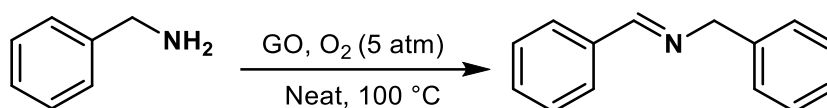
Additionally, GO was discovered to be active in the oxidation of thiol to disulfides with high conversion rates, good selectivity, and no over-oxidation (**Scheme 1.4**).<sup>46</sup> When compared to GO, the catalytic activity of other carbons, including graphite, activated carbon, and hydrazine-reduced GO, was low. Alkyl-functionalized substrates were less reactive than arene-functionalized substrates. Additionally, GO use as a catalyst for the oxidation process of sulfide to sulfoxide was expanded. GO was reduced during the processes and functioned as an oxidant.



---

**Scheme 1.4** GO catalyzed oxidation of thiophenol.

Fan et al. used GO to illustrate the catalytic oxidation process of amines to imines using molecular oxygen as an oxidant (**Scheme 1.5**).<sup>47</sup> The imine product yields are low when using natural flake graphite, multi-walled carbon nanotubes, activated carbon, and rGO in place of GO. ICP-MS measurements of the trace metal's impact in the GO-catalyzed reaction revealed 30 ppb of manganese, whereas the other trace metals were determined to be below the detection limit. Although aliphatic amines and amines without a hydrogen atom at the  $\alpha$ -carbon position were not reactive, primary and secondary amines have also undergone substantial yields of oxidation. Additionally, the synthesis of cyclic and asymmetrical imines was accomplished.



**Scheme 1.5** Oxidation of benzylamine to *N*-benzylidene benzylamine catalyzed by GO.

Using rGO as a catalyst, Ma and co-workers demonstrated the one-pot synthesis method of Bis(aminothiocarbonyl) disulfide from secondary amines and carbon disulfide (**Scheme 1.6**). Under mild reaction conditions, the bis(aminothiocarbonyl)disulfides were produced in good to excellent yields with minimal catalyst loading. The rGO retains its catalytic activity and selectivity even after at least four recycling cycles.<sup>48</sup>



**Scheme 1.6** rGO catalyzed one-pot synthesis of Bis(aminothiocarbonyl)disulfide.

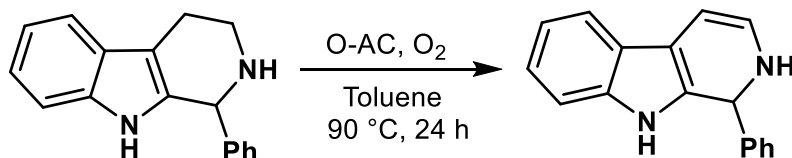
High yields of thiuram disulfide were produced from alkylamine and cyclic secondary

---

amines. Secondary aromatic amines, on the other hand, were said to be less reactive and needed a strong base to speed up the reaction. The unpaired electrons at the graphene's edges, according to the authors, may also activate O<sub>2</sub> to superoxide anion radicals, which in turn start a coupling process with dithiocarbamic acids to produce thiuram disulfide.

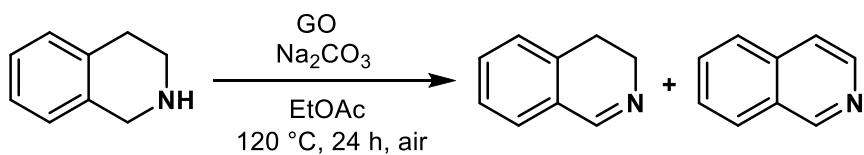
#### 1.4.2 Dehydrogenation of N-heterocycle

In addition to their usual employment, as supports for transition metal nanoparticles or composites, activated carbons are increasingly being employed as catalysts on their own. The air-oxidized activated carbon catalyst for aerobic oxidative aromatization of N-heterocycles was described by Lukas and his co-worker (**Scheme 1.7**). Active carbon is transformed into a weakly oxidized substance with a higher quinoidic content by a straightforward "reagent-free" thermal air treatment, which catalytically dehydrogenates saturated N-heterocycles to the corresponding aromatic compounds.<sup>49</sup>



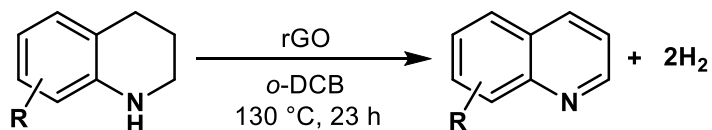
**Scheme 1.7** Air-oxidized activated catalyzed aerobic oxidative aromatizations of N-heterocycles.

GO has been developed as a low-cost, metal-free, eco-friendly carbon catalyst for N-heterocycle dehydrogenation. Important substances have been effectively employed as substrates, including quinazoline, quinoline, 3,4-dihydroisoquinoline, and indole derivatives (**Scheme 1.8**). The analysis of different oxygen-containing compounds with different conjugated systems revealed that this reaction requires both the large  $\pi$ -conjugated systems and oxygen-containing groups in GO sheets.<sup>50</sup>



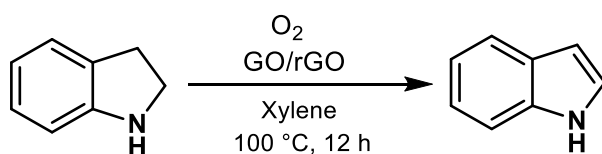
**Scheme 1.8** GO catalyzed dehydrogenation of N-heterocycle.

The acceptorless dehydrogenation of N-heterocycles is used to assess the catalytic capabilities of materials formed from graphene. Reduced graphene oxide (rGO) functions as an appropriate carbon catalyst to facilitate the acceptorless dehydrogenation of N-heterocycles, a more difficult thermodynamically uphill reaction, without the need for metal support. H<sub>2</sub> must be eliminated from the solution for the reaction to begin, and the catalyst must be highly effective at creating equilibrium concentrations (**Scheme 1.9**).<sup>51</sup>



**Scheme 1.9** rGO catalyzed acceptorless dehydrogenation of N-heterocycles.

When molecular oxygen is used as a terminal oxidant in the ODH reaction of indoline, GO and rGO are appealing options (**Scheme 1.10**). The superoxide radical was implicated in the processes, according to electron spin resonance measurements. GO also aided in the reaction, however, due to the irreversible partial reduction of GO brought on by the reactions, it was unable to function as a catalyst. The degree of GO reduction had a significant impact on the catalyst performance because the catalytic activity increased as the recovered GO was further reduced.<sup>52</sup>



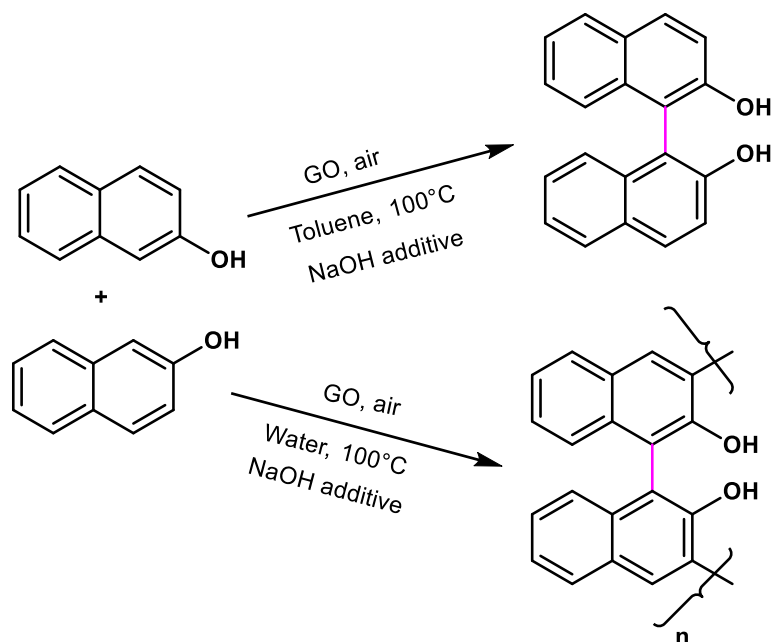
---

**Scheme 1.10** GO/rGO catalyzed ODH of indoline.

**1.4.3 C-C bond formation**

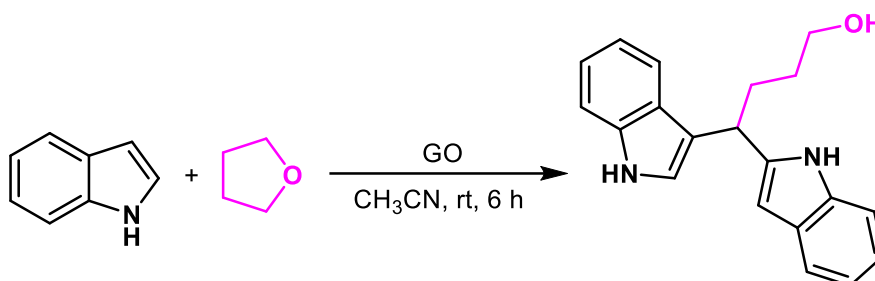
**1.4.3.1 Oxidative coupling reactions**

According to Bielawski and colleagues, GO catalyzed the Claisen-Schmidt coupling reactions of several alkynes or methyl ketones with alcohols and aldehydes to produce compounds related to chalcones.<sup>53</sup> The reactions take place in a tandem fashion: GO first hydrates or oxidizes different alcohols or alkynes to their respective methyl ketones or aldehydes, and then these species go through coupling reactions.  $\beta$ -naphthols undergo an oxidative homo-coupling process to produce binaphthols, which are commonly used as ligands and DNA cross-linking agents.<sup>54</sup> Ranganath mentioned that GO is an effective catalyst for the oxidative coupling of 2-naphthols.<sup>55</sup> When the reaction was carried out in aqueous media, it was found that the solvent was crucial because the result polymerized, but in organic solvents, the reactants selectively reacted with binaphthol (**Scheme 1.11**). Moreover, under ideal reaction circumstances, several carbon materials such as graphite, carbon nanotubes, functionalized carbon nanotubes, and activated charcoal were used as catalysts to counteract the effect of GO; nonetheless, decreased product yields were noted. To produce the product in 90% yield, additives like NaOH or KOH were needed; without the additive, only 20% of the desired product was produced. Although the active site and the impact of solvents are yet unclear, the GO catalyst has the potential to be recycled three times.



**Scheme 1.11** Oxidative coupling of  $\beta$ -naphthol in basic media catalyzed by GO.

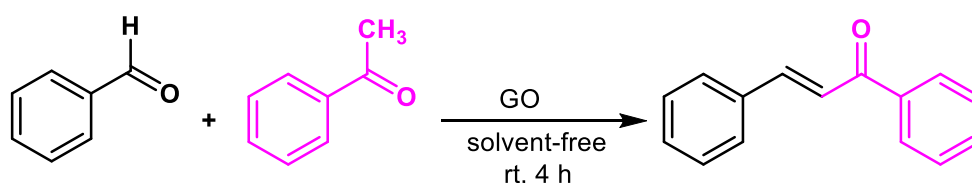
Using a novel GO-promoted oxidation and alkylation approach, mild reaction conditions were created to get 3,3-bisindolylmethane derivatives with superior regioselectivity at 25 °C (**Scheme 1.12**).<sup>56</sup> These findings show that GO has dichotomous catalytic behavior, acting as a Lewis acid in C-O bond cleavage and a transition metal-free catalyst in C-C bond oxidative coupling. According to the preliminary mechanism analysis, the putative mechanism differs from the published literature.



**Scheme 1.12** GO catalyzed oxidative coupling reaction of indole with tetrahydrofuran.

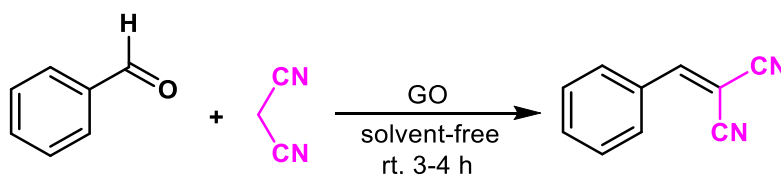
### 1.4.3.2 Aldol-type reaction

The aldol reaction is one of the most significant carbon-carbon bond-forming reactions used in organic synthesis.<sup>57</sup> One type of effective catalyst is an organic base, which helps to accelerate the reaction. However, catalyst separation is challenging since organic bases are typically utilized in homogenous environments. Additionally, because aldol derivatives dehydrate under basic circumstances, their selectivity is typically low.<sup>58</sup> Because of its special surface characteristics and uses, graphene oxide (GO) has attracted a lot more attention in recent years. The aldol reaction between acetophenone and a variety of aromatic aldehydes that donate and withdraw electrons was investigated using GO as a catalyst in a solvent-free environment (**Scheme 1.13**).<sup>59</sup> According to the authors of this study, GO functions as a base catalyst.



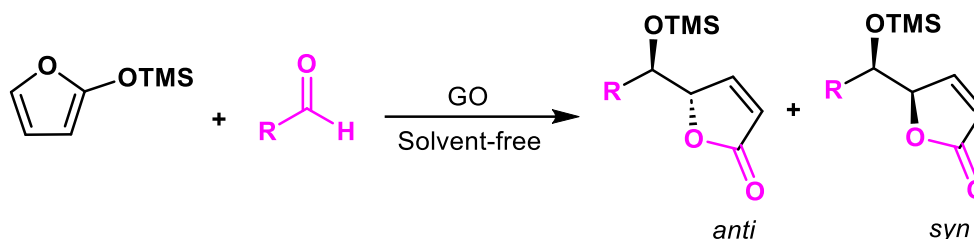
**Scheme 1.13:** Aldol condensation between benzaldehyde and acetophenone catalyzed by GO.

At room temperature and without the use of solvents, the ability of GO to function as a base catalyst for the Knoevenagel condensation of aldehydes and active methylene (malononitrile) compounds was also evaluated (**Scheme 1.14**).<sup>59</sup>



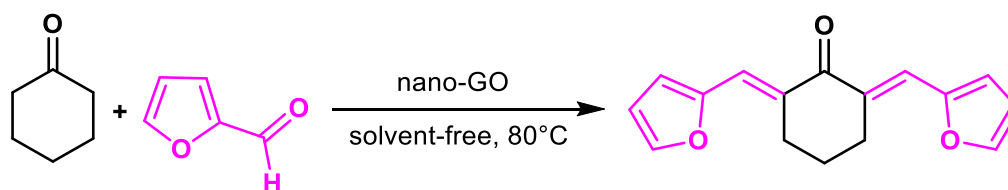
**Scheme 1.14** GO catalyzed Knoevenagel reaction of benzaldehyde with malononitrile.

In solvent-free conditions, GO effectively facilitates the stereoselective Mukaiyama aldol reaction of 2-(trimethylsilyloxy) furan, guaranteeing a high degree of diastereoselectivity (**Scheme 1.15**).<sup>60</sup> The GO capacity to regulate the stereochemical route creates fresh opportunities for potential use in other synthetic reactions.



**Scheme 1.15** GO catalyzed Mukaiyama aldol reaction of 2-(trimethylsilyloxy) furan with aldehyde.

The GO catalytic activity in the Mukaiyama-aldol reaction is accomplished by a straightforward acidic activation by carboxylic and hydroxyl functionalities that can propel the synthesis of the anti-diastereoisomer, which is often seen for H-bond activation.<sup>61</sup> To catalyze the crossed-aldol condensation reaction without the use of solvents, Mohammad and his co-workers studied the novel use of nano-GO catalytic activity as a heterogeneous catalyst made from graphite powder (**Scheme 1.16**).<sup>62</sup>

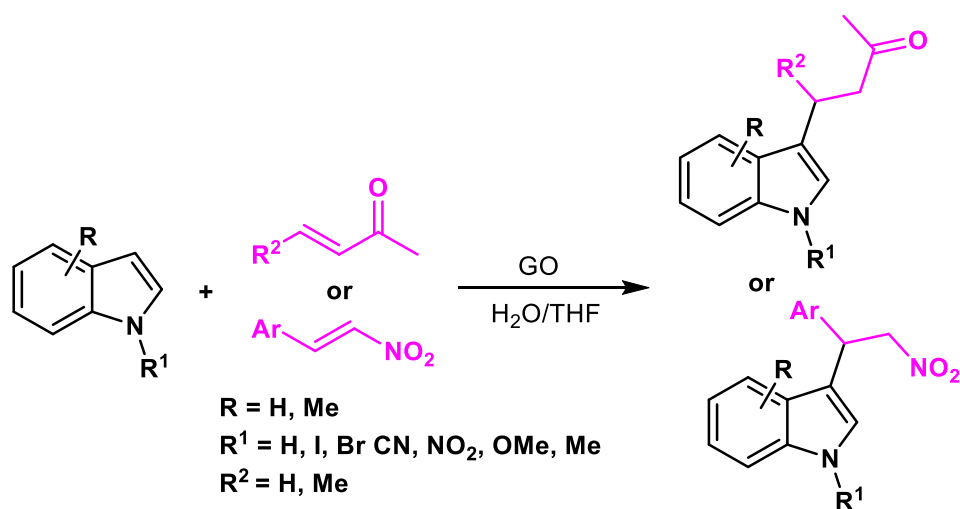


**Scheme 1.16** Nano-GO catalyzed cross aldol condensation of cyclopentanone with substituted benzaldehyde.

In this reaction, the nano-catalyst proved to be quite effective, and good to outstanding yields of products were produced. The catalytic activity of nano-graphene oxide is significantly influenced by the functional groups on its edges and basal planes.

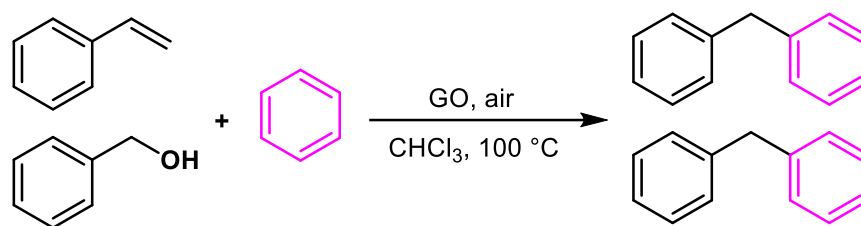
### 1.4.3.3 Friedel Craft-types reaction

When Brønsted or Lewis acids are present, they can be readily synthesized through Friedel-Crafts reactions of indoles with  $\alpha,\beta$ -unsaturated carbonyl compounds.<sup>63-66</sup> A new class of carbon-based solid acids has garnered a lot of interest in the last ten years due to its potential as a stable, affordable, and environmentally friendly catalyst with excellent catalytic activity.<sup>67-70</sup> In water or H<sub>2</sub>O/THF solvents at room temperature, it is worthwhile to investigate the effectiveness of a sulfonated amorphous carbon in catalyzing Friedel-Crafts reactions of indole and its derivatives with different  $\alpha,\beta$ -unsaturated carbonyl compounds.<sup>71</sup> Interestingly, the direct Friedel-Crafts alkylation reaction of indoles with  $\alpha,\beta$ -unsaturated ketone, or nitrostyrene was also successfully catalyzed by graphene-based materials (**Scheme 1.17**).<sup>72</sup> A variety of indole derivatives were produced in yields ranging from satisfactory to outstanding.



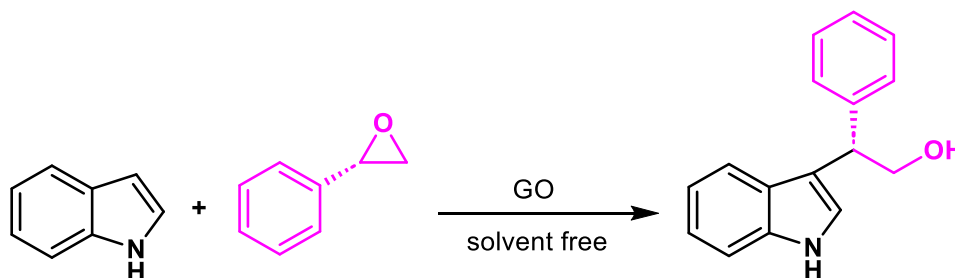
**Scheme 1.17** GO catalyzes Friedel-Crafts alkylation reaction of indoles with  $\alpha, \beta$ -unsaturated ketone, or nitrostyrene.

The electrophilic intermediate is thought to be impacted by graphene's surface electrons. Here, Feng and Michal took advantage of GO's special ability to generate valuable diaryl alkane products in high yields and with exceptional regioselectivity by using it as a catalyst for the Friedel-Crafts-type alkylation reaction of arenes with styrene and alcohol (**Scheme 1.18**).<sup>73</sup>



**Scheme 1.18** Friedel-Crafts alkylation of styrene and alcohol catalyzed by GO.

Guerra claimed that GO acted as a catalyst in the Friedel-Crafts reaction between epoxides and indole (**Scheme 1.19**).<sup>74</sup> Carbon and graphite were tested as comparison catalysts, but they produced very little, indicating that the carboxylic and hydroxyl groups are most likely what gives GO its activity. The GO-catalyzed reaction was in  $\text{S}_{\text{N}}2$  fashion, as evidenced by the product's regioselective and fully inverted formation.



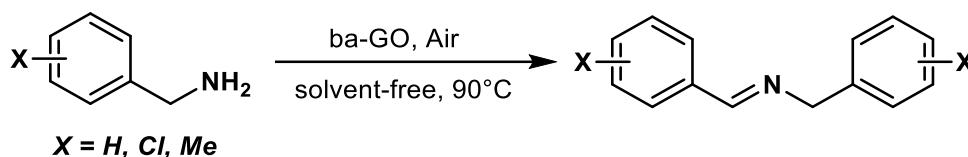
**Scheme 1.19** Regioselective ring-opening reactions of styrene oxide with indole catalyzed by GO.

## 1.4.4 C-N coupling reactions

### 1.4.4.1 Oxidative coupling

The C-N bond's formation is important because it creates pathways for nitrogen to enter organic compounds. The formation of the C-N bond remains a key barrier for organic chemists despite tremendous progress in this field since it frequently requires the employment of costly catalysts or harsh reaction conditions.<sup>75</sup> Under solvent-free,

open-air conditions, the base and acid-treated graphene oxide exhibit efficient catalytic activity in the oxidative C-N coupling conversion of amines to imines yielding up to 98% at 5 wt% percent catalyst loading (**Scheme 1.20**).<sup>76</sup> The synergistic impact of carboxylic acid groups and unpaired electrons at the edge defects is the source of the increased catalytic activity, which is investigated in this work.



**Scheme 1.20** Oxidative coupling of primary amines catalyzed by ba-GO.

High catalytic activity may be influenced by efficient surface modification, such as the creation of holes on the basal plane or the substitution of heteroatoms on the carbon sites,<sup>77,78</sup> but certain oxy-functionalized groups in GO can also serve as active sites for catalytic transformations.<sup>79-81</sup> Under mild reaction conditions GO can be used as an efficient heterogeneous catalyst for the cross-dehydrogenative coupling reaction of  $\alpha$ -ketoaldehyde and amines forming  $\alpha$ -ketoamides with a wide range of substrates (**Scheme 1.21**).<sup>82</sup> The GO surface's oxygen capabilities demonstrated dual activity as an oxidizing and acid catalyst, which was essential for the  $\alpha$ -ketoamide production process.



**Scheme 1.21** GO catalyzed cross-dehydrogenative coupling reaction of  $\alpha$ -ketoaldehyde and amines.

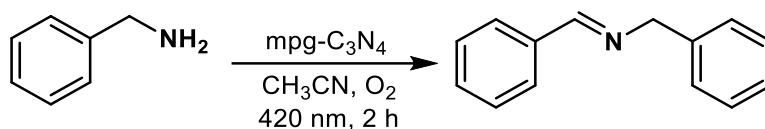
In the presence of air, porous graphene oxide can be employed as a metal-free catalyst for the oxidative coupling of primary amines (**Scheme 1.22**).<sup>83</sup> Remarkably, this tandem approach can also be used to generate classes of potentially physiologically active heterocyclic compounds in moderate to good yields, such as the isoindolo-benzodiazepine derivative and the analog of Tröger's base. Compared to as-made GO, highly porous GO (p-GO) exhibits a higher catalytic activity and a higher density of catalytically active defect sites.



**Scheme 1.22** p-GO-Catalyzed Tandem reactions of benzylamine with nucleophile.

## 1.5 Carbon photocatalysis

Photocatalysis represents a unique class of chemical transformations. Because of its critical significance in addressing the energy crisis and environmental degradation, photocatalysts have drawn more attention as the area of photocatalysis has developed quickly. Graphite carbonitride (g-C<sub>3</sub>N<sub>4</sub>) is a nonmetallic polymeric substance that has been utilized extensively as a visible-light-responsive photocatalyst due to its abundance of sources and ease of manufacture.<sup>84</sup> Using a mesoporous graphite carbon nitride (mpg-C<sub>3</sub>N<sub>4</sub>) photocatalyst, Su and Blechert reported that amines may be aerobically oxidized into imines with excellent yields (**Scheme 1.23**).<sup>85</sup> Even with high-pressure O<sub>2</sub>, no oxidation took place in the absence of light or mpg-C<sub>3</sub>N<sub>4</sub>. N-benzylidene benzylamine was produced by conversion of up to 60% with great selectivity (99%) using mpg-C<sub>3</sub>N<sub>4</sub>, light, and O<sub>2</sub>.



**Scheme 1.23** mpg-C<sub>3</sub>N<sub>4</sub> catalyzed by oxidative coupling of benzylamine under visible light irradiation.

Benzothiazole is a unique structure that is commonly present in medicines and naturally occurring chemicals with biological activity. Benzothiazoles are often made by oxidatively cyclizing thiobenzanilides with a variety of oxidants, including metal salt, bromine, and hypervalent iodine.<sup>86-88</sup> Despite these developments, photo-redox synthesis of benzothiazoles with a recyclable catalyst and a green oxidant in mild conditions is still highly desired. This article describes the first heterogeneous visible light-driven aerobic synthesis of benzothiazoles employing carbon nitride as a photocatalyst and intramolecular C-H functionalization/C-S bond formation of thiobenzanilides in ambient air (**Scheme 1.24**).<sup>89</sup>

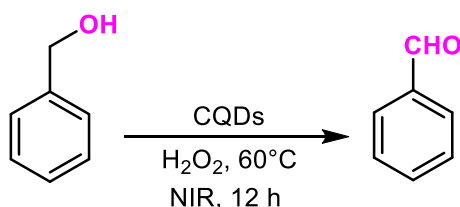


**Scheme 1.24** Synthesis of benzothiazoles via intramolecular C-H functionalization.

For desilylative and decarboxylative additions, allylations, and heteroarylations, visible light-induced g-C<sub>3</sub>N<sub>4</sub> can function as a potent photo-redox catalyst. The recently developed techniques employ gentle reaction conditions, offer good yields, and cover a wide range of substrates. The catalyst can be recovered and reused without losing its reactivity due to the reaction system's heterogeneous character. The feasibility of this heterogeneous photocatalysis technique is demonstrated by the fact that the reaction may also be carried out in continuous flow form, even on a gram-scale, utilizing a straightforward and reusable continuous-flow photoreactor.<sup>90</sup>

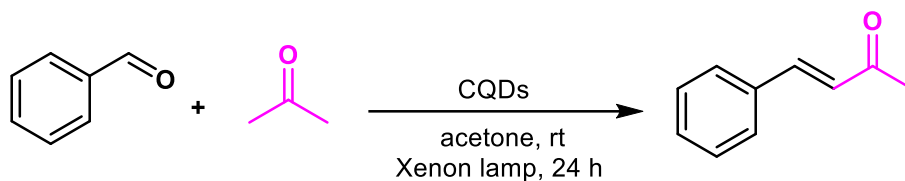
---

Carbon quantum dots (CQDs), a novel form of carbon allotrope, are monodisperse, quasi-spherical carbon nanoparticles with a diameter less than 10 nm.<sup>91</sup> When compared to other allotropic forms, graphene quantum dots have a comparatively high degree of crystallinity.<sup>92</sup> Water solubility and the potential for additional functionalization are provided by the lattice spacings of graphite and oxygenic functional groups (5–50 wt%) on the surface of CQDs, which contain an amorphous or nanocrystalline core primarily composed of sp<sup>2</sup> carbon.<sup>93-95</sup> Because of their special characteristics, CQDs can be used in photocatalysis, where photogenerated electrons and holes carry out the task.<sup>96-98</sup> An important and crucial transformation for the large-scale manufacture of fine chemicals is the selective oxidation of alcohols. Although UV and visible light-driven photocatalytic systems have been developed for the oxidation of alcohol, the long wavelength near-infrared (NIR) and infrared light have not been adequately utilized by the current photocatalytic systems. According to Haitao and his co-worker, when H<sub>2</sub>O<sub>2</sub> is present as an oxidant, CQDs can serve as an efficient NIR light-driven photocatalyst for the selective oxidation of benzyl alcohol to benzaldehyde with high conversion (92%) and selectivity (100%) (**Scheme 1.25**).<sup>99</sup>



**Scheme 1.25** Selective oxidation of benzyl alcohol to benzaldehyde with high conversion and selectivity under the irradiation of NIR light.

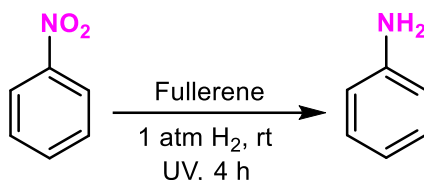
In the aldol condensation, CQDs with a diameter of roughly 5 nm were effective photocatalysts for H-bond catalysis (**Scheme 1.26**). For H-bond catalysis with a range of aromatic aldehydes, CQDs demonstrated exceptional photo-enhanced catalytic capabilities. The effective electron-accepting characteristics of CQDs enhanced the O-H bond and activated the C-O bond to speed up the aldol condensation according to control catalytic tests.<sup>100</sup>



**Scheme 1.26** Room-temperature aldol condensation between aromatic aldehydes and acetone in the presence of CQDs with visible light.

Compared to 1-4 nm CQDs and 10-2000 nm graphite, which do not have as good catalytic activity, 5-10 nm CQDs are an efficient visible-light-driven and controlled acid-catalyst that can catalyze many organic reactions (esterification, Beckmann rearrangement, and aldol condensation) in water solution with high conversion (34-46%, respectively). An innovative use of carbon-based nanomaterials, 5–10 nm CQDs can be used as a light-responsive and controllable photocatalyst. This might greatly advance research in the existing catalytic industry, as well as environmental pollution and energy challenges.<sup>101</sup>

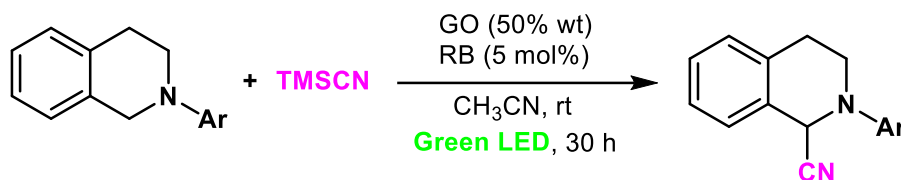
Fullerene can activate molecular hydrogen<sup>102</sup> and showed excellent nonmetal hydrogenation catalysts for the reduction of aromatic nitro compounds to the corresponding amine with excellent selectivity and conversion under 1 atm pressure of H<sub>2</sub> and UV irradiation at ambient temperature (**Scheme 1.27**). The reaction mechanism might involve a synergistic excimer under light irradiation. Additionally, inductively coupled plasma (ICP) emission spectroscopy was used to detect and determine metal contaminants in fullerenes, and control experiments explained that traces of metal impurities in fullerene did not affect the catalytic hydrogenation of nitrobenzene.<sup>103,104</sup>



**Scheme 1.27** Fullerene catalyzed photoinduced reduction of nitrobenzene to aniline.

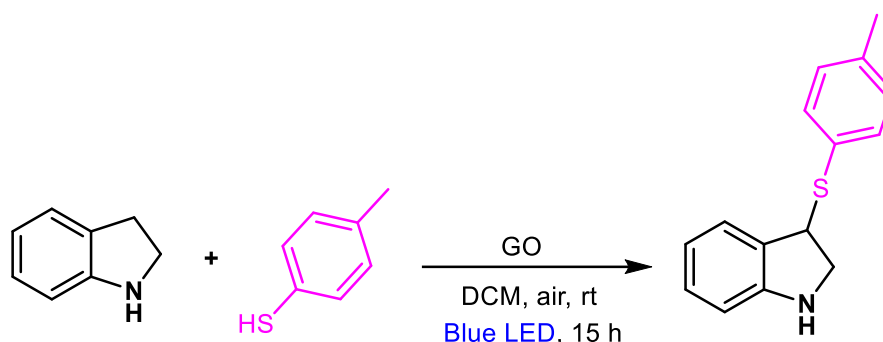
---

The distinctive characteristics and possible uses of GO make its photocatalytic activity in organic processes a subject of intense study interest. Pan and his colleague reported that GO and Rose Bengal together catalyzed the visible-light-responsive oxidative C-H functionalization of tertiary amines (**Scheme 1.28**). Stoichiometric quantities of peroxy compounds are not used as terminal oxidants in this reaction. Tri-alkyl amines, particularly chiral tertiary amines, benefit from this process. This reaction was demonstrated to involve both trifluoromethyl and cyanide nucleophiles, yielding  $\alpha$ -cyano and  $\alpha$ -trifluoromethylated tertiary amines. The intrinsic high surface area of GO and the stabilization of iminium intermediates by slightly acidic GO may contribute to the rate enhancement.<sup>105</sup>



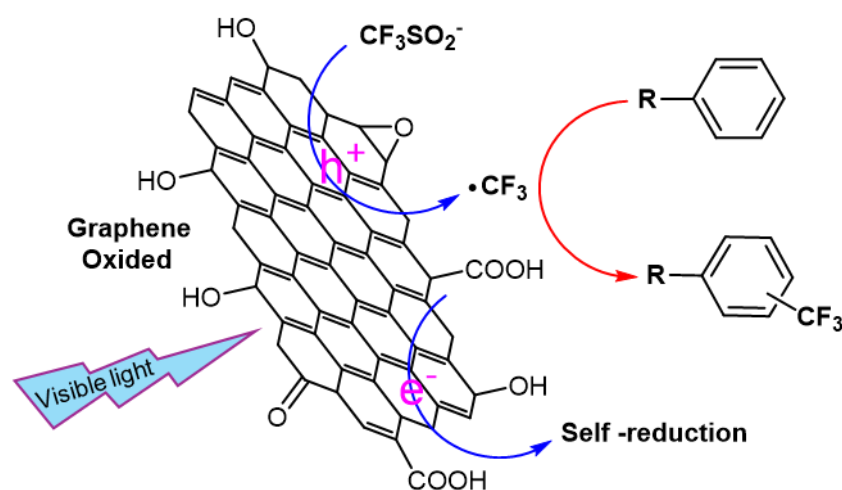
**Scheme 1.28** GO and Rose Bengal catalyzed oxidative C-H functionalization of tertiary amines.

Organosulfur and organoselenium compounds have therapeutic value in the field of medicinal chemistry.<sup>106-109</sup> The C3-chalcogenylation of indolines was developed, employing GO and visible light irradiation at room temperature under an air atmosphere. The reactions characteristics include gram-scalable synthesis, good yields, easy operation, and metal-free conditions. A variety of 3-arylthioindoles, 3-arylselenylindoles, and even 3-thiocyanatoindoles can be obtained with this technique in good to exceptional yields (**Scheme 1.29**). Based on the results of control experiments, GO could act as a radical initiator for progressing the reactions.<sup>110</sup>



**Scheme 1.29** C3-chalcogenylation of indolines catalyzed by GO.

Trifluoromethyl ( $\text{CF}_3$ ) group is a crucial component in the agrochemical and pharmaceutical sectors because it can significantly increase solubility, lipophilicity, and antioxidizability.<sup>7,8</sup> GO has been used as a metal-free photocatalyst for the trifluoromethylation of arenes, using cheap  $\text{CF}_3\text{SO}_2\text{Na}$  as the source  $\text{CF}_3$  radical. It is demonstrated that when exposed to visible light, GO has appropriate bandgaps that activate  $\text{CF}_3\text{SO}_2\text{Na}$  to produce the electrophilic  $\text{CF}_3$  radical, which effectively triggers the trifluoromethylation of common benzene molecules and certain of their derivatives (**Scheme 1.30**).<sup>111</sup>



**Scheme 1.30** Trifluoromethylation of aromatic hydrocarbons using GO sheets as photocatalysts.

---

GO is a two-dimensional nanocarbon that has garnered a lot of attention lately because of its exceptional changeable characteristics under both thermal and photoexcitation modes. In sharp contrast to the behavior shown for the thermal reduction of hydroxyl and epoxy groups, photoexcitation selectively removes the oxygen atoms of epoxy groups from the basal plane of GO. When exposed to light, epoxide groups are selectively photoexcited which produces radicals reversibly. This observation has enabled the preparation of the optimum GO for the intended applications and expanded the application scope of organic transformation under visible light irradiation.<sup>112,113</sup>

## 1.6 Conclusion

Carbon-based materials have emerged as versatile and sustainable catalysts for a wide range of thermal and photochemical reactions. Their unique properties, such as tunable porosity, high surface area, and diverse functionalization potential, make them highly adaptable to various catalytic processes. Thermal carbon-based catalysts demonstrate instability in high-temperature applications, while photoactive carbon materials exhibit remarkable efficiency in light-driven reactions. The review highlights that the integration of carbon nanostructures such as activated carbon, graphite carbo nitride, CQDs, fullerene, CNT, and GO has significantly advanced catalytic efficiency and selectivity.

## 1.7 Objectives and scope of this thesis

In thermal carbon catalysis (**Table 1**), carbon materials act as electron acceptors or donors, influencing reaction rates through charge transfer processes, adsorption-desorption equilibria, acid-base assisted, and heat-driven activation of reactants. Driven by heat energy, which activates the carbon catalyst and the reactants. Reactions are conducted at high temperatures (ranging from 200°C to over 1000°C) depending on the process. Often highly efficient at elevated temperatures, with faster reaction rates. Selectivity can sometimes be lower due to excessive heat, which might cause side reactions. Energy-intensive due to high-temperature requirements. Conversely, photo

carbon catalysis (**Table 1**) involves photon absorption by the carbon catalyst, which can result in electron excitation and the generation of reactive species such as free radicals, singlet oxygen, or hydroxyl radicals. Driven by light energy typically from UV, visible, or infrared light. Photons activate the catalyst, leading to the generation of reactive species such as electrons and holes. Usually occurs at ambient temperatures but can be coupled with slight thermal activation for enhanced performance. Energy efficient since it leverages sunlight or artificial light, reducing the need for external heating. It tends to be more selective since the catalyst can be tuned to absorb specific wavelengths of light, minimizing side reactions.

**Table 1** Comparison of thermal and photo carbon catalysis.

<b>Feature</b>	<b>Thermal Carbon Catalysis</b>	<b>Photo Carbon Catalysis</b>
Energy Source	Heat	Light (UV, visible, NIR)
Temperature	High (200-1000 °C)	Ambient or slightly elevated
Mechanism	Heat-driven charge transfer, adsorption-desorption, acid-base assisted	Photon-driven electron excitation, radicals, reversible
Efficiency	Efficiency is high at elevated temperatures but energy-intensive	Efficiency depends on the light,
Selectivity	Moderate (heat-induced side reactions)	Higher (light wavelength-specific reactions)
Environmental Impact	High energy consumption, potential toxic by-products	Low energy consumption, cleaner reactions

Scope	Oxidation, aldol condensation, esterification, Friedel craft reaction, amidation, C-C bond formation	Oxidation, aldol condensation, radical coupling reaction
Advantages	High reactivity	Reusable, sustainable
Disadvantages	Non-reusable, use oxidant, high catalyst loading	Low reactivity

Based on the above observation the main drawbacks of thermal carbon catalysts are low stability, non-reusable, and high loading. However, in the photo carbon catalysis system reactions are proceeded by homolytic bond cleavage with reversible pathways. The supremacy of photo carbon catalysis system catalyst stability is high, reusable, and sustainable but reactivity is low. By using the unique feature of carbon photocatalysts and overcoming the drawbacks, I have focused on designing and synthesizing highly active, durable, easily recyclable nanocarbon photocatalysts for organic transformations under visible light irradiation. This dissertation also aims to provide an in-depth understanding of how the carbon photocatalyst works and participates in reactions for progressing organic transformation.

## 1.8 References

1. E. Alexander, *Chem-ZTG*, **1911**, 35, 753-755.
2. E. C. C. Baly, I. M. Heilbron, and W. F. Barker, *J. Chem. Soc., Trans.*, **1921**, 119, 1025-1035.
3. E. Baur, and A. Perret, *Helv. Chim. Acta*, **1924**, 7, 910.
4. A. Fujishima, and K. Honda, *Nature*, **1972**, 238, 37-38.
5. A. Kudo, K. Sayama, A. Tanaka, K. Asakura, K. Domen, K. Maruya, and T. Onishi, *J. Catal.*, **1989**, 120, 337.

- 
6. C. Kormann, D. W. Bahnemann, and M. R. Hoffmann, *J. Photochem. Photobiol. A: Chem.*, **1989**, *48*, 161-169.
  7. M. Hara, T. Kondo, M. Komoda, S. Ikeda, N. J. Kondo, K. Domen, M. Hara, K. Shinohara, and A. Tanaka, *Chem. Commun.*, **1998**, *3*, 357-358.
  8. G. E. M. Crisenza, and P. Melchiorre, *Nat. Commun.*, **2020**, *11*, 803.
  9. S. Zhu, and D. Wang, *Adv. Energy Mater.*, **2017**, *7*, 1700841.
  10. A. B. Djurisic, Y. He, A. and M. C. Ng, *APL Mater.*, **2020**, *8*, 030903.
  11. M. A. Hassaan, M. A. El-Nemr, M. R. Elkatory, S. Ragab, V. C. Niculescu, and A. E. Nemr, *Top Curr Chem.*, **2023**, *381*.
  12. A. F. Guzik, *Materials*, **2023**, *16*, 193.
  13. M. V. Bobo, J. J. Kuchta, and A. K. Vannucci, *Org. Biomol. Chem.*, **2021**, *19*, 4816-4834.
  14. L. Wang and J. Yu, *Interface. Sci. Tech.*, **2023**, *35*, 1-52.
  15. S. Gisbertz, and B. Pieber, *ChemPhotoChem*, **2020**, *4*, 456-475.
  16. D. D. Thongam and H. Chaturvedi, *Nano Ex.*, **2021**, *2*, 012005.
  17. D. S. Su, G. Wen, S. Wu, F. Peng, and R. Schlegl, *Angew. Chem. Int. Ed.*, **2017**, *56*, 936-964.
  18. Y. Zhai, Z. Zhu, and S. Dong, *ChemCatChem*, **2015**, *7*, 2806-2815
  19. L. Pacosov, C. Kartusch, P. Kukula, and J. A. Bokhoven, *ChemCatChem*, **2011**, *3*, 154-156.
  20. K. Gong, F. Du, Z. Xia, M. Durstock, and L. Dai, *Science*, **2009**, *323*, 760-764.
  21. S. Dommele, K. P. de Jong, and J. H. Bitter, *Chem. Commun.*, **2006**, 4859-4861.
  22. X. Wang, X. Li, L. Zhang, Y. Yoon, P. K. Weber, H. Wang, J. Guo, and H. Dai, *Science*, **2009**, *324*, 768-771.
  23. C. N. Rao, A. K. Sood, K. S. Subrahmanyam, and A. Govindaraj, *Angew. Chem. Int. Ed.*, **2009**, *48*, 7752-7777.
  24. J. Lu, P. S. Yeo, C. K. Gan, P. Wu, and K. P. Loh, *Nat. Nanotech.*, **2011**, *6*, 247-252.
  25. S. Yasuda, L. Yu, J. Kim, and K. Murakoshi, *Chem. Commun.*, **2013**, *49*, 9627-9629.
  26. B. Fahimirad, A. Asghari, and M. Rajabi, *Micro. Acta*, **2017**, *184*, 3027-3035.
  27. N. Zhao, Y. Wang, S. Hou, and L. Zhao, *Microchim. Acta*, **2020**, *187*, 351.
  28. P. P. Brisebois and M. Siaj, *J. Mater. Chem. C*, **2020**, *8*, 1517-1547.

- 
29. M. Ismael, *J. Alloys Com.*, **2020**, 846, 156446.
30. Y. Li, X. Li, H. Zhang, J. Fan, and Q. Xiang, *J. Mat. Sci. & Tech.*, **2020**, 56, 69-88.
31. A. Akhundi, A. Badiei, G. M. Ziarani, A. H. Yangieh, M. J. Batista, and R. Luque, *Mole. Cata.*, **2020**, 488, 110902.
32. Y. Yu, Q. Zeng, S. Tao, C. Xia, C. Liu, P. Liu, and B. Yang, *Adv. Sci.*, **2023**, 10, 2207621.
33. H. Jung, V. S. Sapner, A. Adhikari, B. R. Sathe and R. Patel, *Front. Chem.*, **2022**, 10.
34. F. Rodríguez-reinoso, *Carbon*, **1998**, 36, 159-175.
35. E. K. Rideal and W. M. Wright, *J. Chem. Soc. Trans.*, **1925**, 127, 1347–1357.
36. E. Keightley Rideal and W. Mary Wright, *J. Chem. Soc. Resumed*, **1926**, 129, 1813–1821.
37. L. E. Cadus, L. A. Arrua, O. F. Gorriz and J. B. Rivarola, *Ind. Eng. Chem. Res.*, **1988**, 27, 2241–2246.
38. F. Lücking, H. Köser, M. Jank and A. Ritter, *Water Res.*, **1998**, 32, 2607–2614.
39. H. J. H. Fenton, *J. Chem. Soc. Trans.*, **1894**, 65, 899–910.
40. G. Tojo, and M. Fernandez, *Oxidation of Alcohols to Aldehydes and Ketones*, **2006**.
41. Y. Kuang, N. M. Islam, Y. Nabae, T. Hayakawa, and M. Kakimoto, *Angew. Chem. Int. Ed.*, **2010**, 49, 436-440.
42. B. H. R. Suryanto and C. Zhao, *Chem. Commun.*, **2016**, 52, 6439-6442.
43. Y. Ohkatsu, Y. Yamazaki, and Tetsuo, *J. Japan Petrol. Inst.*, **1979**, 22, 164-169.
44. S. Nishida and M. Hayashi, *SYNLETT*, **2012**, 23, 1683-1685.
45. D. R. Dreyer, H. Jia and C. W. Bielawski, *Angew. Chem. Int. Ed.*, **2010**, 49, 6813-6816.
46. D. R. Dreyer, H. Jia, A. D. Todd, J. Geng and C. W. Bielawski, *Org. Biomol. Chem.*, **2011**, 9, 7292-7295.
47. H. Huang, J. Huang, Y. Liu, H. He, Y. Cao, and K. Fan, *Green Chem.*, **2012**, 14, 930-934.
48. M. Wang, X. Song, and N. Ma, *Catal. Lett.*, **2014**, 144, 1233-1239.
49. L. Enders, D. S. Casadio, S. Aikonen, A. Lenarda, T. Wirtanen, T. Hu, S. Hietala, L. S. Ribeiro, M. F. R. Pereira and J. Helaja, *Catal. Sci. Technol.*, **2021**, 11, 5962-5972.
50. J. Zhang, S. Chen, F. Chen, W. Xu, G. Deng, and H. Gong, *Adv. Synth. Catal.*, **2017**,

- 
- 359, 2358-2363.
51. A. Mollar-Cuni, D. Espinosa, S. Martín, H. García, and J. A. Matais, *ACS Catal.*, **2021**, *11*, 14688-14693.
52. N. Morimoto, Y. Takeuchi, and Y. Nishina, *Chem. Lett.*, **2016**, *45*, 21-23.
53. H. Jia, D. R. Dreyer, and C. W. Bielawska, *Adv. Synth. Catal.*, **2011**, *353*, 528-532.
54. H. Fan and X. Peng, *J. Org. Chem.*, **2021**, *86*, 493-506.
55. M. Shaikh, A. Sahu, A. K. Kumar, M. Sahu, S. K. Singha, and K. V. S. Ranganath, *Green Chem.*, **2017**, *19*, 4533-4537.
56. X. Peng, Y. Zen, Q. Liu, L. Liu, and H. Wang, *Org. Chem. Front.*, **2019**, *6*, 3615-3619.
57. S. Ding, X. Liu, W. Xiao, M. Li, Y. Pan, J. Hu, and N. Zhang, *Catal. Commun.*, **2017**, *92*, 5-9.
58. C. Ghobril, C. Sabot, C. Mioskowski, and R. Baati, *Eur. J. Org. Chem.*, **2008**, 4104-4108.
59. S. M. Islam, A. S. Roy, R. C. Dey, and S. Paul, *J. Mole. Cata. A: Chemical*, **2014**, *394*, 66-73.
60. M. R. Acocella, M. D. Pascale, M. Maggio, and G. Guerra, *J. Mole. Cata. A: Chemical*, 2015, *408*, 237-241.
61. N. Zhu, B. C. Ma, Y. Zhang, and W. Wang, *Adv. Synth. Catal.*, **2010**, *352*, 1291-1295.
62. M. A. Nasser, A. Allahresani, H. Raissi, *Ir. J. of Cata.*, **2014**, *4*, 33-40.
63. G. Bartoli, M. Bartolacci, M. Bosco, G. Foglia, A. Giuliani, E. Marcantoni, L. Sambri, and E. Torregiani, *J. Org. Chem.*, **2003**, *68*, 4594-4597.
64. M. Bandini, M. Fagioli, A. Umani-Ronchi, *Adv. Synth. Catal.*, **2004**, *346*, 545-548.
65. H. Firouzabadi, N. Iranpoor, and F. Nowrouzi, *Chem. Commun.*, **2005**, *6*, 789-791.
66. H. Tang, A. Lu, Z. Zhou, G. Zhao, L. He, and C. Tang, *Eur. J. Org. Chem.*, **2008**, *2008*, 1406-1410.
67. X. Mo, E. Lotero, C. Lu, Y. Liu, and J. G. Goodwin, *Cat. Lett.*, **2008**, *123*, 1-6.
68. M. Zong, Z. Duan, W. Lou, T. J. Smith, and H. Wua, *Green Chem.*, **2007**, *9*, 434-437.
69. M. Toda, A. Takagaki, M. Okamura, J. N. Kondo, S. Hayashi, K. Domen, and M. Hara, *Nature*, **2005**, *438*, 178.

- 
70. V. L. Budarin, J. H. Clark, R. Luque, and D. J. Macquarrie, *Chem. Commun.*, **2007**, 6, 634-636.
71. J. Ma, S. Ng, Y. Yong, X. Luo, X. Wang, and X. Liu, *Chem. Asian J.*, **2010**, 5, 778-782.
72. A. V. Kumar and K. R. Rao, *Tetrahedron Lett.*, **2011**, 52, 5188-5191.
73. F. Hu, M. Patel, F. Luo, C. Flach, R. Mendelsohn, E. Garfunkel, H. He, and M. Szostak, *J. Am. Chem. Soc.*, **2015**, 137, 14473-14480.
74. M. R. Acocella, M. Mauro and G. Guerra, *ChemSusChem*, **2014**, 7, 3279-3283.
75. J. Bariwal and E. V. Eycken, *Chem. Soc. Rev.*, **2013**, 42, 9283-9303.
76. C. Su, M. Acik, K. Takai, J. Lu, S. Hao, Y. Zheng, P. Wu, Q. Bao, T. Enoki, Y. J. Chabal, and K. P. Loh, *Nat. Commun.*, **2012**, 3, 1298.
77. A. Primo, V. Parvulescu, H. Garcia, *J. Phys. Chem. Lett.*, **2017**, 8, 264-278.
78. J. Long, X. Xie, J. Xu, Q. Gu, L. Chen, X. Wang, *ACS Catal.*, **2012**, 2, 622-631.
79. S. Verma, H. P. Mungse, N. Kumar, S. Choudhary, S. L. Jain, B. Sain, O. P. Khatri, *Chem. Commun.*, **2011**, 47, 12673-12675.
80. A. Dhakshinamoorthy, M. Alvaro, P. Concepcion, V. Fornes, H. Garcia, *Chem. Commun.*, **2012**, 48, 5443-5445.
81. T. Bhattacharya, B. Majumdar, D. Dey, and T. K. Sarma, *RSC Adv.*, **2014**, 4, 45831-45837.
82. B. Majumdar, D. Sarma, T. Bhattacharya, and T. K. Sarma, *ACS Sustainable Chem. Eng.*, **2017**, 5, 9286-9294.
83. C. Su, R. Tandiana, J. Balapanuru, W. Tang, K. Pareek, C. T. Nai, T. Hayashi, and K. P. Loh, *J. Am. Chem. Soc.*, **2015**, 137, 685-690.
84. R. Huang, J. Wu, M. Zhang, B. Liu, Z. Zheng, and D. Luo, *Material & Design*, **2021**, 210, 110040.
85. F. Su, S. C. Mathew, L. Mohlmann, M. Antonietti, X. Wang, and S. Blechert, *Angew. Chem.*, **2011**, 123, 683-686.
86. K. Inamoto, C. Hasegawa, K. Hiroya, and T. Doi, *Org. Lett.*, **2008**, 10, 5147-5150.
87. C. Shen, H. Xia, H. Yan, X. Chen, S. Ranjit, X. Xie, D. Tan, R. Lee, Y. Yang, B. Xing, K. Huang, P. Zhang, and X. Liu, *Chem. Sci.*, **2012**, 3, 2388-2393.
88. Y. Xu, B. Li, X. Zhang, and X. Fan, *J. Org. Chem.*, **2017**, 82, 9637-9646.

- 
89. J. Bai, S. Yan, Z. Zhang, Z. Guo, and C. Zhou, *Org. Lett.*, **2021**, *23*, 4843-4848.
90. Y. Cai, Y. Tang, L. Fan, Q. Lefebvre, H. Hou, and M. Rueping, *ACS Catal.*, **2018**, *8*, 9471-9476.
91. W. Liu, C. Li, Y. Ren, X. Sun, W. Pan, Y. Li, J. Wang, and W. Wang, *J. Mater. Chem. B*, **2016**, *4*, 5772-5788.
92. X. Li, M. Rui, J. Song, Z. Shen, and H. Zeng, *Adv. Funct. Mater.*, **2015**, *25*, 4929-4947.
93. S. Yang, X. Wang, H. Wang, F. Lu, P. G. Luo, L. Cao, M. J. Meziani, J. Liu, Y. Liu, M. Chen, Y. Huang, and Y. Sun, *J. Phys. Chem. C*, **2009**, *113*, 18110-18114.
94. S. Yang, L. Cao, P. G. Luo, F. Lu, X. Wang, H. Wang, M. J. Meziani, Y. Liu, G. Qi, and Y. Sun, *J. Am. Chem. Soc.*, **2009**, *131*, 11308-11309.
95. S. N. Baker, and G. A. Baker, *Angew. Chem. Int. Ed.*, **2010**, *49*, 6726-6744.
96. G. Murali, J. Modigunta, S. Park, S. Lee, H. Lee, J. Yeon, H. Kim, Y. Park, S. Y. Park, J. R. Durrant, H. Cha, T. K. An, and I. In, *ACS Appl. Mater. Interfaces*, **2021**, *13*, 34648-34657.
97. N. Syed, J. Huang, and Y. Feng, *Carbon Lett.*, **2021**, *32*, 81-97.
98. J. Yao, L. Yang, L. Huang, C. Wang, J. Liu, L. Huang, and Y. Song, *Appl. Surf. Sci.*, **2021**, *578*, 151913.
99. H. Li, R. Liu, S. Lian, Yang Liu, H. Huang, and Z. Kang, *Nanoscale*, **2013**, *5*, 3289-3297.
100. Y. Han, H. Huang, H. Zhang, Y. Liu, X. Han, R. Liu, H. Li, and Z. Kang, *ACS Catal.*, **2014**, *4*, 781-787.
101. H. Li, R. Liu, W. Kong, J. Liu, Y. Liu, L. Zhou, X. Zhang, S. Lee, and Z. Kang, *Nanoscale*, **2014**, *6*, 867-873.
102. M. Wu, X. Wei, L. Qi, and Z. Xu, *Tetra. Lett.*, **1996**, *37*, 7409.
103. B. Li and Z. Xu, *J. Am. Chem. Soc.*, **2009**, *131*, 16380-16382.
104. A. Corma, P. Concepción, and P. Serna, *Angew. Chem. Int. Ed.*, **2007**, *46*, 7266-7269.
105. Y. Pan, S. Wang, C. W. Kee, E. Dubuisson, Y. Yang, K. P. Loha, and C. Tan, *Green Chem.*, **2011**, *13*, 3341-3344.
106. M. Feng, B. Tang, S. Liang, and X. Jiang, *Curr. Top. Med. Chem.*, **2016**, *16*, 1200-1216.

- 
107. J. T. Jarrett, *J. Biol. Chem.*, **2015**, *290*, 3972-3979.
108. M. Ninomiya, D. R. Garud, and M. Koketsu, *Coord. Chem. Rev.*, **2011**, *255*, 2968-2990.
109. C. W. Nogueira, and J. B. T. Rocha, *Arch. Toxicol.*, **2011**, *85*, 1313-1359.
110. C. Liu, X. Peng, D. Hu, F. Shi, P. Huang, J. Luo, Q. Liu, and L. Liu, *New J. Chem.*, **2020**, *44*, 17245-17251.
111. Y. Tong, H. Pan, W. Huang, W. Qiu, Z. Ding, C. Xu, and R. Yuan, *New J. Chem.*, **2019**, *43*, 8741-8745.
112. M. Hada, K. Miyata, S. Ohmura, Y. Arashida, K. Ichiyanagi, I. Katayama, T. Suzuki, W. Chen, S. Mizote, T. Sawa, T. Yokoya, T. Seki, J. Matsuo, T. Tokunaga, C. Itoh, K. Tsuruta, R. Fukaya, S. Nozawa, S. Adachi, J. Takeda, K. Onda, S. Koshihara, Y. Hayashi, and Y. Nishina, *ACS Nano*, **2019**, *13*, 10103-10112.
113. Y. Saida, R. Shikata, K. En-ya, S. Ohmura, Y. Nishina, and M. Hada, *J. Phys. Chem. A*, **2022**, *126*, 6301-6308.

---

## Chapter II

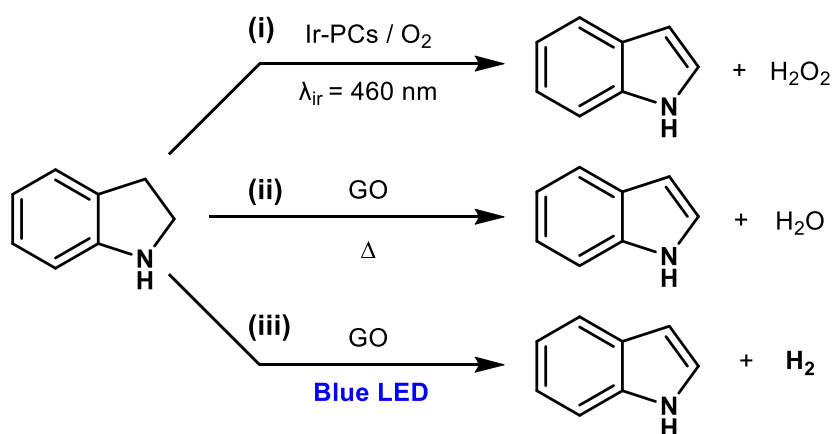
### **Photocatalytic Dehydrogenation of N-Heterocycles Promoted by Radicals from Graphene Oxide**

Visible light-induced photocatalytic dehydrogenation of N-heterocycles was achieved by graphene oxide (GO). Unlike previously reported thermally induced GO-promoted reactions, this system generates radicals and molecular hydrogen, which are confirmed by electron spin resonance and gas chromatography. A metal-free, oxidant-free, and recyclable photocatalytic reaction were achieved by a carbon-based system for the first time.

## 2.1 Introduction

Metal-based catalysis has been extensively studied for decades. However, metal-based catalysts have some drawbacks; toxicity, removal difficulty, and limited natural resources.<sup>1,2</sup> Therefore, non-metallic systems in catalysis are attractive and valuable because of their environment friendliness, sustainability, and abundance of resources.<sup>3-7</sup> Graphene oxide (GO) is a two-dimensional carbon material with various unique properties such as high surface area, durability, and tunable electron conductivity, and reactivity.<sup>8,9</sup> GO works as a catalyst in several organic transformations, such as oxidation of benzyl alcohol to benzaldehyde,<sup>10</sup> aerobic oxidative coupling of amine to imine,<sup>11</sup> arylation of benzene for biaryl construction,<sup>12</sup> thiolation of indoles,<sup>13</sup> cross-coupling of indoles with ethers,<sup>14</sup> and Mannich type reactions.<sup>15</sup> Recently, researchers have focused on the photocatalytic behaviour of GO, including oxidative C–H functionalization of tertiary amine,<sup>16</sup> chalcogenylation of indoline,<sup>17</sup> and carbon dioxide to methanol.<sup>18</sup> Photocatalytic dehydrogenation was reported using Ir complex;<sup>19</sup> however, there has been no report on such a reaction using a carbon-based catalyst. In contrast, GO was reported to undergo redox-type reactions under thermal conditions.<sup>20</sup>

Herein, delineate the use of GO as a metal-free and recyclable photocatalyst for the dehydrogenation of N-heterocycles by releasing molecular hydrogen under visible light irradiation (**Scheme 2.1**).



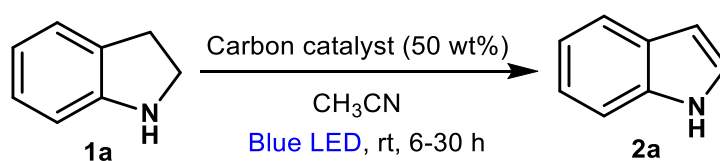
**Scheme 2.1** Dehydrogenation of indoline by (i) Ir catalyst under photo-irradiation, generating hydrogen peroxide, (ii) GO under heating, generating water, and (iii) GO under photo-irradiation, generating molecular hydrogen.

## 2.2 Result and discussion

### 2.2.1 Screening of the reaction

To optimize the reaction conditions for photocatalytic dehydrogenation, indoline (**1a**) was selected as a model substrate (**Table 2.1** and **2.2**). The mixture of indoline **1a** (24 mg, 0.2 mmol), GO (12 mg) and CH<sub>3</sub>CN (1.0 mL) was stirred with irradiating Blue LED light under an air atmosphere at room temperature for up to 30 hours. After the reaction, the reaction mixture was analyzed by GC using n-dodecane as an internal standard. To check up screening of the reaction time dehydrogenation product was analyzed every six-hour interval during the reaction course (**Table 2.1**). An optimum yield was found at 24 hours reaction time up to 93% (**Table 2.1**, Entry 4).

**Table 2.1** Screening of reaction time<sup>a</sup>

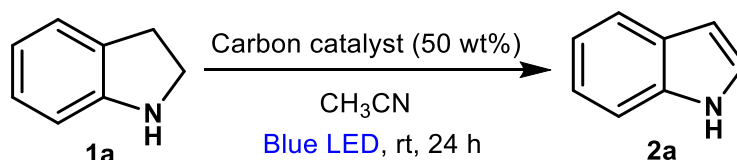


Entry	Time (hour)	Yield (%) <sup>b</sup>
1	6	27
2	12	50
3	18	71
4	24	90±3 <sup>c</sup>
5	30	93

<sup>a</sup>Reaction conditions: Indoline **1a** (0.2 mmol), GO (12 mg), CH<sub>3</sub>CN (1.0 mL) under air atmosphere, room temperature, 6-30 h. <sup>b</sup>GC yield, <sup>c</sup>n=5.

For checking reaction conditions different carbon materials were synthesized. Among various carbon materials, GO showed the highest catalytic activity, and indole (**2a**) was obtained in 93% yield under blue LED irradiation (**Table 2.2**, Entry 1). Other carbon materials such as reduce graphene oxide (rGO), nitrogen-doped reduced graphene oxide (N-rGO), activated carbon, natural graphite, and carbon quantum dot (CQD) showed very low yield or no catalytic performance on the photocatalytic dehydrogenation of **1a** (**Table 2.2**, Entries 2-6). As reported previously, GO worked as an oxidant under thermal treatment without photoirradiation (**Table 2.2**, Entry 7). Both light and carbon catalysts were proved to be essential for this reaction; no desired product was observed when the reaction was conducted in the dark and absence of GO (**Table 2.2**, Entries 8 and 9). Interestingly, the reaction proceeded in the absence of molecular oxygen (**Table 2.2**, Entry 10), which is totally different from the thermally induced reaction using GO.<sup>20</sup>

**Table 2.2** Screening of the reaction conditions



Entry	Carbon Catalyst	Yield (%) <sup>b</sup>
1	GO	93
2	rGO	10
3	N-rGO	5
4	activated carbon	5
5	graphite	0
6	CQD	0
7	GO <sup>c</sup>	73
8	GO <sup>d</sup>	0
9	none	0
10	GO <sup>e</sup>	91

<sup>a</sup>Reaction conditions: indoline **1a** (0.2 mmol), carbon catalyst (12 mg), CH<sub>3</sub>CN (1.0 mL)

---

under air atmosphere at room temperature for 24 h. <sup>b</sup>GC yield. <sup>c</sup>Heating at 100 °C without photo-irradiation. <sup>d</sup>Under dark without photo-irradiation. <sup>e</sup>Reaction was performed under Ar atmosphere.

### 2.2.2 Radical properties analysis

To elucidate the reaction mechanism, in-situ electron spin resonance (ESR) experiments were designed in the absence and presence of blue LED irradiation. A mixture of **1a** and GO in acetonitrile was subjected to irradiation and performed ESR analysis (**Figure 2.1**). No ESR signal appeared in the absence of light, in contrast, a strong ESR signal was observed in the presence of light. However, no peak was detected in the ESR spectra when rGO, activated carbon, or graphite was used. These results suggest the radicals are generated from GO, and they promoted the dehydrogenation reaction.

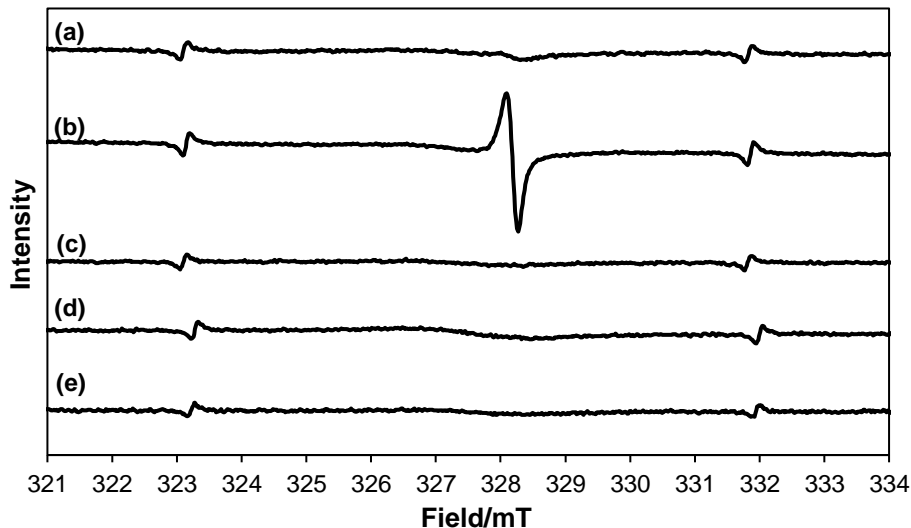


**Figure 2.1** ESR spectrum of the reaction mixture (a) with GO in the absence of light, (b) with GO under light irradiation, (c) with rGO under light irradiation, (d) with activated carbon under light irradiation, and (e) with graphite under light irradiation.

### 2.2.3 Mechanistic investigation

To gain better insight into the mechanism of the reaction, tried to trap the radical intermediate by in-situ ESR analysis using 5,5-dimethyl-1-pyrroline N-oxide (DMPO). A mixture of indoline **1a**, GO, and DMPO in acetonitrile was photo-irradiated and subjected to ESR analysis (**Figure 2.2**). A signal derived from the DMPO-hydroxyl radical adduct (DMPO- $\cdot$ OH)<sup>21</sup> was observed only in the first cycle; in contrast, from the second to the fifth cycles, only carbon radical was detected. These results suggest that, in the first cycle, the reaction was promoted by  $\cdot$ OH radical and/or carbon radical, and later cycles proceeded via only carbon radical. To confirm the radical pathway, radical scavenger 2,2,6,6-tetramethyl piperidine 1-oxyl (TEMPO) in the reaction mixture was added; as a result, only 3% of the product was obtained, suggesting the radical pathway.

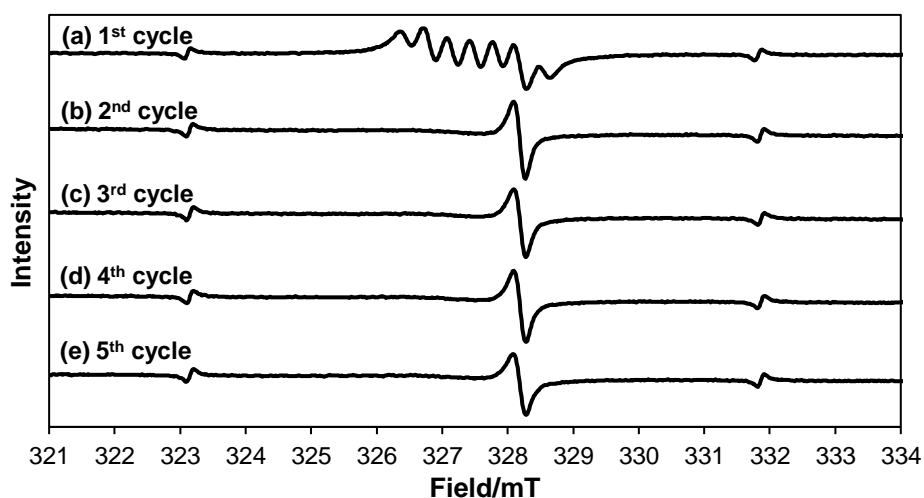
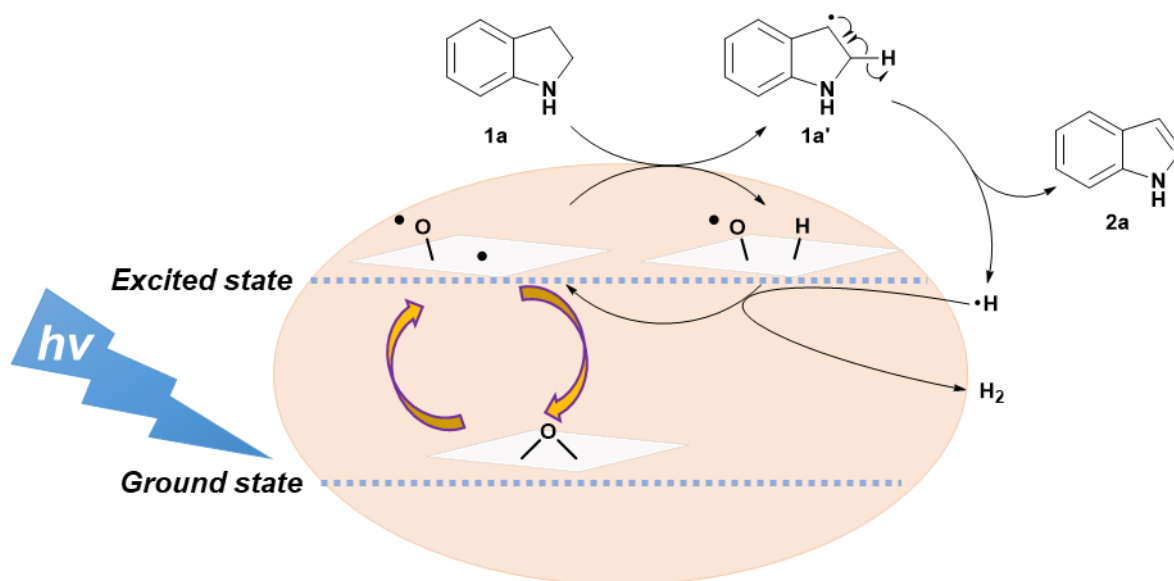


**Figure 2.2** ESR spectrum of the reaction mixture with DMPO. (a) 1<sup>st</sup> cycle, (b) 2<sup>nd</sup> cycle, (c) 3<sup>rd</sup> cycle, (d) 4<sup>th</sup> cycle, and (e) 5<sup>th</sup> cycle.

Based on the above observation, a plausible reaction mechanism after the second cycle is proposed (**Scheme 2.2**). Under the irradiation of blue LED light, band gap excitation generates radical species on GO (for simplicity, only epoxide functional group is shown).<sup>22</sup> Indoline (**1a**) is activated by the GO radical, generating indoline radical (**1a'**). Finally, dehydrogenation from **1a'** gives indole (**2a**) and H<sub>2</sub>.



**Scheme 2.2** Proposed reaction mechanism.

Different from meta-catalyzed systems that require molecular oxygen as a terminal oxidant,<sup>23</sup> GO photocatalytic system worked even under Ar atmosphere. It is reported that rGO produces molecular hydrogen in the dehydrogenation of N-heterocycles under thermal conditions.<sup>24</sup> Also investigated to obtain evidence that molecular hydrogen was released from the reaction. The reaction was performed in a capped test tube reactor, the upper gas was pumped off by a syringe after the reaction, and the gas was measured by GC. As a result, molecular hydrogen was observed, revealing that GO photocatalytic system is dehydrogenative even in the presence of molecular oxygen (**Figure 2.3**).

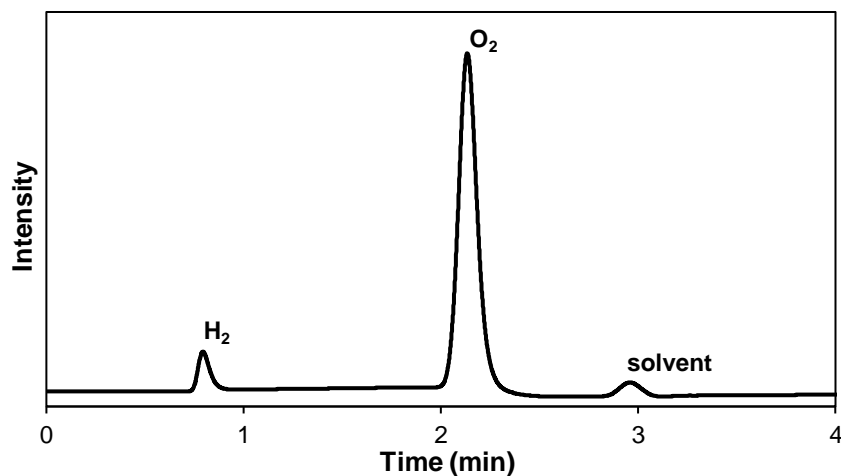


**Figure 2.3** GC spectrum of the gas phase of the reaction mixture.

#### 2.2.4 Recyclability test

Next, the recyclability of the GO photocatalyst was investigated. The structural analysis before and after the reaction was investigated by FTIR spectroscopy) and X-ray photoelectron spectroscopy (XPS). The reactivity was maintained for at least five cycles (**Figure 2.4**) without significant structural changes of GO, explained in **Figures 2.5** and **2.6**.

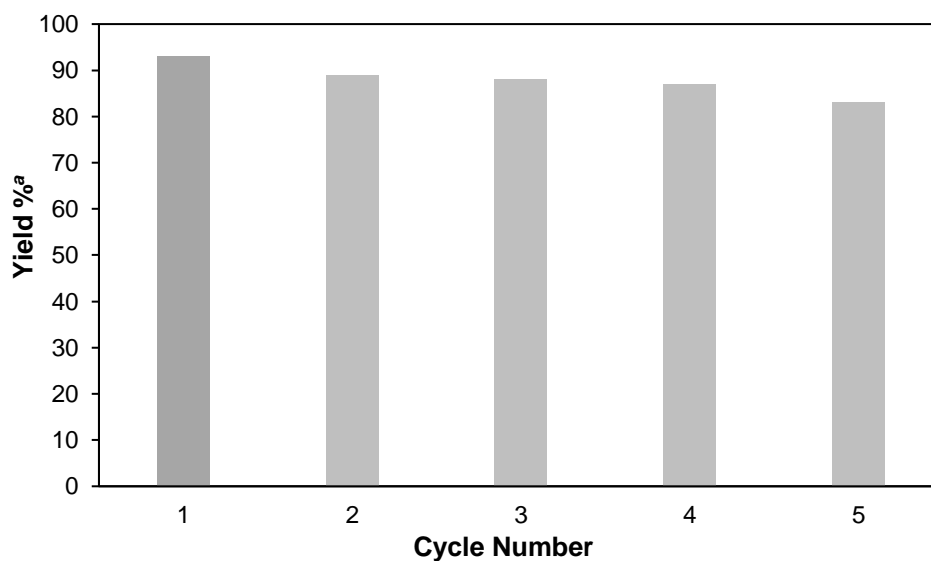


**Figure 2.4** Recyclability test of GO photocatalyzed dehydrogenation of indoline **1a**. Reaction conditions: **1a** (1.0 mmol), GO (60 mg), CH<sub>3</sub>CN (5.0 mL) under air atmosphere, room temperature, irradiation of blue LED for 24 h. <sup>a</sup>GC yield.

FTIR spectroscopy is a powerful technique to characterize the presence of different functional groups in graphene oxide including oxygen-containing functional groups. The FTIR spectrum of GO (**Figure 2.5**), shows a broad peak appearing at 3381 cm<sup>-1</sup> in the high-frequency area attributed to the stretching mode of the O-H bond, revealing the presence of hydroxyl groups in GO. The band observed at 1724 cm<sup>-1</sup> was assigned to the C=O stretch of the carboxyl group while the peak around 1616 cm<sup>-1</sup> is attributed to C=C stretches. The peaks at 1395 cm<sup>-1</sup> and 1065 cm<sup>-1</sup> correspond to the C-OH and C-O-C groups, respectively. All peaks were reserved up to the fifth cycle of the reaction.

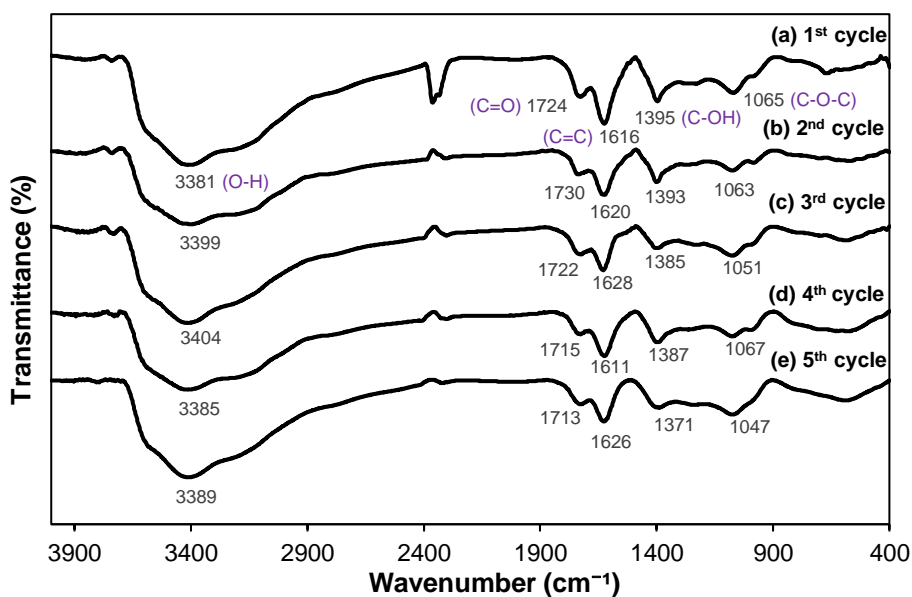


**Figure 2.5** FTIR spectra of GO. (a) 1<sup>st</sup> cycle, (b) 2<sup>nd</sup> cycle, (c) 3<sup>rd</sup> cycle, (d) 4<sup>th</sup> cycle, and (e) 5<sup>th</sup> cycle.

The XPS spectra of GO before reaction and after the reaction were also analyzed (**Figure 2.6**). In the expanded XPS spectrum before the reaction, the C1s peak binding energies of 284.1 eV, 286.8 eV, and 288.3 eV correspond to the C-C bond, C-O bond,

and C=O bond respectively. After the fifth cycle of reaction the C1s peak binding energies of 284.1 eV for C-C bond, 286.2 for C-O bond, and 287.8 for C=O bond. All peaks were retained the same after the fifth cycle of the photocatalytic reaction.

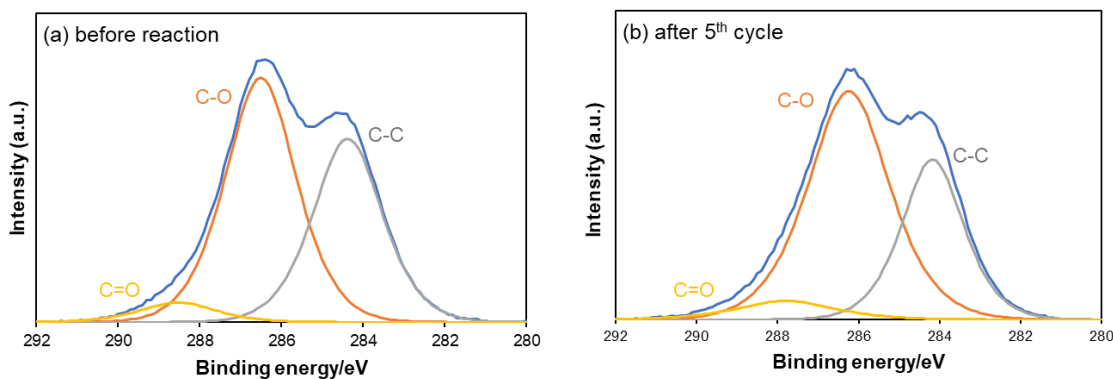


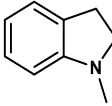
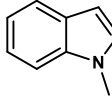
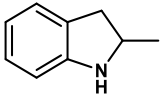
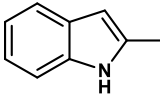
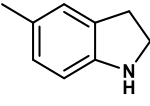
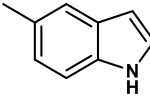
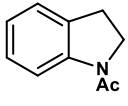
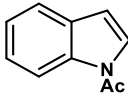
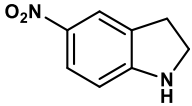
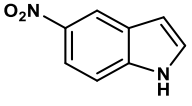
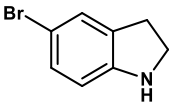
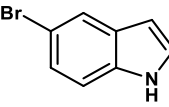
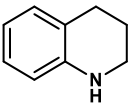
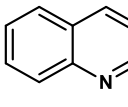
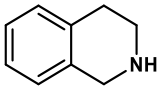
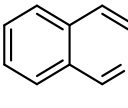
**Figure 2.6** XPS spectra of GO. (a) before reaction, and (b) after the 5<sup>th</sup> cycle.

These results suggested that GO remained unchanged until the fifth cycle of the photocatalytic dehydrogenation reaction. These results also indicate that the  $\cdot\text{OH}$  formed in the first cycle is negligible and does not significantly affect the product yield.

### 2.2.5 Substrate scope

Then examined the substrate scope of the photocatalytic dehydrogenation reaction. The reaction proceeded with good to excellent yields (**Table 2.3**, Entries 1-3) when indoline derivatives having a methyl group at the C1, C2, or C5 position (**3a-c**) were used. In contrast, an acetyl group on the nitrogen atom of indoline inhibited the reaction due to the steric or electronic effect, and most of *N*-acetylindoline (**3d**) was recovered (**Table 2.3**, Entry 4). Electron withdrawing groups such as nitro and bromo groups at the C5 position (**3e** and **3f**) did not affect the reactivity and formed corresponding indole derivatives (**4e** and **4f**) in good yields (**Table 2.3**, Entries 5 and 6). Furthermore, not only indoline derivatives but also 1,2,3,4-tetrahydroquinoline and 1,2,3,4-tetrahydroisoquinoline (**3g** and **3h**) worked as substrates to give the corresponding dehydrogenation products (**4g** and **4h**) in moderate to good yields (**Table 2.3**, Entries 7 and 8).

**Table 2.3** Substrate scope using GO as a photocatalyst<sup>a</sup>

Entry	Substrate	Product	Yield (%) <sup>b</sup>
1	 <b>3a</b>	 <b>4a</b>	90
2	 <b>3b</b>	 <b>4b</b>	91
3	 <b>3c</b>	 <b>4c</b>	92
4	 <b>3d</b>	 <b>4d</b>	Trace
5	 <b>3e</b>	 <b>4e</b>	85
6	 <b>3f</b>	 <b>4f</b>	93
7	 <b>3g</b>	 <b>4g</b>	75
8	 <b>3h</b>	 <b>4h</b>	74

---

<sup>a</sup>Reaction conditions: N-heterocycles (0.2 mmol), GO (12 mg), CH<sub>3</sub>CN (1.0 mL) under air atmosphere, room temperature, irradiation of blue LED for 24 h. <sup>b</sup>GC yield.

## 2.3 Conclusion

In conclusion, developed a metal-free carbon-based photocatalytic system for the dehydrogenation of N-heterocycles. The reactions proceeded smoothly under mild reaction conditions and afforded the desired products in good to excellent yields. The mechanistic study revealed that the reaction proceeded with the formation of radicals from GO under irradiation of blue LED light. Both GO and light synergistically worked for the dehydrogenation reactions. This is the first example of the detection of molecular hydrogen in dehydrogenation of N-heterocycles using GO photocatalyst. Based on the proposed reaction mechanism, the scope of the photocatalytic reaction would be expanded by tuning the band gap and functional group of carbon materials.

## 2.4 Experimental

### 2.4.1 Materials

Graphite was purchased from NIPPON GRAPHITE Industries, Ltd. and activated carbon (Vulcan XC72) was purchased from Cabot Corporation. KMnO<sub>4</sub>, H<sub>2</sub>SO<sub>4</sub>, 30% aq. H<sub>2</sub>O<sub>2</sub>, hydrazine monohydrate, 5,5-dimethyl-1-pyrroline N-oxide (DMPO), 1-acetylundoline, and 5-nitroindoline were purchased from FUJIFLIM Wako Pure Chemical Industries, Ltd. Indoline, 1-methylindoline, 2-methylindoline, 5-methylindoline, 5-bromoindoline, 1,2,3,4-tetrahydroquinoline and 1,2,3,4-isoquinoline were purchased from Tokyo Chemical Industry Co., Ltd. All above-mentioned reagents were used directly without further purification. Products (**4a**, **4b**, **4c**, **4d**, **4e**, **4f**, **4g**, and **4h**) are commercially available and identical to known data.

### 2.4.2 General information

---

The light source was used as Kessil A360X tuna blue LED light, wavelength 470 nm and power  $55 \times 10^3$  lux. The products were quantified by gas chromatography-mass spectrometry (GCMS-QP2010 *Plus*, Shimadzu), equipped with a flame ionization detector (FID). Hydrogen gas was detected by gas chromatography (GC-2014, Shimadzu), connected with a thermal conductivity detector (TCD). ESR analysis was performed using an electron spin resonance spectrometer (JES-X310) with microwave frequency 9.542 GHz, modulation frequency 100 kHz, power 1 mW, and sweep time 1 min. The functional groups on the surface of the GO were recorded by Fourier transform infrared spectrophotometer (FTIR; Shimadzu IRTracer-100). The samples for the FTIR were dried and mixed with KBr and then pressed into 1.3 cm-diameter pellets. Freeze-drying of the carbon catalysts was performed using ADVANTEC DRZ350WC. The surface chemistry of GO was performed using an X-ray photoelectron spectroscopy (XPS; JPS-9030) with a pass energy of 20 eV.

### **2.4.3 Preparation of carbon materials**

#### **Preparation of GO**

Graphite (3.0 g) was stirred in 95%  $\text{H}_2\text{SO}_4$  (75 mL).  $\text{KMnO}_4$  (9.0 g) was gradually added to the solution keeping the temperature. The mixture was then stirred at 35 °C for 2 h. The resulting mixture was diluted by water (75 mL) under vigorous stirring and cooling so that temperature does not exceed 50 °C. The suspension was further treated by 30% aq.  $\text{H}_2\text{O}_2$  (7.5 mL). The resulting graphite oxide suspension was purified by centrifugation with water until neutralization and freeze-dried.

#### **Preparation of rGO**

GO (2.0 g) was dispersed in water (200 mL), then hydrazine monohydrate (2.0 mL) was added and stirred at 180 °C for 4 h. After cooling, rGO was purified by washing with water, and freeze-dried.

---

## Preparation of (N-rGO)

Nitrogen doping onto GO was conducted by dissolving 1 g of nitrogen source (Guanidine Carbonate) in 100 mL of 0.1 wt% GO solution to attain a 10:1 ratio of nitrogen source to GO. The mixture was transferred into a steel-based autoclave and subjected to hydrothermal treatment at 180 °C for 8 h. The autoclave was then allowed to cool down to room temperature naturally, after which the black precipitate was filtered and washed five times with deionized water and once with isopropanol. Finally, the product was dried in a freeze drier and labeled as N-rGO.

## Preparation of CQD

Here, the solvothermal method was used for the synthesis of CQD. The solution was made using 0.76 g (3 mmol) of pyromellitic acid, 0.76 g (10 mmol) of thiourea, 0.108 ml (1 mmol) of diethylene triamine in 10 ml of DMF, and then ultrasonicated for 15 min. The final solution was transferred into a Teflon-lined autoclave (50 ml) and heated at 180 °C for 8 h and then the autoclave was allowed to cool naturally, resulting in a strong fluorescent orange emissive CQD.

### 2.4.4 ESR measurement technique

The mixture of indoline **1a** (24 mg, 0.2 mmol), GO (12 mg), CH<sub>3</sub>CN (1.0 mL), and DMPO (22 mg, 0.2 mmol) was stirred at room temperature for 5 minutes. After 5 minutes the reaction mixture was taken in a 1-mm-internal-diameter, 50-mm-long quartz capillary tube and irradiated Blue LED light at room temperature for 24 h. After every 6 h intervals, ESR analysis was performed.

### 2.4.5 Light on/off experiment

The mixture of indoline **1a** (24 mg, 0.2 mmol), GO (12 mg) and CH<sub>3</sub>CN (1.0 mL) was stirred with irradiating Blue LED light under an air atmosphere at room temperature for

6 h and kept in the dark at 6 h intervals. After every 6 h, the reaction mixture was analyzed by GC using n-dodecane as an internal standard (**Figure 2.7**). Light is necessary for the progress of dehydrogenation reactions. Reactions did not proceed in the absence of light.

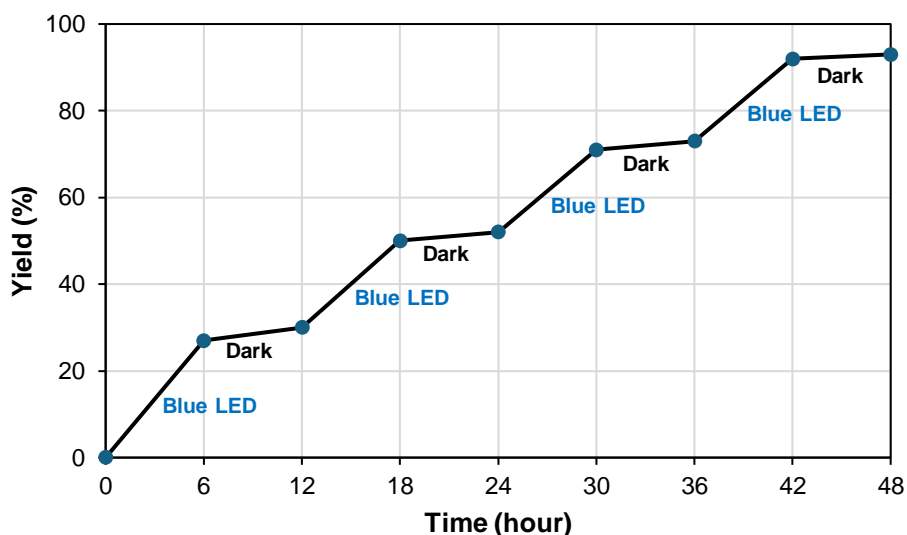


**Figure 2.7** Profile of reactions with light on/off over time.

#### 2.4.6 The reaction with radical scavenger

The mixture of indoline **1a** (24 mg, 0.2 mmol), GO (12 mg), 2,2,6,6-tetramethylpiperidine 1-oxyl (31 mg, 0.2 mmol) and CH<sub>3</sub>CN (1.0 mL) was stirred with irradiating Blue LED light under air atmosphere at room temperature for 24 h. After the reaction, the reaction mixture was analyzed by GC using n-dodecane as an internal standard.



#### 2.4.7 GC analysis of air and H<sub>2</sub>

---

The Air gave only one peak of O<sub>2</sub> and H<sub>2</sub> also gave one peak (**Figure 2.8**). Both Air (O<sub>2</sub>) and H<sub>2</sub> peaks were matched with standard O<sub>2</sub> and H<sub>2</sub> peaks. GC spectrum of Air and H<sub>2</sub> were compared with reaction mixture spectrum for identification of O<sub>2</sub> and H<sub>2</sub>.

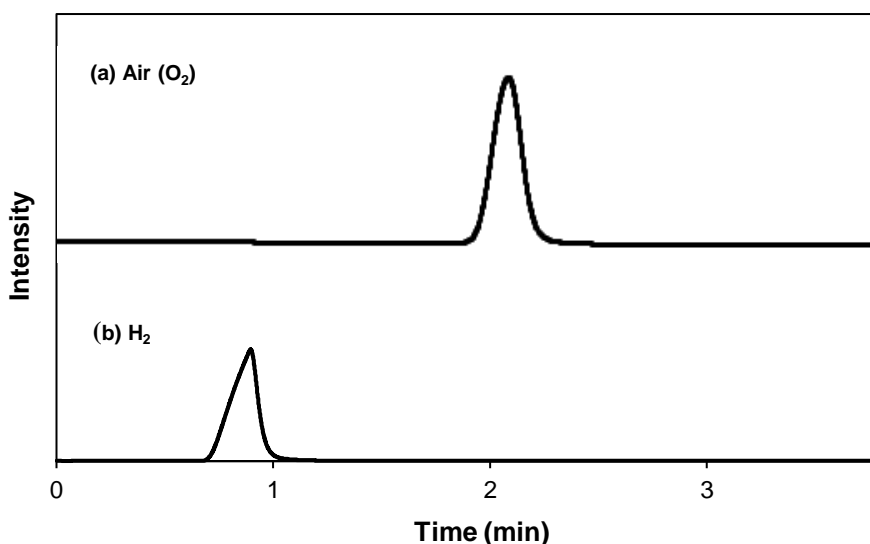


**Figure 2.8** GC spectrum of (a) Air (O<sub>2</sub>) and (b) H<sub>2</sub>.

## 2.5 References

1. Y. Chen, D. M. Ho, C. Lee, *J. Am. Chem. Soc.*, **2005**, *127*, 12184–12185.
2. L. Ackermann, L. T. Kaspar, *Journal of Organic Chemistry*, **2007**, *72*, 6149–6153.
3. D. S. Su, J. Zhang, B. Frank, A. Thomas, X. Wang, J. Paraknowitsch, R. Schlögl, *ChemSusChem*, **2010**, *3*, 169–180.
4. P. I. Dalko, L. Moisan, *Angewandte Chemie - International Edition*, **2004**, *43*, 5138–5175.
5. D. W. C. MacMillan, *Nature*, **2008**, *455*, 304–308.
6. D. S. Su, G. Wen, S. Wu, F. Peng, R. Schlögl, *Angewandte Chemie - International Edition*, **2017**, *129*, 956–985.
7. J. L. Figueiredo, M. F. R. Pereira, *Catal. Today*, **2010**, *150*, 2–7.
8. C. Su, K. P. Loh, *Acc. Chem. Res.*, **2013**, *46*, 2275–2285.

- 
9. F. Gao, S. Zhang, Q. Lv, B. Yu, *Chinese Chemical Letters*, **2022**, *33*, 2354–2362.
  10. D. R. Dreyer, H. P. Jia, C. W. Bielawski, *Angewandte Chemie - International Edition*, **2010**, *122*, 6965–6968.
  11. H. Huang, J. Huang, Y. M. Liu, H. Y. He, Y. Cao, K. N. Fan, *Green Chemistry*, **2012**, *14*, 930–934.
  12. Y. Gao, P. Tang, H. Zhou, W. Zhang, H. Yang, N. Yan, G. Hu, D. Mei, J. Wang, D. Ma, *Angewandte Chemie - International Edition*, **2016**, *128*, 3176–3180.
  13. M. Chen, Y. Luo, C. Zhang, L. Guo, Q. Wang, Y. Wu, *Organic Chemistry Frontiers*, **2019**, *6*, 116–120.
  14. X. Peng, Y. Zen, Q. Liu, L. Liu, H. Wang, *Organic Chemistry Frontiers*, **2019**, *6*, 3615–3619.
  15. N. Saravana Ganesan, P. Suresh, *Research on Chemical Intermediates*, **2021**, *47*, 1197–1210.
  16. Y. Pan, S. Wang, C. W. Kee, E. Dubuisson, Y. Yang, K. P. Loh, C. H. Tan, *Green Chemistry*, **2011**, *13*, 3341–3344.
  17. C. Liu, X. Peng, D. Hu, F. Shi, P. Huang, J. Luo, Q. Liu, L. Liu, *New Journal of Chemistry*, **2020**, *44*, 17245–17251.
  18. H. C. Hsu, I. Shown, H. Y. Wei, Y. C. Chang, H. Y. Du, Y. G. Lin, C. A. Tseng, C. H. Wang, L. C. Chen, Y. C. Lin, K. H. Chen, *Nanoscale*, **2013**, *5*, 262–268.
  19. I. Echevarría, M. Vaquero, B. R. Manzano, F. A. Jalón, R. Quesada, G. Espino, *Inorg. Chem.*, **2022**, *61*, 6193–6208.
  20. N. Morimoto, Y. Takeuchi, Y. Nishina, *Chem. Lett.*, **2016**, *45*, 21–23.
  21. M. M. Sajid, N. A. Shad, Y. Javed, S. B. Khan, Z. Zhang, N. Amin, *Research on Chemical Intermediates*, **2020**, *46*, 1201–1215.
  22. M. Hada, K. Miyata, S. Ohmura, Y. Arashida, K. Ichianagi, I. Katayama, T. Suzuki, W. Chen, S. Mizote, T. Sawa, T. Yokoya, T. Seki, J. Matsuo, T. Tokunaga, C. Itoh, K. Tsuruta, R. Fukaya, S. Nozawa, S. Adachi, J. Takeda, K.

- 
- Onda, S. Koshihara, Y. Hayashi, Y. Nishina, *ACS Nano*, **2019**, *13*, 10103–10112.
23. X. Niu, L. Yang, *Adv. Synth. Catal.*, **2021**, *363*, 4209–4215.
24. M. Cuni, D. Ventura-Espinosa, S. Martín, H. García, J. A. Mata, *ACS Catal.*, **2021**, *11*, 14688–14693.

---

## Chapter III

# **Investigating the Radical Properties of Oxidized Carbon Materials Under Photo-Irradiation: Behavior of Carbon Radicals and Their Application in Catalytic Reactions**

Oxidized carbon materials have abundant surface functional groups and customizable properties, making them an excellent platform for generating radicals. Unlike reactive oxygen species such as hydroxide or superoxide radicals that have been reported previously, oxidized carbon also produces stable carbon radicals under photo-irradiation. This has been confirmed through electron spin resonance. Among the various oxidized carbon materials synthesized, graphene oxide shows the largest number of carbon radicals when exposed to blue LED light. The light absorption capacity, high surface area, and unique structural characteristics of oxidized carbon materials offer a unique function for radical-mediated oxidative reactions.

---

### 3.1 Introduction

Free radicals play a crucial role in many fields such as catalysis, chemical synthesis, biomedicine, and antioxidants in personal care products.<sup>1-3</sup> Various free radicals used in many industries are toxic and explosive, and due to the coupling of individual radicals, they lack sufficient stability for long-term storage.<sup>4,5</sup> Developing stable, low-cost, and environmentally friendly radicals remains challenging. Carbon-based materials have received growing interest due to their unique properties, such as high surface area, electron conductivity, biocompatibility, environmental sustainability, and versatility.<sup>6,7</sup> Carbon materials can generate free radicals under thermal treatment<sup>8-10</sup> and photo-irradiation.<sup>11,12</sup> However, in the thermal process, carbon materials are concurrently decomposed, and radicals rapidly disappear.<sup>13,14</sup> Conversely, in the photo-irradiation process, carbon materials are mildly activated to produce free radicals.<sup>15-18</sup> Electrons tend to localize at the edge or defect sites of the carbon plane, which enhances their reactivity and stability as free radicals.<sup>19-22</sup> In this study, various oxidized carbon materials were produced, and investigated their properties for generating carbon radicals under visible light irradiation. The resulting radical species are utilized for catalysis in the oxidative dehydrogenation of indoline and the oxidative coupling of benzylamine.

### 3.2 Result and discussion

Various carbon materials such as graphite, activated carbon (AC), carbon black (CB), carbon nanotube (CNT), and nanodiamond (ND) were oxidized. After oxidation, oxidized carbon materials were described as follows: graphene oxide (GO) from graphite, oxidized activated carbon (O-AC) from AC, oxidized carbon black (O-CB) from CB, oxidized carbon nanotube (O-CNT) from CNT, oxidized nanodiamond (O-ND) from ND.

### 3.2.1 Characterization

Oxidized carbon materials were characterized by Fourier transform infrared (FTIR) and X-ray photoelectron spectroscopy (XPS). A broad peak of FTIR spectra ranging from  $3600\text{ cm}^{-1}$  to  $2600\text{ cm}^{-1}$  indicates the presence of hydroxyl groups (**Figure 3.1**). Characteristic peaks centered at  $1735\text{ cm}^{-1}$  and  $1030\text{ cm}^{-1}$  are carbonyl and epoxide groups, respectively. FTIR spectra showed that GO, O-AC, O-CB, and O-CNT have hydroxyl, carbonyl, and epoxide functional groups, but O-ND contains only carbonyl and epoxide groups (**Figure 3.1e**). In all oxidized carbon materials, the intensity of carbonyl group peaks was significant. In the case of GO (**Figure 3.1a**) and O-CNT (**Figure 3.1d**), the intensity of the epoxide peaks is higher than other oxidized carbon materials, probably because graphite and CNT have large  $\text{sp}^2$  domains.

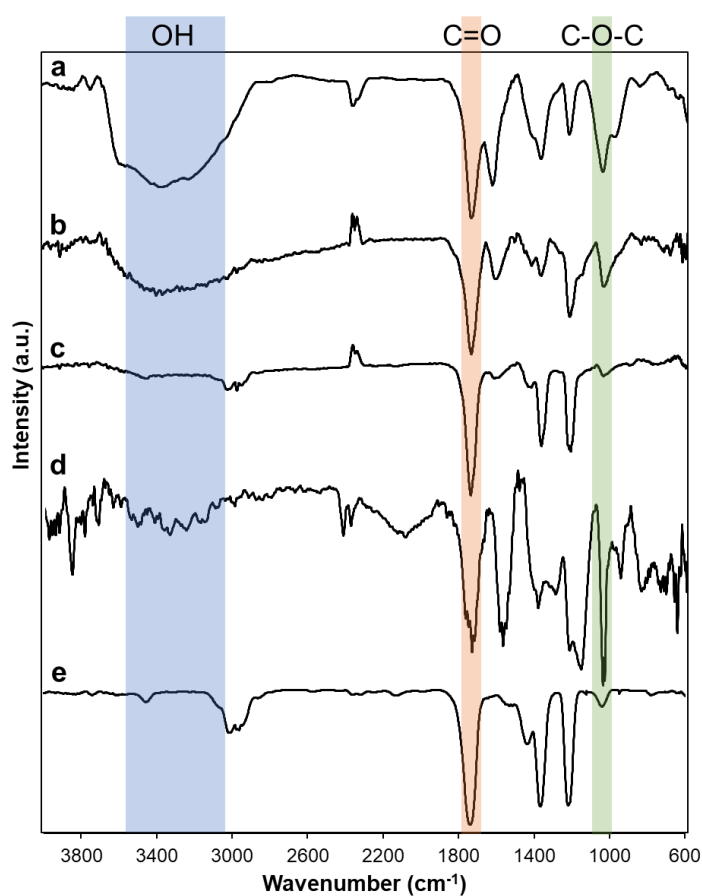


**Figure 3.1** FTIR spectra of (a) GO, (b) O-AC, (c) O-CB, (d) O-CNT, and (e) O-ND.

All XPS survey spectra showed a similar pattern; a typical example of GO is shown in **Figure 3.2a**, and others are listed in **Figures 3.3a-d**. XPS survey spectra indicate that GO has more oxygen-containing groups than other oxidized carbons (**Figure 3.2a**). High-resolution XPS represents the C=C/C-C bonds at 284.2 eV, C-O bonds at 286.2 eV, and C=O bonds at 287.8 eV. XPS spectra at the C 1s region of GO show a larger number of C-O bonds than C=C bonds and C=O bonds (**Figure 3.2b**). O-AC has a lower quantity of C-O bonds than GO (**Figure 3.2c**) but higher than that of O-CB (**Figure 3.2d**). Moreover, O-CNT (**Figure 3.2e**) contains a greater number of C-O bonds than C=C bonds like GO. O-ND (**Figure 3.2f**) has a lower number of C-O and C=O bonds than all other oxidized carbon materials.

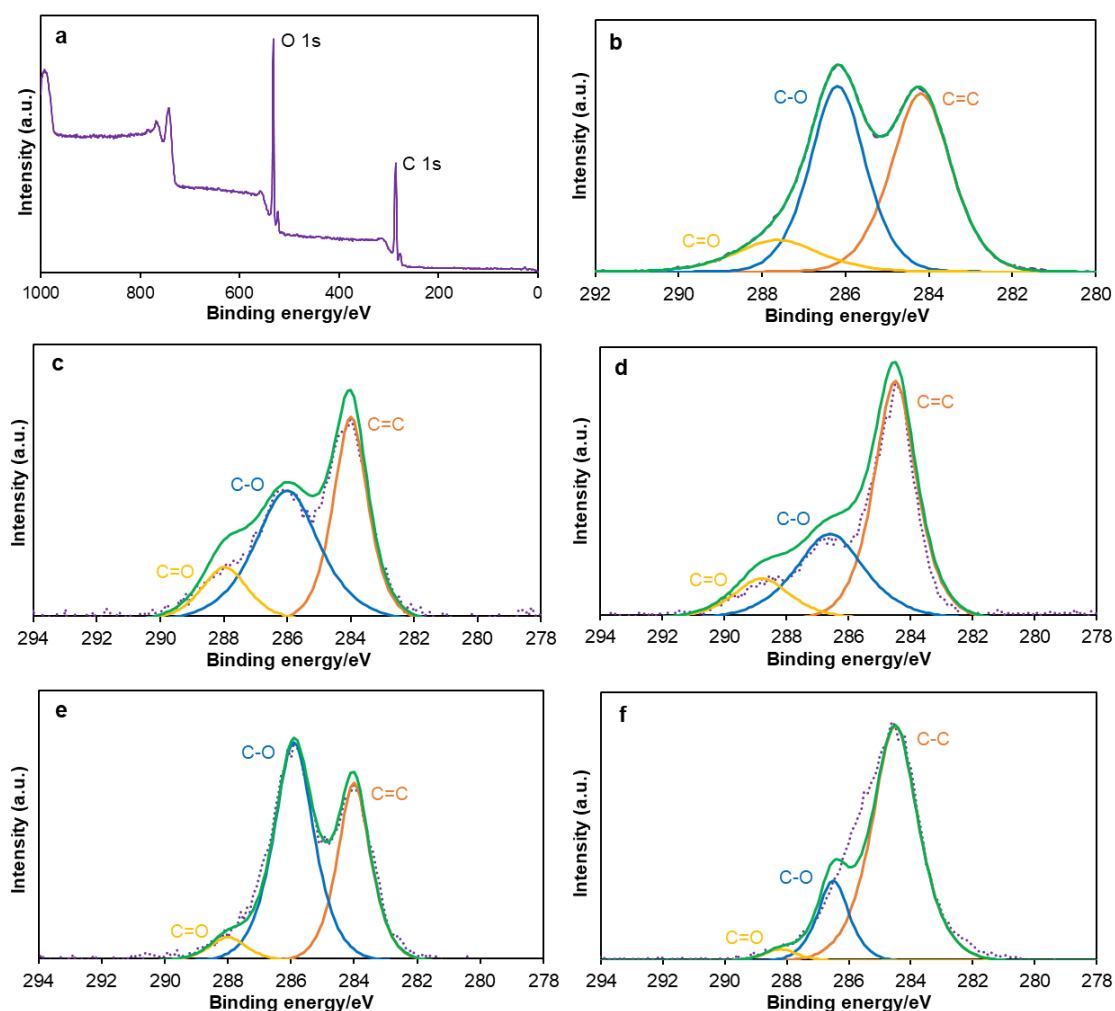


**Figure 3.2** XPS (a) survey spectra of GO, (b) C 1s region of GO, (c) C 1s region of O-AC, (d) C 1s region of O-CB, (e) C 1s region of O-CNT, and (f) C 1s region of O-ND.

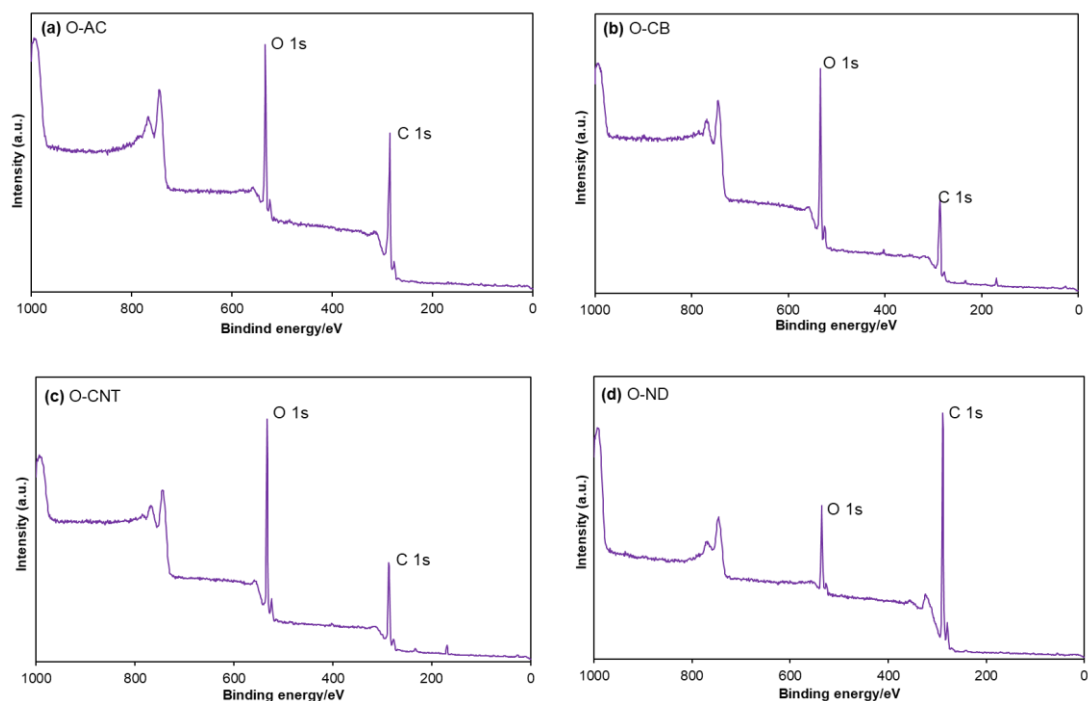


**Figure 3.3** XPS survey spectra of (a) O-AC, (b) O-CB, (c) O-CNT, (e) O-ND.

### 3.2.2 Photo-radical properties

To elucidate the photo-radical properties, in-situ electron spin resonance (ESR) experiments were designed in the absence and presence of blue LED light irradiation (**Figures 3.4a** and **3.4b**). A mixture of oxidized carbon materials in acetonitrile was irradiated and subjected to ESR analysis. For all oxidized carbon materials, a negligible ESR signal appeared in the absence of light (**Figure 3.4a**), in contrast, a strong ESR signal was observed by the irradiation of blue LED light (**Figure 3.4b**). Among oxidized carbons, GO showed the highest ESR peak intensity, suggesting that more carbon radicals are generated from GO than other oxidized carbon materials under the irradiation of blue LED light. It has been reported that epoxide can be selectively photoexcited under light irradiation, resulting in the reversible generation of carbon radicals.<sup>23,24</sup> GO contains a greater number of epoxides, as evidenced by FTIR and XPS analysis, which explains why GO generates more carbon radicals under the irradiation of blue LED light. For the

consideration of the stability of GO radicals, it is more interesting that GO radicals are stable over 6 months (**Figure 3.5**).

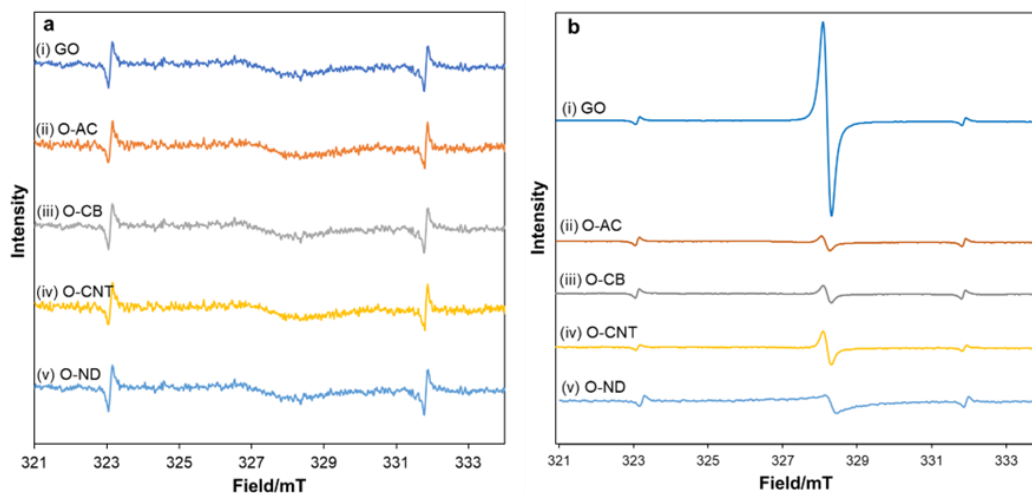


**Figure 3.4** ESR spectra of (i) GO, (ii) O-AC, (iii) O-CB, (iv) O-CNT, and (v) O-ND. (a) in the absence of light, and (b) under irradiation of blue LED light. The standard  $\text{Mn}^{2+}$  peaks are observed at 323 and 332 mT.

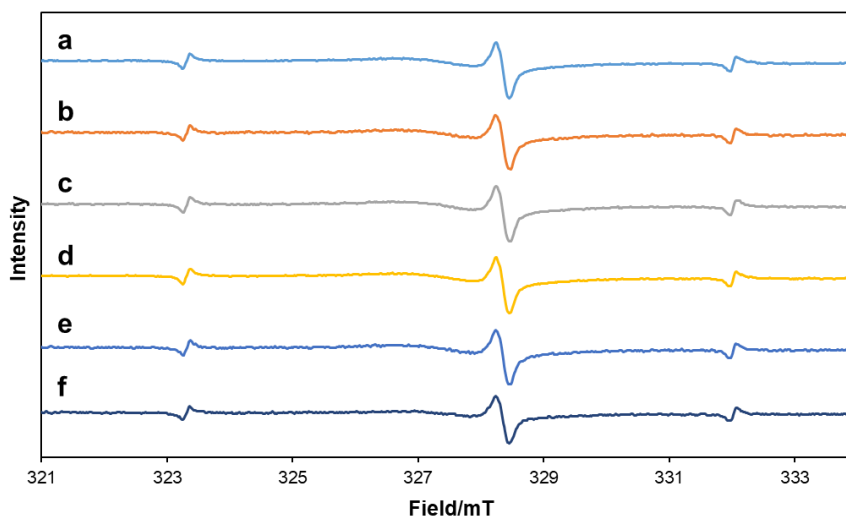


**Figure 3.5** ESR spectra of GO after (a) 1<sup>st</sup> month, (b) 2<sup>nd</sup> month, (c) 3<sup>rd</sup> month, (d) 4<sup>th</sup> month, (e) 5<sup>th</sup> month, and (f) 6<sup>th</sup> month.

### 3.2.3 Mechanistic investigation

To confirm that the carbon radicals are derived from epoxide, epoxide on GO was reacted with amine. The amine-functionalized GO (Am-GO) was synthesized by following the reported literature.<sup>25,26</sup> GO (300 mg) was dispersed in distilled water (150 mL) in a glass beaker using an ultrasonic probe sonicator. In a separate beaker, n-butylamine (450 mg) was dispersed in 45 mL water via bath sonication for 10 min. The GO suspension was then transferred to a 500 mL round bottom flask in which the n-butylamine suspension was also moved and the mixture was stirred in an oil bath at 80 °C for 20 h. The black solution eventually obtained was left to stand undisturbed for 24 h after which it showed a separation of the functionalized GO from the solvent suggesting its hydrophobic nature. The functionalized GO was then extracted via centrifugation. The obtained solid product was purified by centrifugation with water five times and freeze-dried to afford the pure amine functionalized GO. GO and Am-GO were irradiated under blue LED light and measured ESR. As a result, GO gave a significant ESR signal (**Figure 3.6a**), however, an insignificant ESR signal appeared for Am-GO (**Figure 3.6b**). This evidence proved that the epoxide bond opens under irradiation of light and gives radical species (**Scheme 3.1**).

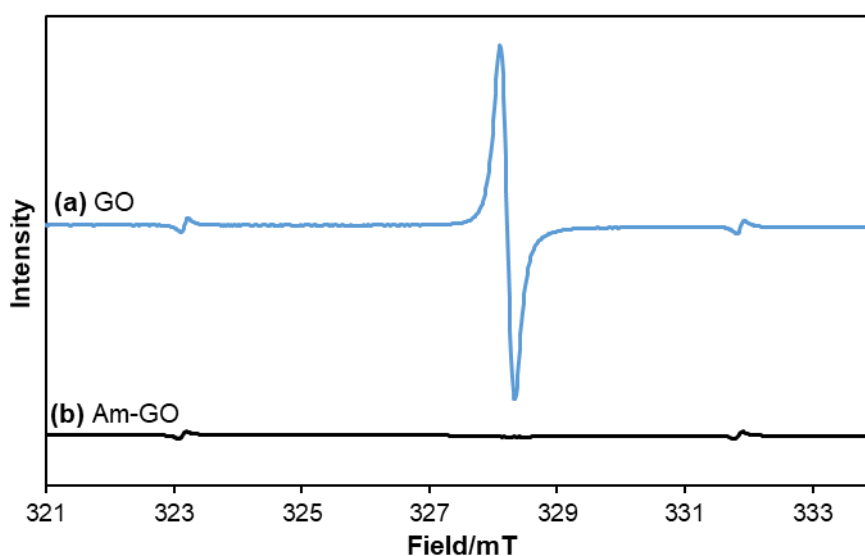
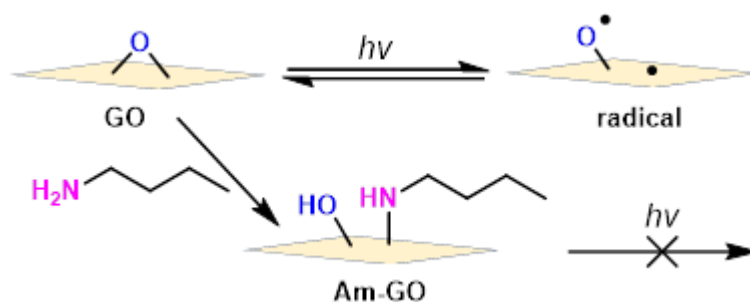


**Figure 3.6** ESR spectra of (a) GO and (b) Am-GO under irradiation of blue LED. The standard Mn<sup>2+</sup> peaks are observed at 323 and 332 mT.

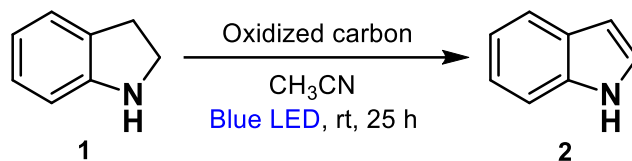


**Scheme 3.1** Mechanistic route of generation of radicals from GO and Am-GO under light irradiation (for simplicity, only the epoxide functional group is shown).

### 3.2.4 Evaluation of catalytic performance

It has been reported that carbon radicals function as catalysts; activation of  $O_2$  to generate reactive oxygen species for oxidation of various substrates has been well studied.<sup>27-29</sup> Also reported was the oxidation of indoline by photo-irradiation of GO.<sup>24</sup> In this research, the catalytic activity of oxidized carbon materials was evaluated by oxidation of indoline and oxidative coupling of benzylamine under irradiation of blue LED light. Using these reactions as models, the photocatalytic oxidation reactions of each oxidized carbon material were investigated. **Table 3.1** shows the results of the oxidation reaction of indoline (**1**) to indole (**2**). From all oxidized carbon materials, GO showed a highest yield of 85% (**Table 3.1**, Entry 1); however, other oxidized carbon materials such as O-AC, O-CB, O-CNT, and O-ND gave lower yields of 12%, 10%, 7%, and 5%, respectively (**Table 3.1**, Entries 2-5). No desired product was observed when the reaction was conducted in the darkness and in the absence of oxidized carbon (**Table 3.1**, Entries 6-7). The reaction also proceeded under Ar atmosphere (**Table 3.1**, Entry 8), suggesting the dehydrogenative oxidation as reported previously.<sup>24</sup>

**Table 3.1** Evaluation of the catalytic activity of oxidized carbon materials by oxidation of indoline<sup>a</sup>

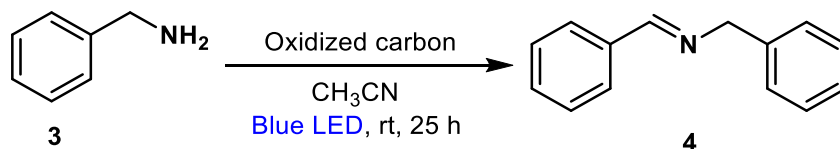


Entry	Oxidized carbon	Yield (%) <sup>b</sup>
1	GO	85
2	O-AC	12
3	O-CB	10
4	O-CNT	7
5	O-ND	5
6 <sup>c</sup>	GO	0
7	-	0
8 <sup>d</sup>	GO	85

<sup>a</sup>Reaction conditions: Indoline **1** (0.2 mmol), GO (5 mg), CH<sub>3</sub>CN (1.0 mL) under air atmosphere at room temperature, irradiation of blue LED for 25 h. <sup>b</sup>GC yield. <sup>c</sup>Under dark. <sup>d</sup>Under Ar.

**Table 3.2** shows the results of the oxidative coupling reaction of benzylamine (**3**) to imine (**4**). Of all oxidized carbon materials, GO showed a highest yield of 90% (**Table 3.2**, Entry 1); however, other oxidized carbon materials gave lower yields (**Table 3.2**, Entries 2-5). Both light and oxidized carbon were proved to be essential for this reaction; no desired product was observed when the reaction was conducted in the darkness and the absence of oxidized carbon (**Table 3.2**, Entries 6-7). The reaction also proceeded under Ar atmosphere (**Table 3.2**, Entry 8).

**Table 3.2** Evaluation of the catalytic activity of oxidized carbon materials by oxidative coupling of benzylamine<sup>a</sup>



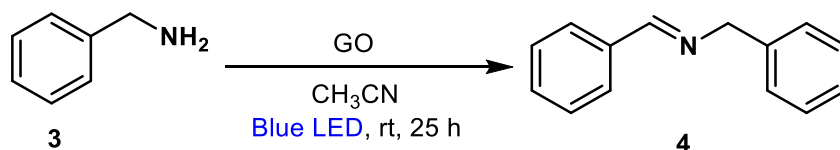
Entry	Oxidized carbon	Yield (%) <sup>b</sup>
1	GO	90
2	O-AC	10
3	O-CB	5
4	O-CNT	7

5	O-ND	3
6 <sup>c</sup>	GO	0
7	-	0
8 <sup>d</sup>	GO	90

<sup>a</sup>Reaction conditions: benzylamine **3** (0.2 mmol), GO (5 mg), CH<sub>3</sub>CN (1.0 mL) under air atmosphere at room temperature, irradiation of blue LED for 25 h. <sup>b</sup>GC yield. <sup>c</sup>Under dark. <sup>d</sup>Under Ar.

**Table 3.3** shows the screening results of the oxidative coupling reaction of benzylamine (**3**) to imine (**4**). Gave the highest yield of 90% in 25 hours when 5 mg of GO was used. In solvent screening, acetonitrile gave the best performance than tetrahydrofuran and dimethyl formamide.

**Table 3.3** Screening Reaction Conditions of Oxidative Coupling of Benzylamine<sup>a</sup>



Entry	GO (mg)	Time (hour)	Solvent	Yield (%) <sup>b</sup>
1	5	5	CH <sub>3</sub> CN	30
2	5	10	CH <sub>3</sub> CN	51
3	5	15	CH <sub>3</sub> CN	70
4	5	20	CH <sub>3</sub> CN	80
<b>5</b>	<b>5</b>	<b>25</b>	<b>CH<sub>3</sub>CN</b>	<b>88±2<sup>c</sup></b>
6	5	30	CH <sub>3</sub> CN	90
7	3	25	CH <sub>3</sub> CN	72
8	6	25	CH <sub>3</sub> CN	90
9	10	25	CH <sub>3</sub> CN	88
10	5	25	DMF	61
11	5	25	THF	55

<sup>a</sup>Reaction conditions: benzylamine **3** (0.2 mmol), GO (5 mg), CH<sub>3</sub>CN (1.0 mL) under air atmosphere at room temperature, irradiation of blue LED for 25 h. <sup>b</sup>GC yield. <sup>c</sup>n=3.

All oxidized carbon materials showed the presence of carbon radicals under irradiation

---

of blue LED light as shown in **Figure 3.4b**. Among them, GO radical peak intensity was the highest and gave the highest yield for oxidation of indoline and oxidative coupling of benzylamine. The radical peak intensity of O-AC, O-CB, O-CNT, and O-ND were lower and yielded lower for the oxidation product. Moreover, both of the reactions also proceeded under Ar atmosphere, suggesting dehydrogenative reactions and carbon radicals were responsible for the proceeding of these reactions.

### 3.3 Conclusion

In conclusion, the radical properties of oxidized carbon materials are a consequence of their unique structure, functional groups, and chemical reactivity, allowing them to generate radicals. The amount of radicals differs in the types of oxidized carbons; GO showed a higher number of radicals under blue LED irradiation. The photoexcitation of GO under blue LED light irradiation offers a progression of various chemical transformations by radical pathways such as the oxidation of indoline and benzylamine. These properties will make them versatile materials for future applications in areas such as catalysis, environmental remediation, energy storage, and biomedical engineering.

### 3.4 Experimental

#### 3.4.1 General information

All the chemicals used in this study were purchased from commercial sources and used as received unless otherwise mentioned. Kessil A360X tuna blue LED light with a wavelength centered at 470 nm was used. The products were quantified by gas chromatography-mass spectrometry (GCMS-QP2010 *Plus*, Shimadzu), equipped with a flame ionization detector (FID). ESR analysis was performed using an electron spin resonance spectrometer (JES-X310) with microwave frequency 9.542 GHz, modulation frequency 100 kHz, power 1 mW, and sweep time 1 min. The functional groups on the surface of the oxidized carbon materials were recorded by Fourier transform infrared spectrophotometer (FTIR; Shimadzu IRTracer-100). The samples for the FTIR were

---

dried and mixed with KBr and then pressed into 1.3 cm-diameter pellets. Freeze-drying of the oxidized carbon materials was performed using ADVANTEC DRZ350WC. The surface chemistry was performed using an X-ray photoelectron spectroscopy (XPS; JPS-9030) with a pass energy of 20 eV.

### 3.4.2 General procedure for synthesis of oxidized carbon materials

Various carbon materials such as graphite, AC, CB, CNT, and ND were oxidized using the following procedure. Carbon material (1.0 g) was dispersed in 95% H<sub>2</sub>SO<sub>4</sub> (30 mL). After cooling the mixture in an ice bath, KMnO<sub>4</sub> (3.0 g) was gradually added to the solution, keeping the temperature below 55 °C. The mixture was stirred at 35 °C for 2 h. The generated suspension was again cooled down, after which 60 mL of deionized water was added slowly to keep the temperature below 50 °C. The suspension was further treated by 30% aq. H<sub>2</sub>O<sub>2</sub>. The resulting suspension was purified by centrifugation with water five times and freeze-dried to afford oxidized carbon materials.

### 3.4.3 FTIR spectra of Am-GO

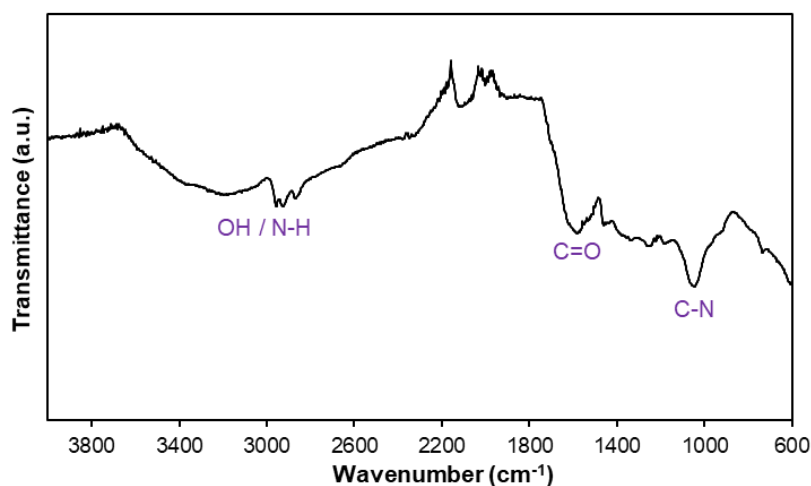


**Figure 4.7** FTIR spectra of Am-GO.

### 3.4.4 XPS Spectra of GO and Am-GO

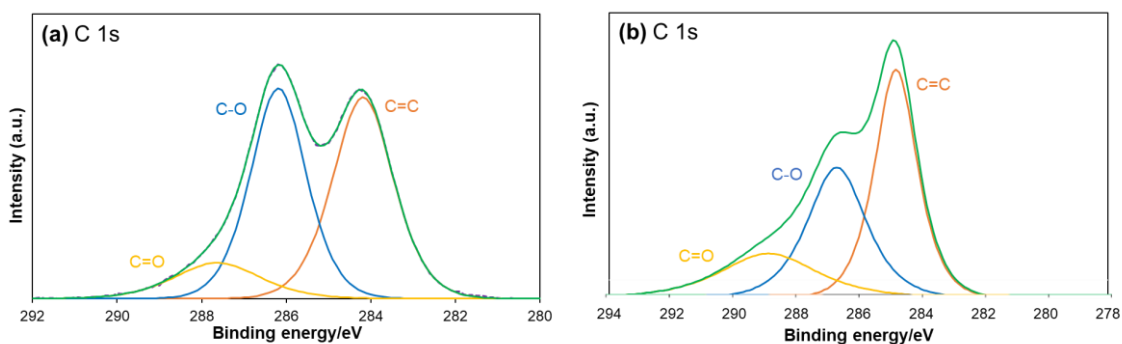


**Figure 3.8** XPS spectra at C 1s region of (a) GO and (b) Am-GO.

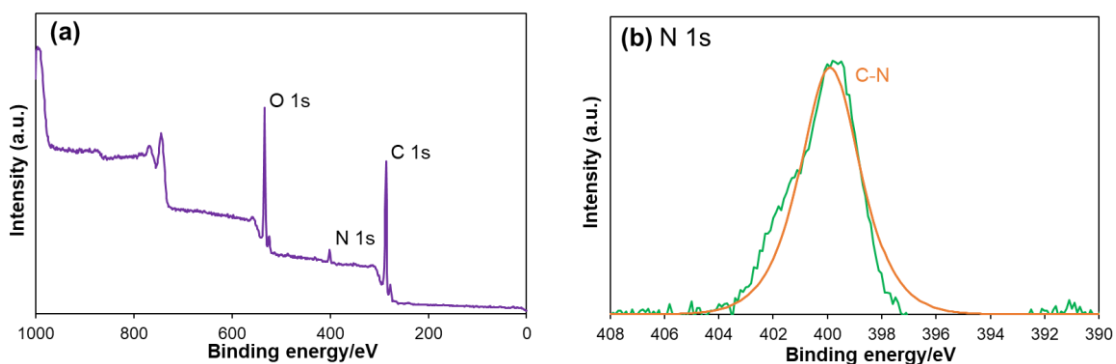


**Figure 3.9** XPS spectra (a) survey and (b) N 1s region of Am-GO.

### 3.4.5 EI-Mass spectra of product 4

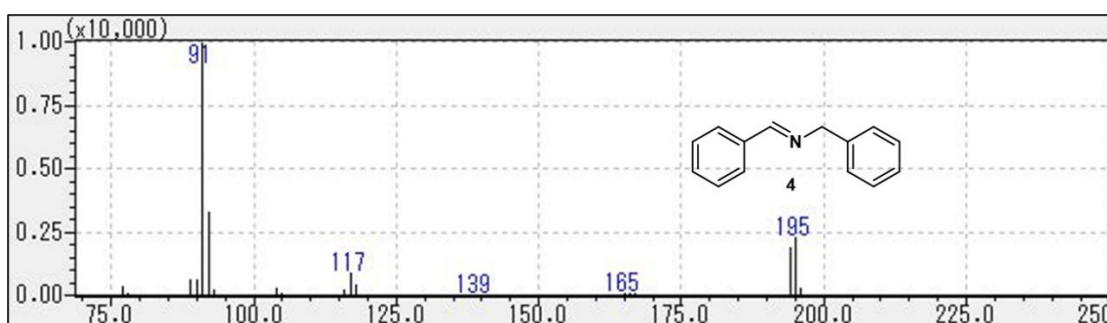


**Figure 3.10** EI-Mass spectra of Product 4.

---

### 3.5 References

1. P. Eskandari, Z. A. Rezvani, H. R. Mamaqani and M. S. Kalajahi, *Adv. Coll. and Interf. Sci.*, **2021**, *294*, 102471.
2. A. Phaniendra, D. B. Jestadi and L. Periyasamy, *Ind. J. Clin. Biochem.*, **2015**, *30*, 11.
3. C. Kingston, R. Zepp, A. Andrady, D. Boverhof, R. Fehir, D. Hawkins, J. Roberts, P. Sayre, B. Shelton, Y. Sultan, V. Vejins and W. Wohlleben, *Carbon*, **2014**, *68*, 33.
4. M. Chen, M. Zhong and J. A. Johnson, *Chem. Rev.*, **2016**, *116*, 10167.
5. T. Yoshikawa, and F. You, *Int. J. Mol. Sci.*, **2024**, *25*, 3360.
6. S. Pandey, M. Karakoti, D. Bhardwaj, G. Tatrari, R. Sharma, L. Pandey, M. J. Lee and N. G. Sahoo, *Nanoscale Adv.*, **2023**, *5*, 1492.
7. C. Cha, S. R. Shin, N. Annabi, M. R. Dokmeci and A. Khademhosseini, *ACS Nano*, **2013**, *7*, 2891.
8. M. S. Ahmad, H. He and Y. Nishina, *Org. Lett.*, **2019**, *21*, 8164.
9. N. Morimoto, K. Morioku, H. Suzuki, Y. Nakai and Y. Nishina, *Chem. Commun.*, **2017**, *53*, 7226.
10. Y. Matsuki, N. Ohnishi, Y. Kakeno, S. Takemoto, T. Ishii, K. Nagao and H. Ohmiya, *Nat. Commun.*, **2021**, *12*, 3848.
11. W. Shi, S. Yang, H. Sun, J. Wang, X. Lin, F. Guo and J. Shi, *J. Mat. Sci.*, **2021**, *56*, 2226.
12. R. X. Seng, L. L. Tan, W. P. C. Lee, W. J. Ong and S. P. Chai, *J. Environ. Manage.*, **2020**, *255*, 109936.
13. L. J. Konwar, P. M. Arvela and J. P. Mikkola, *Chem. Rev.*, **2019**, *119*, 11576.
14. Z. Li, L. Jin and C. Cai, *Org. Chem. Front.*, **2017**, *4*, 2039.
15. Y. Zhang, W. Schilling, D. Riemer and S. Das, *Nat. Prot.*, **2020**, *15*, 822.
16. J. Bai, S. Yan, Z. Zhang, Z. Guo and C. Y. Zhou, *Org. Lett.*, **2021**, *23*, 4843.
17. M. R. Ahmed, Y. K. Cheng and Y. Nishina, *Ind. Eng. Chem. Res.*, **2024**, *63*, 7475.
18. S. Cailotto, M. Negrato, S. Daniele, R. Luque, M. Selva, E. Amadio and A. Perosa, *Green Chem.*, **2020**, *22*, 1145.
19. F. Meng, T. Hao, W. Tian, J. Zhao, S. Wang and H. Zhang, *Surf. Interf.*, **2024**, *44*, 103717.
20. H. He, S. Liu, Y. Liu, L. Zhou, H. Wen, R. Shen, H. Zhang, X. Guo, J. Jiang and B. Li, *Green Chem.*, **2023**, *25*, 9501.

- 
21. P. Chettri, A. Tripathi and A. Tiwari, *Mat. Res. Bull.*, **2022**, *150*, 111752.
  22. M. Alimohammadian and B. Sohrabi, *Nat. Res.*, **2020**, *10*, 21325.
  23. M. Hada, K. Miyata, S. Ohmura, Y. Arashida, K. Ichiyanagi, I. Katayama, T. Suzuki, W. Chen, S. Mizote, T. Sawa, T. Yokoya, T. Seki, J. Matsuo, T. Tokunaga, C. Itoh, K. Tsuruta, R. Fukaya, S. Nozawa, S. Adachi, J. Takeda, K. Onda, S. Koshihara, Y. Hayashi and Y. Nishina, *ACS Nano*, **2019**, *13*, 10103.
  24. M. R. Ahmed and Y. Nishina, *Bull. Chem. Soc. Jpn.*, **2023**, *96*, 568.
  25. S. Chakraborty, S. Saha, V. R. Dhanak, K. Biswas, M. Barbezat, G. P. Terrasi and A. K. Chakraborty, *RSC Adv.*, **2016**, *6*, 67916.
  26. N. A. Carvajal, D. A. A. Guzman, V. M. Laguna, M. H. Farias, L. A. P. Rey, E. A. Morales, V. A. G. Ramirez, V. A. Basiuk and E. V. Basiuk, *RSC Adv.*, **2018**, *8*, 15253.
  27. C. Su, M. Acik, K. Takai, J. Lu, S. J. Hao, Y. Zheng, P. Wu, Q. Bao, T. Enoki, Y. J. Chabal and K. P. Loh, *Nat. Commun.*, **2012**, *3*, 1298.
  28. J. Zhang, Y. Yang, J. Fang, G. J. Deng and H. Gong, *Chem. Asian J.*, **2017**, *12*, 2524.
  29. N. Morimoto, Y. Takeuchi and Y. Nishina, *Chem. Lett.*, **2016**, *45*, 21.

---

## Chapter IV

# Synthesis of Visible-Light-Responsive Nanocarbon and Application for Photocatalytic Carbon-Carbon Bond Formation

Visible-light-responsive nanocarbon was systematically synthesized via a one-step hydrothermal method, using citric acid and Congo Red; this nanocarbon exhibited visible-light absorption at 516 nm and photocatalytic activity for the carbon-carbon bond-forming reaction between benzylamine and ethyl cyanoacetate. Mechanistic investigations proved that this system generates radicals, and the reactions proceed via radical pathways, which are confirmed by electron spin resonance. A metal-free, mildly conditioned, and recyclable photocatalytic reaction was achieved by the visible-light-responsive nanocarbon system.

---

## 4.1 Introduction

Visible-light-responsive photocatalysis presents an environmentally sustainable approach to synthesis, offering substantial avenues for developing synthetic methodologies for fine chemicals.<sup>1,2</sup> The past decade has witnessed the rapid development of photo-redox systems in homogeneous catalysis using transition metal complexes, enabling C-H arylation,<sup>3</sup> enone cycloaddition,<sup>4</sup> reductive dehalogenations,<sup>5</sup> C-C bond formation,<sup>6</sup> acylations of C(sp<sup>3</sup>)-H bond,<sup>7</sup> thioetherification,<sup>8</sup> C-N bond formation,<sup>9</sup> C-H hydroxyalkylation.<sup>10</sup> In addition, metal catalyst light absorption capability directly impacts the catalytic performance in the C-C bond formation.<sup>11-13</sup> However, metal-based catalysts have some drawbacks; they are often expensive, toxic, difficult to remove, and limited natural resources.<sup>14,15</sup> Like as metal catalysts, organic dyes have been used as photocatalysts in several organic transformations, such as oxidative hydroxylation of arylboronic acid,<sup>16</sup> arylation of heteroarene with aryl diazonium salt,<sup>17</sup> functionalization of thiazole derivatives,<sup>18</sup> dehydrogenative coupling,<sup>19</sup> and C-C bond forming radical reaction.<sup>20</sup> Furthermore, using dyes as catalysts introduces disadvantages, necessitating additional additives for catalyst activation, complicating catalyst-product separation, and hindering catalyst recyclability.<sup>21,22</sup> To solve these problems, focus on carbon-based photocatalysts because of their high surface area, electron conductivity, easy separation, reusability, and environment friendliness.<sup>23-25</sup> There are reports on nanocarbon-based photocatalysis, including oxidation,<sup>26</sup> esterification,<sup>27</sup> transamidation,<sup>28</sup> and reductive photocleavage.<sup>29</sup> This indicates that only a few reaction systems have been developed by nanocarbon-based photocatalysis. Moreover, there is no report on the C-C bond formation reaction using nanocarbon photocatalyst. This is attributed to the predominant absorption of most nanocarbons in the ultra-violet region, while weakly absorbing the visible light.<sup>25,26</sup> Therefore, focused on the synthesis of visible-light-responsive nanocarbons from visible-light-responsive dye molecules and investigated their application for photocatalysts in the C-C bond-forming reactions.

---

## 4.2 Result and discussion

### 4.2.1 Optimization course

First, optimize the nanocarbon synthesis. Our strategy is to use citric acid as a main component of nanocarbon and add another component to express visible-light absorption properties. investigated various combinations, using citric acid as a carbon source with various chromophore molecules as a result, found the combination of citric acid and Congo Red with a 3:1 ratio showed visible-light absorption (516 nm) (**Table 4.1**, Entry 1). As controls, only citric acid or Congo Red was treated under the same condition, but the products adsorbed shorter wavelengths (**Table 4.1**, Entries 2 and 3). Other chromophore molecules such as methyl orange, methylene blue, rose bengal, and eosin Y gave absorption in lower wavelengths (**Table 4.1**, Entries 4-7). Previously reported functional nanocarbon using urea,<sup>30</sup> thiourea,<sup>30</sup> D-proline,<sup>31</sup> ammonia,<sup>32</sup> and ethylenediamine<sup>33</sup> were also investigated, but they did not show visible-light absorption (**Table 4.1**, Entries 8-12).

**Table 4.1** Synthesis of various carbon materials<sup>a</sup>

**Carbon source + Chromophore molecule**  $\xrightarrow[\text{Temperature, Time}]{\text{Hydrothermal treatment}}$  **Product**

Entry	Carbon source	Chromophore molecule	Product	Temperature (°C)	Time (hour)	λ-max (nm)
1	citric acid	Congo Red	<b>C1</b>	185	4	516
2	citric acid	none	<b>C2</b>	185	4	294, 370
3	none	Congo Red	<b>C3</b>	185	4	390
4	citric acid	methyl orange	<b>C4</b>	160	4	260
5	citric acid	methylene blue	<b>C5</b>	160	4	-
6	citric acid	rose bengal	<b>C6</b>	180	2	290
7	citric acid	Eosin Y	<b>C7</b>	200	3	295
8	citric acid	urea	<b>C8</b>	220	5	340

9	citric acid	thiourea	<b>C9</b>	185	4	314
10	citric acid	D-proline	<b>C10</b>	185	4	286
11	citric acid	ammonia	<b>C11</b>	185	4	265
12	citric acid	ethylenediamine	<b>C12</b>	185	4	354

<sup>a</sup>Carbon source (600 mg), chromophore molecule (200 mg), and water (5 mL) were mixed in an autoclave and heated in an oven.

#### 4.2.2 Characterization

Among the synthesized carbon material, **C1** composed of citric acid and Congo Red only showed visible-light absorption; therefore, this material was extensively characterized. An elemental analysis technique was used to understand the elemental composition of **C1**, presenting 66% carbon, 5% hydrogen, 6% nitrogen, 4% sulfur, and 19% oxygen. This result confirms the presence of carbon, hydrogen, nitrogen, sulfur, and oxygen, respectively.

The UV-visible spectra of **C1** showed a broad characteristic absorption peak at around 516 nm is attributed to the absorption of hydroxyl, amine, thiol, and carboxyl groups on the surface of **C1** (**Figure 4.1a**). Furthermore, as it is evident from the UV-vis spectrum, the presence of a tail ranging from about 450 nm to 650 nm (visible region) suggests that the **C1** possesses photocatalytic activity under visible light irradiation. Fourier transform infrared (FTIR) spectroscopy showed the presence of surface functional groups of **C1** (**Figure 4.1b**); a broad absorption peak ranging from 3600  $\text{cm}^{-1}$  to 2600  $\text{cm}^{-1}$  was detected, suggesting the presence of a plethora of hydroxyl and amine groups, and a shoulder peak at 2526  $\text{cm}^{-1}$  corresponds to the S-H stretch. Similarly, a characteristic peak centered at 1701  $\text{cm}^{-1}$  confirmed the presence of carbonyl groups. The peaks at 1385  $\text{cm}^{-1}$ , 1178  $\text{cm}^{-1}$ , and 1083  $\text{cm}^{-1}$  were assigned to the stretching vibration of C-OH, C-C, and C-N bonds, respectively.

The X-ray diffraction (XRD) patterns of **C1** exhibit two significant broad peaks at 9° and 20°, indicating that carbonization and surface modification have occurred (**Figure**

---

**4.2).** The characteristic diffraction peak of **C1** corresponding to the (001) plane was observed at  $2\theta = 9^\circ$ , which suggests the stacking of carbon frameworks containing functional groups on the surface.<sup>34</sup> The broad diffraction peak centered at  $2\theta = 20^\circ$  suggests the amorphous carbon of **C1**.<sup>35</sup> The chemical composition and surface modification structure of the **C1** was analyzed by X-ray photoelectron spectroscopy (XPS). High-resolution XPS at the C 1s region presents predominant C-C/C=C bonds at 284.5 eV and minor C-OH/C-N/C-S bonds at 286.4 eV, indicating the carbonization while maintaining functional groups of the starting materials. The other significant peaks at 288.5 eV and 290.7 eV are assigned to C=O and  $\pi$ - $\pi$  interaction, respectively (**Figure 4.1c**).<sup>36</sup> The S 2p region can be deconvoluted into two peaks at 163.5 eV and 165.1 eV, which could be ascribed to the S 2p<sub>3/2</sub> and S 2p<sub>1/2</sub> of the C-S-H bond, respectively (**Figure 4.1d**).<sup>37,38</sup>

Raman spectra of a general amorphous carbon material are composed of two peaks: D-band (1320-1360 cm<sup>-1</sup>) and G-band (1500-1600 cm<sup>-1</sup>).<sup>39</sup> Raman spectra of **C1** gave two peaks corresponding to the D-band at around 1315 cm<sup>-1</sup> and the G-band at 1588 cm<sup>-1</sup> (**Figure 4.1e**). This observation reveals the amorphous structure of **C1**. Scanning electron microscopy (SEM) image of **C1** showed spherical particles ranging from 35-45 nm in size (**Figure 4.1f**). The average diameter of **C1** is  $40 \pm 5$  nm, suggesting the narrow particle size distribution.

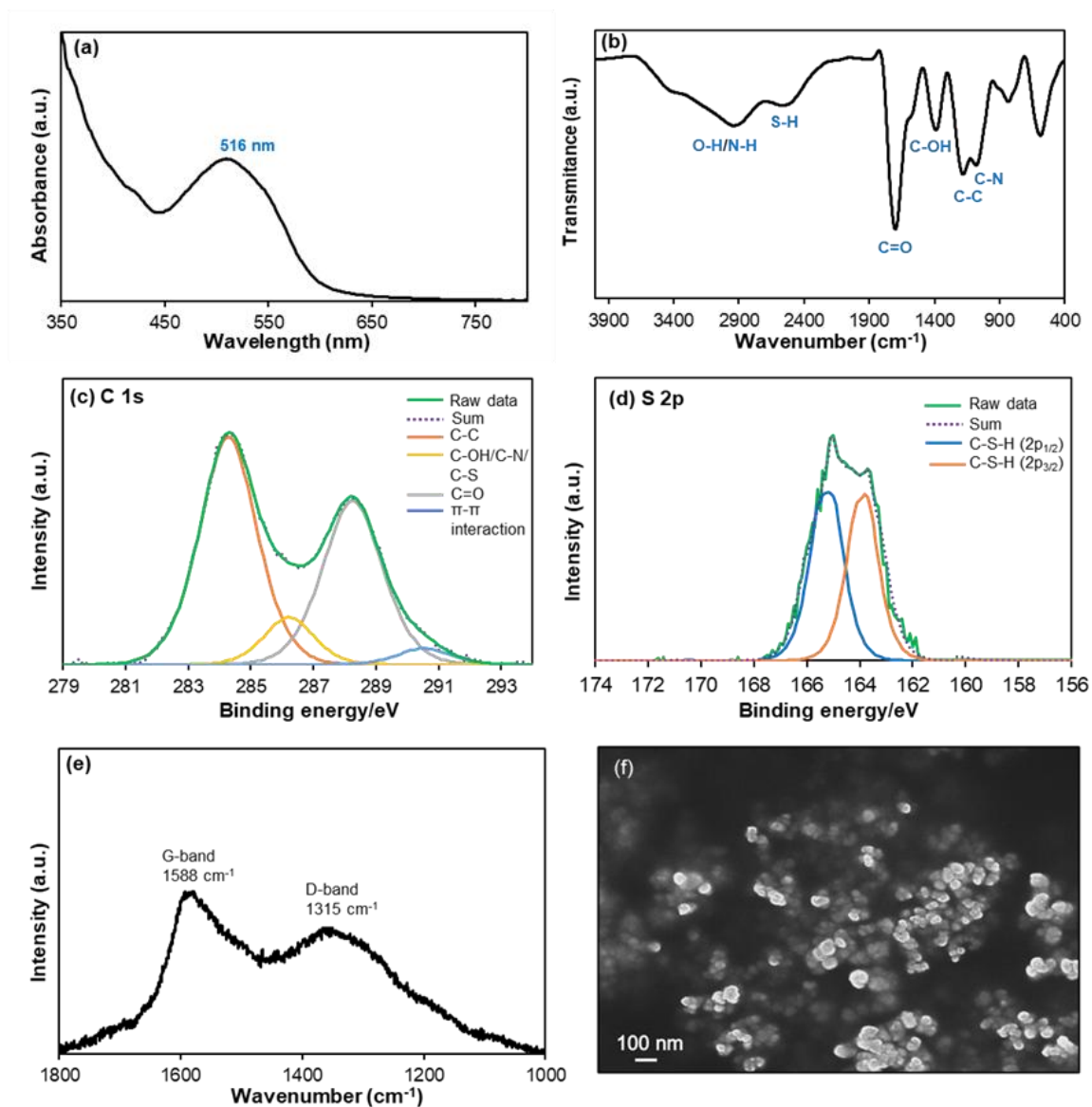


**Figure 4.1** Characterization of C1 by (a) UV-vis, (b) FTIR spectra, (c) XPS at C 1s region, (d) XPS at S 2p region, (e) Raman, and (f) SEM.

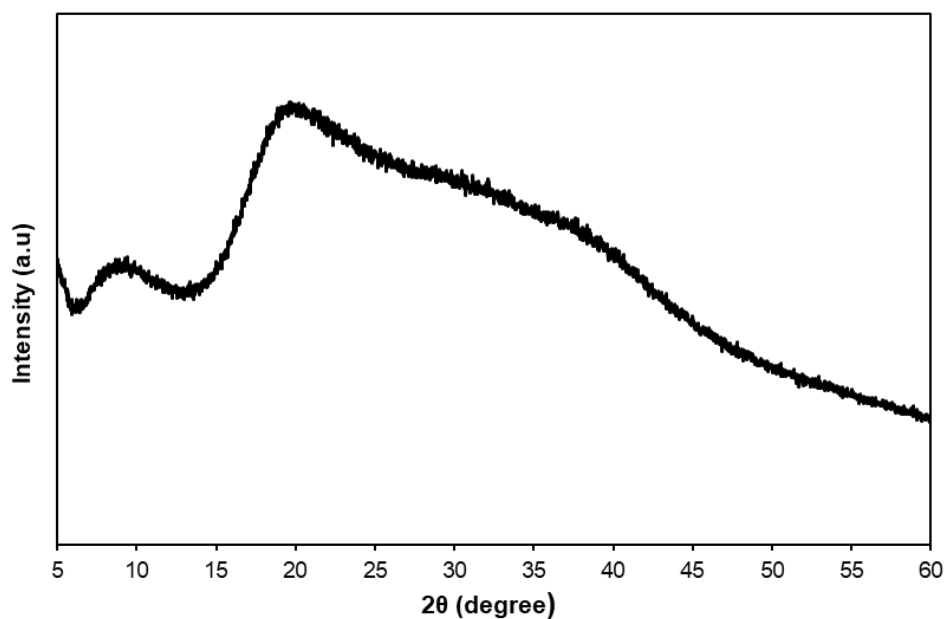
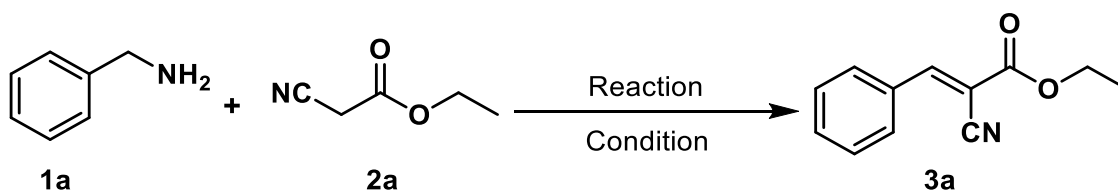


**Figure 4.2** XRD pattern of **C1**.

### 4.2.3 Reaction screening

First, optimized the reaction conditions for the C-C bond formation reaction of benzylamine with ethyl cyanoacetate under irradiation of blue LED light (**Table 4.2**). Nanocarbon **C1** gave maximum yield when using a 5 mg sample and an optimum reaction time of 28 h (**Table 4.2**, Entries 1-8). The yield was higher when using acetonitrile (CH<sub>3</sub>CN) as a solvent (**Table 4.2**, Entry 4) while using other solvents such as DMF and THF was not so effective and gave a low yield (**Table 4.2**, Entry 9 and 10).

**Table 4.2** Screening of the Reaction Conditions<sup>a</sup>



Entry	<b>C1</b> (mg)	Time (hour)	Solvent	Yield (%) <sup>b</sup>
-------	----------------	-------------	---------	------------------------

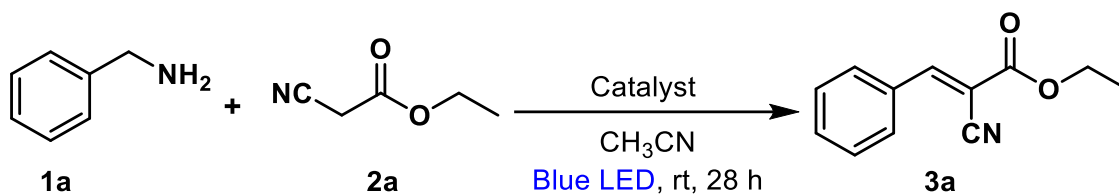
1	5	7	CH <sub>3</sub> CN	28
2	5	14	CH <sub>3</sub> CN	50
3	5	21	CH <sub>3</sub> CN	71
<b>4</b>	<b>5</b>	<b>28</b>	<b>CH<sub>3</sub>CN</b>	<b>88±2<sup>c</sup></b>
5	5	30	CH <sub>3</sub> CN	90
6	3	28	CH <sub>3</sub> CN	76
7	6	28	CH <sub>3</sub> CN	90
8	10	28	CH <sub>3</sub> CN	88
9	5	28	DMF	67
10	5	28	THF	58

<sup>a</sup>Reaction conditions: **1a** (0.2 mmol), **2a** (0.3 mmol), **C1** (5-10 mg), CH<sub>3</sub>CN (1.0 mL) under air atmosphere at room temperature, irradiation of blue LED for 7-30 h. <sup>b</sup>GC yield, <sup>c</sup>n=3

#### 4.2.4 Evaluation of catalytic activity

Then applied nanocarbon **C1** to catalyze the C-C bond formation reaction. The condensation of primary amines with active methylene compounds furnishes substituted electrophilic alkenes. In this research, the coupling reaction of benzylamine with ethyl cyanoacetate was evaluated under irradiation of blue LED light (wavelength: 470 nm). Nanocarbon **C1** showed a high yield of 90% (**Table 4.3**, Entry 1); however, a carbon material prepared without Congo Red **C2** showed only 5% yield (**Table 4.3**, Entry 2), other carbons **C3** – **C12** and Congo Red itself showed no catalytic performance (**Table 4.3**, Entries 3-12). Both light and visible-light-responsive carbon were proved to be essential for this reaction. No desired product was observed when the reaction was conducted in the darkness and in the absence of **C1** (**Table 4.3**, Entries 14 and 15). Moreover, the reaction also proceeded under Ar atmosphere and gave a low yield under control UV light irradiation (**Table 4.3**, Entries 16 and 17).

**Table 4.3** Evaluation of the catalytic activity of nanocarbon **C1**<sup>a</sup>



Entry	Catalyst	Yield (%) <sup>b</sup>
1	<b>C1</b>	90
2	<b>C2</b>	5
3	<b>C3</b>	0
4	<b>C4</b>	0
5	<b>C5</b>	0
6	<b>C6</b>	0
7	<b>C7</b>	0
8	<b>C8</b>	0
9	<b>C9</b>	0
10	<b>C10</b>	0
11	<b>C11</b>	0
12	<b>C12</b>	0
13	<b>Congo Red</b>	0
14 <sup>c</sup>	<b>C1</b>	0
15	<b>none</b>	0
16 <sup>d</sup>	<b>C1</b>	88
17 <sup>e</sup>	<b>C1</b>	30

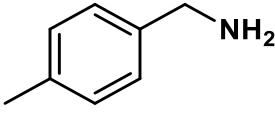
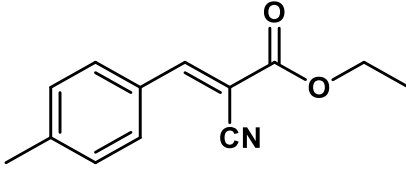
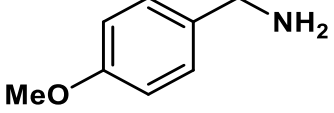
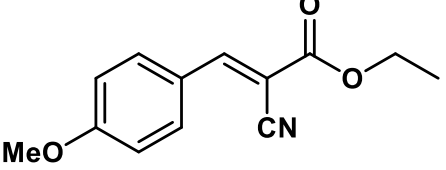
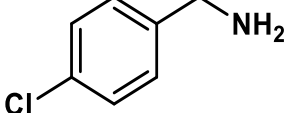
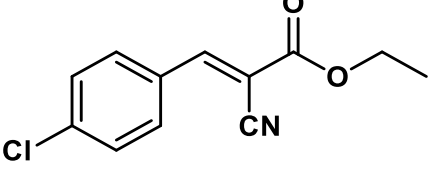
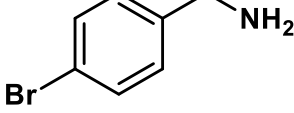
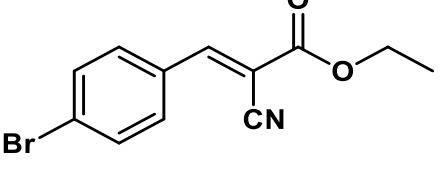
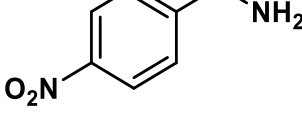
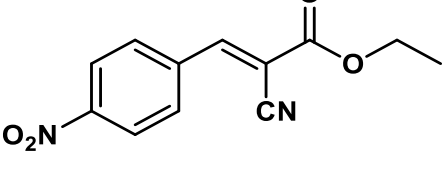
<sup>a</sup>Reaction conditions: 1a (0.2 mmol), 2a (0.3 mmol), **C1** (5 mg), CH<sub>3</sub>CN (1.0 mL) under air atmosphere at room temperature, irradiation of blue LED for 28 h. <sup>b</sup>GC yield. <sup>c</sup>Under dark. <sup>d</sup>Under Ar. <sup>e</sup>Under UV.

#### 4.2.5 Substrate scope

After that, the substrate scope of the photocatalytic C-C bond formation reaction of benzylamine derivatives was examined. The reaction proceeded with good to excellent yields of 90% and 91% (**Table 4.4**, Entries 1 and 2) when benzylamine contained electron-donating methyl and methoxy groups. Electron-withdrawing halogen groups

such as chloro and bromo at the *para* position (**1d** and **1e**) did not affect the reactivity and formed corresponding acrylate derivatives (**3d** and **3e**) in good yields (**Table 4.4**, Entries 3 and 4). Furthermore, the benzylamine having a strong electron-withdrawing nitro group also worked as a substrate to give the corresponding products (**3f**) in good yield (**Table 4.4**, Entry 5).

**Table 4.4** Substrate scope using C1 as a photocatalyst<sup>a</sup>

Entry	Substrate	Product	Yield (%) <sup>b</sup>
1	 <b>1b</b>	 <b>3b</b>	90
2	 <b>1c</b>	 <b>3c</b>	91
3	 <b>1d</b>	 <b>3d</b>	87
4	 <b>1e</b>	 <b>3e</b>	88
5	 <b>1f</b>	 <b>3f</b>	85

<sup>a</sup>Reaction conditions: benzylamine derivatives **1** (0.2 mmol), **2a** (0.3 mmol), **C1** (5 mg), CH<sub>3</sub>CN (1.0 mL) under air atmosphere at room temperature, irradiation of blue LED for 28 h. <sup>b</sup>GC yield.

#### 4.2.6 Mechanism investigation

To gain better insight into the mechanism of the reaction, tried to trap the radical intermediate by in-situ electron spin resonance (ESR) analysis using 5,5-dimethyl-1-pyrroline N-oxide (DMPO) as a spin trap agent. A mixture of benzylamine, ethyl cyanoacetate, nanocarbon **C1**, and DMPO in acetonitrile was prepared. No ESR signal appeared in the absence of light (**Figure 4.3a**); in contrast, a strong ESR signal derived from the DMPO-sulfur radical adduct (DMPO-•S) was observed under blue LED irradiation (**Figure 4.3b**).<sup>40</sup> These results suggest that the reaction was promoted by sulfur radicals. To confirm the radical pathway, radical scavenger 2,2,6,6-tetramethyl piperidine 1-oxyl (TEMPO) in the reaction mixture was added; as a result, only 4% of the product was obtained, suggesting the radical plays an important role in the reaction.

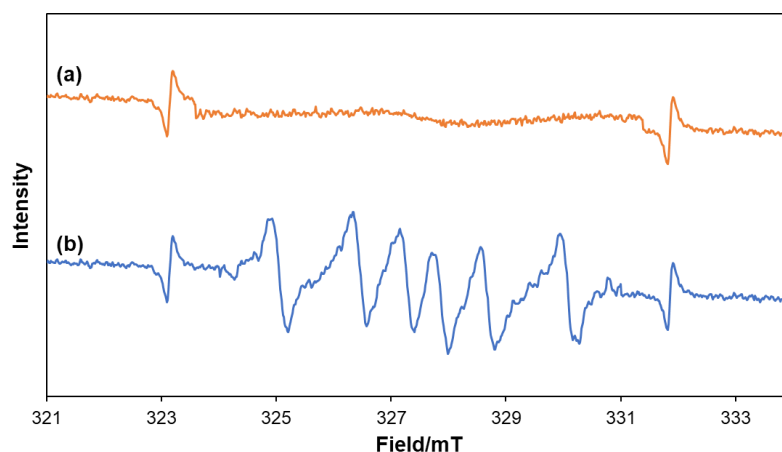


**Figure 4.3** ESR spectra of the reaction mixture with DMPO (a) in the absence of light, and (b) under irradiation of blue LED. 323 and 332 mT are the standard Mn<sup>2+</sup> peaks.

Next, confirmed the role of the SH group on **C1**. I employed H<sub>2</sub>O<sub>2</sub> to oxidize the SH group, which was confirmed by FTIR (**Figure 4.4**).<sup>41</sup> After oxidation, **C1** was used as a catalyst; as a result, most of the benzylamine and ethyl cyanoacetate recovered, and only 5% of the product was found. This observation confirmed that SH is the reactive functional group of nanocarbon **C1**, which generates the radical intermediate.

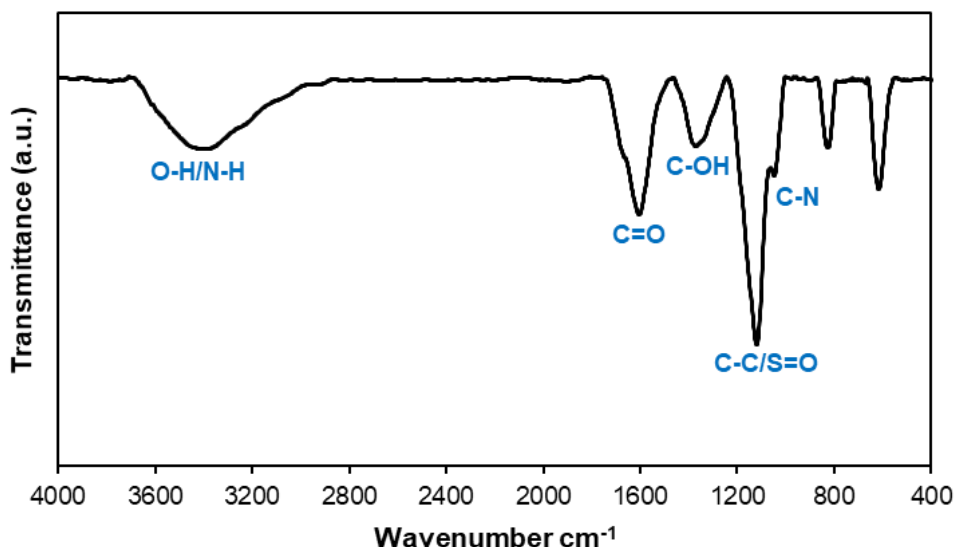
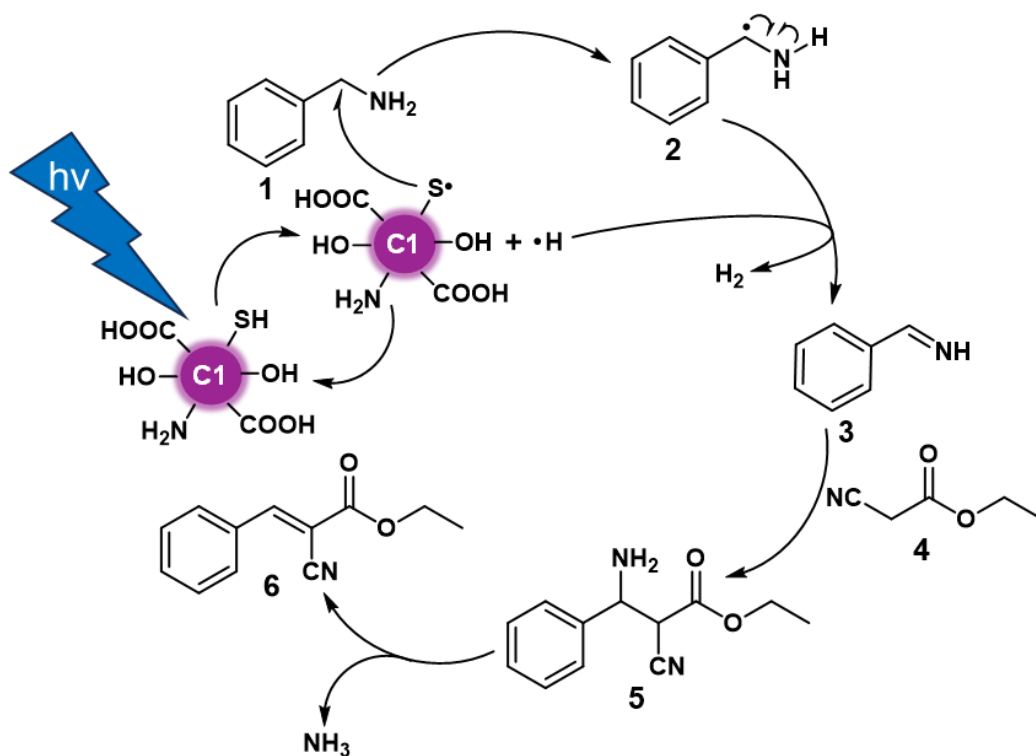


**Figure 4.4** FTIR spectra of **C1** after oxidation by H<sub>2</sub>O<sub>2</sub>.

Based on the above observations, a plausible reaction mechanism is proposed (**Scheme 4.1**). Nanocarbon **C1** produces sulfur radical under irradiation of blue LED light. The resulting sulfur radical attacks the benzylamine **1** to form aminomethyl radical **2** and then furnishes imine intermediate **3** with H<sub>2</sub> generation, as reported previously.<sup>42,43</sup> The formation of imine intermediate **3** was confirmed by the following experiment:<sup>44</sup> in the presence of water, benzylamine was converted to benzaldehyde identified by GC-MS. Subsequently, imine intermediate **3** coupled with ethyl cyanoacetate **4** to form intermediate **5**, and finally give the product **6** through the release of ammonia.<sup>45,46</sup>



**Scheme 4.1** Proposed reaction mechanism.

#### 4.2.7 Recyclability test

Finally, the stability and recyclability of nanocarbon **C1** were investigated, an important indicator for the practical applicability of the heterogeneous catalyst. Notably, **C1** was recycled and reused at least five times without any significant loss of reactivity (**Figure 4.5**).

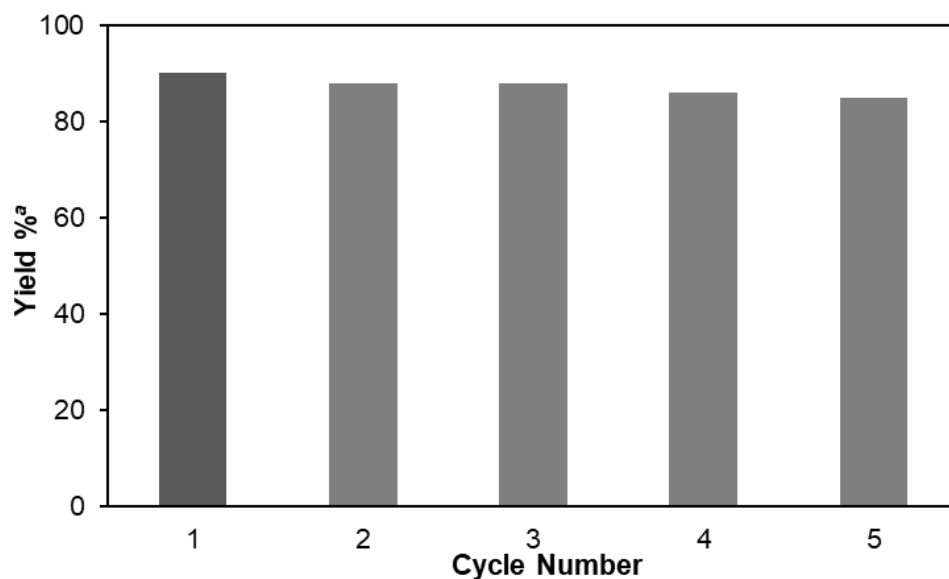


**Figure 4.5** Recyclability test of nanocarbon **C1**. Reaction conditions: **1a** (1.0 mmol), **2a** (1.5 mmol), **C1** (25 mg), CH<sub>3</sub>CN (5.0 mL) under air atmosphere at room temperature, irradiation of blue LED for 28 h. <sup>a</sup>GC yield.

The structural analysis after the reaction was investigated by FTIR and XPS. All characterization peaks were reserved up to the 5<sup>th</sup> reaction cycle, confirming the negligible structural change (**Figures 4.6** and **4.7**).

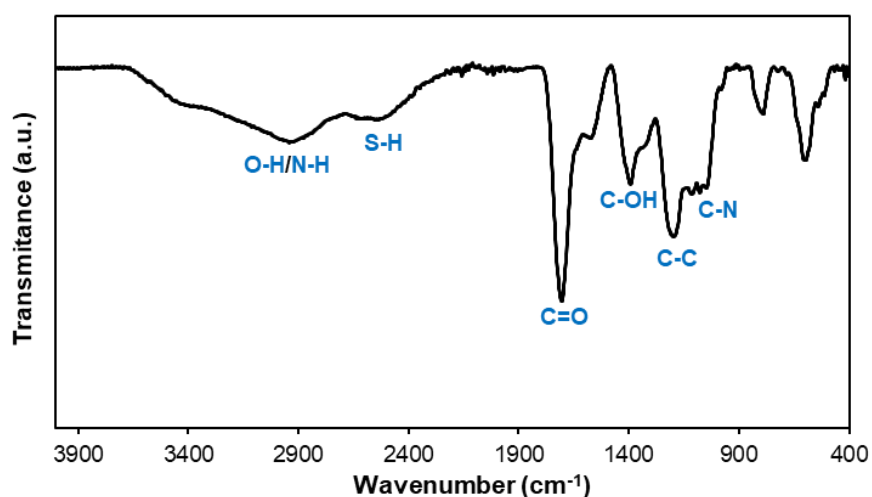


**Figure 4.6** FTIR spectra of **C1** after the 5<sup>th</sup> reaction cycle.

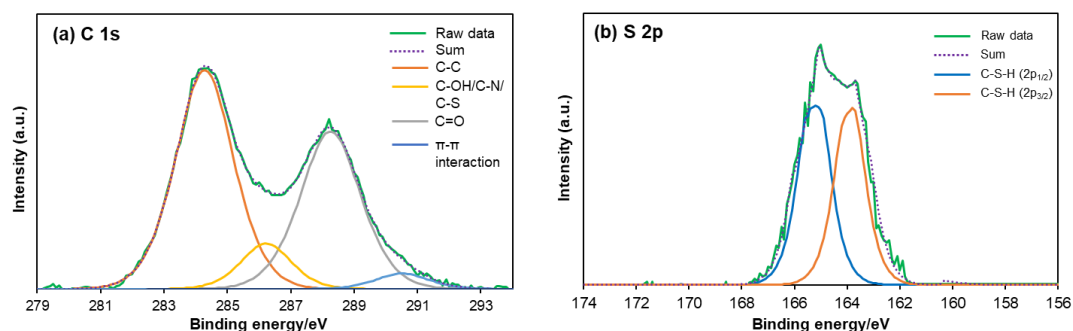


**Figure 4.7** XPS spectra (a) at the C 1s region, and (b) at the S 2p region after the 5<sup>th</sup> reaction cycle.

### 4.3 Conclusion

In summary, a visible-light-absorbing amorphous nanocarbon **C1** was synthesized by hydrothermal treatment of citric acid and Congo Red. Various characterization methods confirmed the structure and surface functional groups of **C1**. More interestingly, **C1** exhibited high catalytic performance under irradiation of blue LED for the C-C bond formation reaction of benzylamine with ethyl cyanoacetate. The reactions proceeded smoothly under mild reaction conditions and afforded the desired product in high yield. The mechanistic study revealed that the reaction proceeded with forming sulfur radical from nanocarbon **C1** under irradiation of blue LED light. Both **C1** and visible light synergistically worked for the progress of the reactions. This report on the synthesis of visible-light-responsive nanocarbon photocatalysts for carbon-carbon bond-forming reactions will enhance the opportunity for future photocatalytic applications.

### 4.4 Experimental

#### 4.4.1 General Information

All the chemicals used in this study were purchased from commercial sources and used as received unless otherwise mentioned. Kessil A360X tuna blue LED light with a wavelength centered at 470 nm was used. The products were quantified by gas

---

chromatography-mass spectrometry (GCMS-QP2010 *Plus*, Shimadzu), equipped with a flame ionization detector (FID). ESR analysis was performed using an electron spin resonance spectrometer (JES-X310) with microwave frequency 9.542 GHz, modulation frequency 100 kHz, power 1 mW, and weep time 1 min. The functional groups on the surface of the synthesized nanocarbon were recorded by Fourier transform infrared spectrophotometer (FTIR; Shimadzu IRTracer-100). The samples for the FTIR were dried and mixed with KBr and then pressed into 1.3 cm-diameter pellets. Freeze-drying of the carbon catalysts was performed using ADVANTEC DRZ350WC. The surface chemistry was performed using an X-ray photoelectron spectroscopy (XPS; JPS-9030) with a pass energy of 20 eV. Particle size was measured by scanning electron microscope technique (SEM; HITACHI-9000). Inductively coupled plasma mass spectrometry (ICP-MS) was analyzed by Agilent7500cx.

#### **4.4.2 Experimental procedure for synthesis of carbon**

Synthesis of carbon materials from citric acid and dye molecules was performed by a one-step hydrothermal method. In more detail, 600 mg of citric acid and 200 mg of Congo Red were added to 5 mL of water. Then the mixture was sonicated and heated in a Teflon-lined autoclave at 185 °C with a constant heating rate of 10 °C per minute. Finally, the solution was kept at that temperature for 4 h. The obtained product was cooled down naturally to room temperature, redispersed in water, and centrifuged at 10000 rpm for 20 min (three times). Finally, the dark brown color residue part was collected and dried in a freeze drier.

#### **4.4.3 UV-visible spectra**

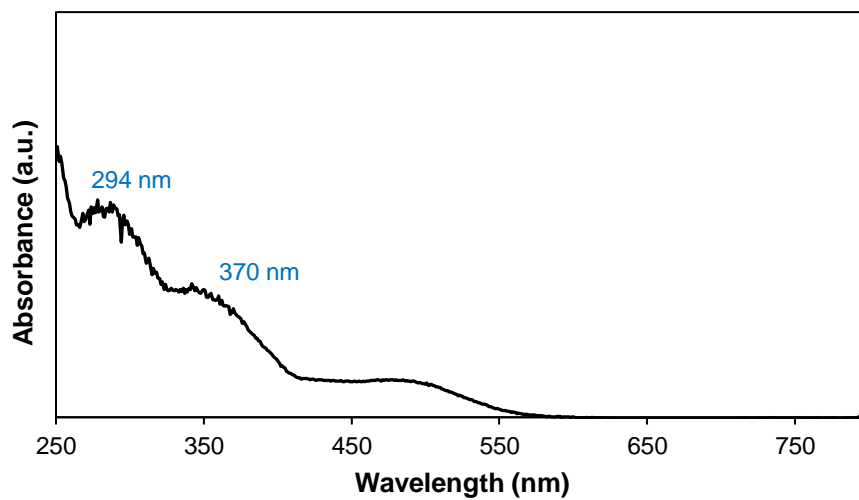


**Figure 4.8** UV-vis absorption spectra of **C2**.

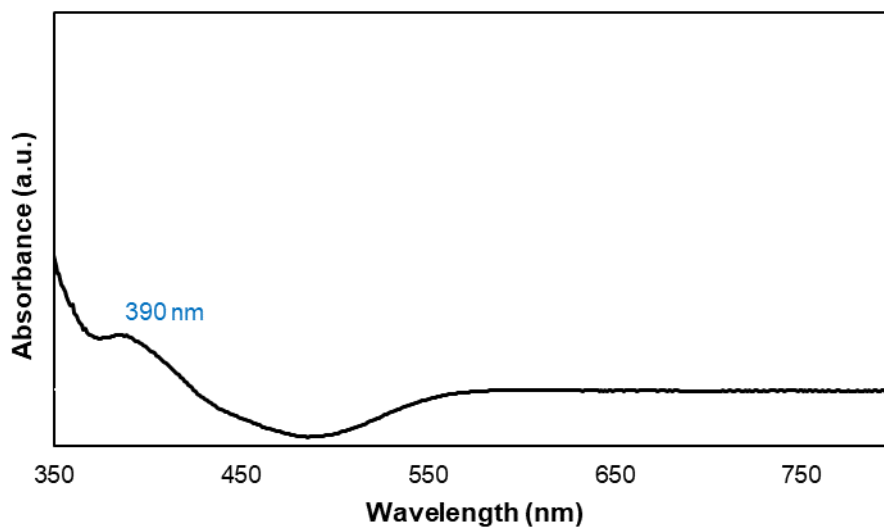


**Figure 4.9** UV-vis absorption spectra of **C3**.

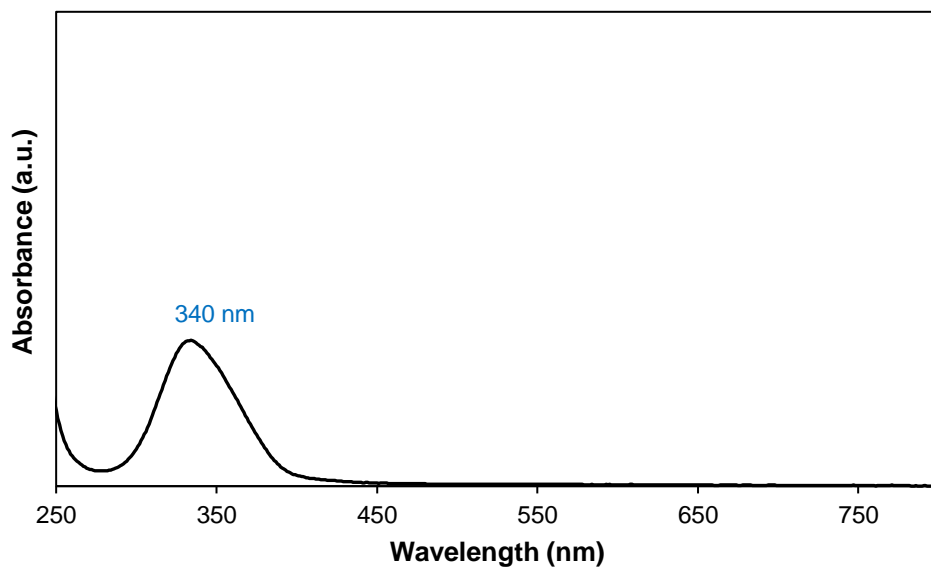


**Figure 4.10** UV-vis absorption spectra of **C4**.

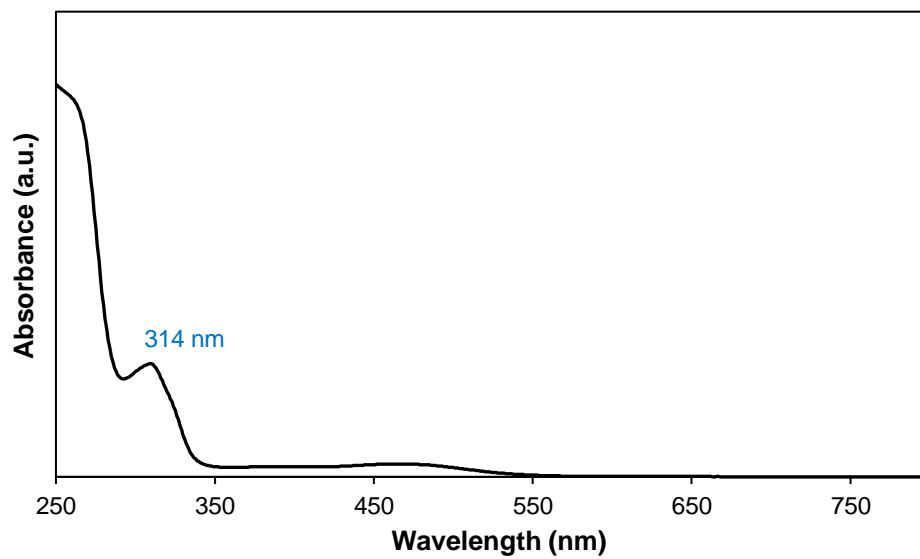


**Figure 4.11** UV-vis absorption spectra of **C5**.

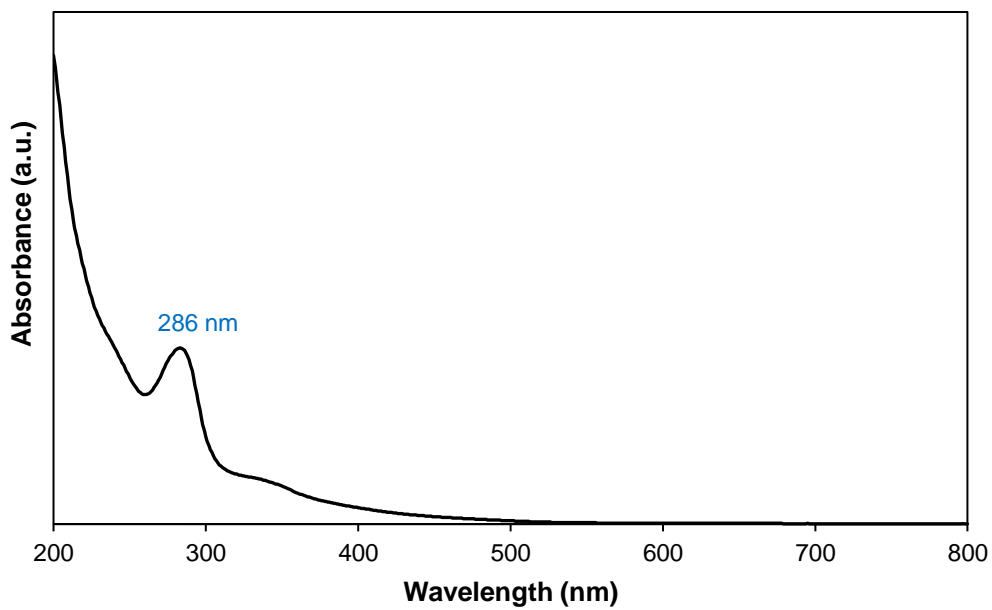


**Figure 4.12** UV-vis absorption spectra of **C6**.

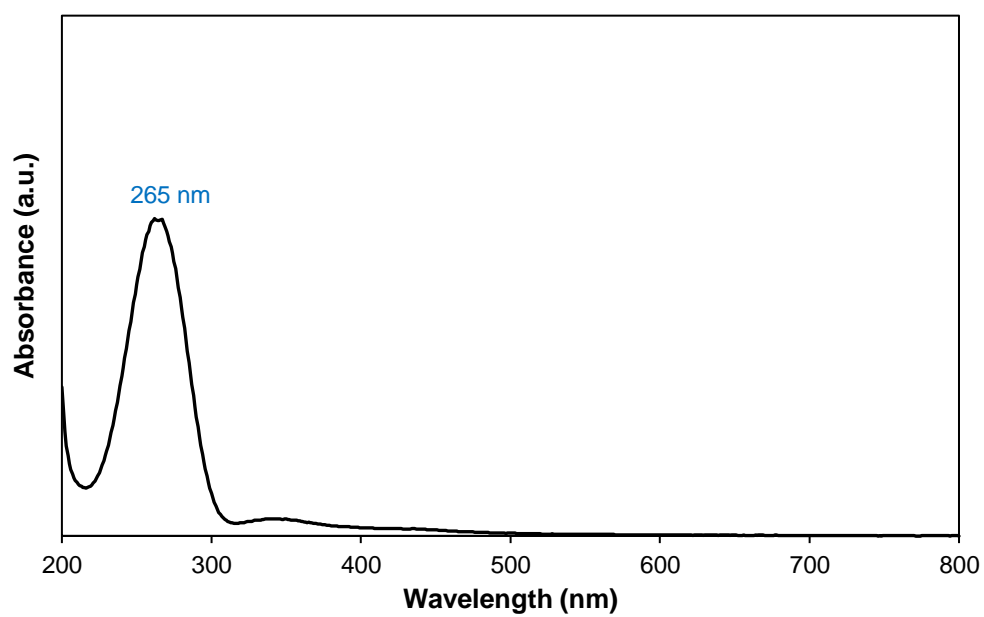


**Figure 4.13** UV-vis absorption spectra of **C7**.

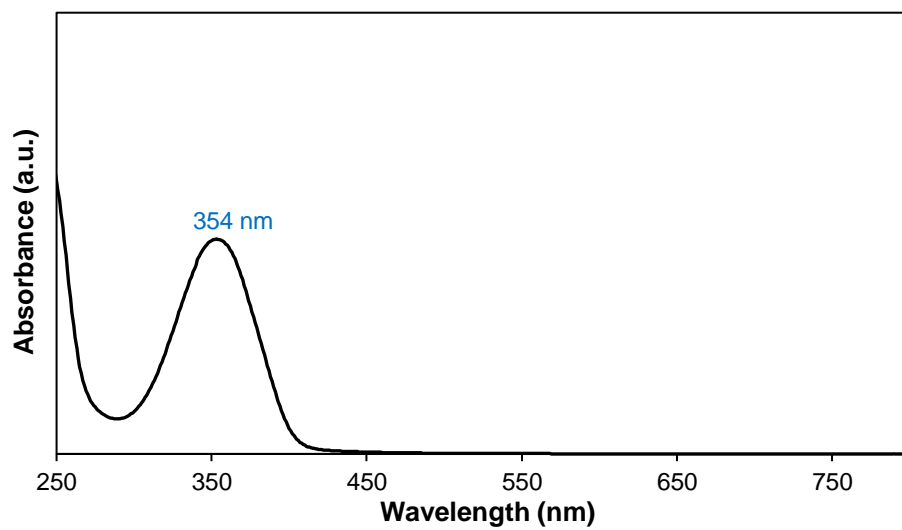


**Figure 4.14** UV-vis absorption spectra of **C8**.

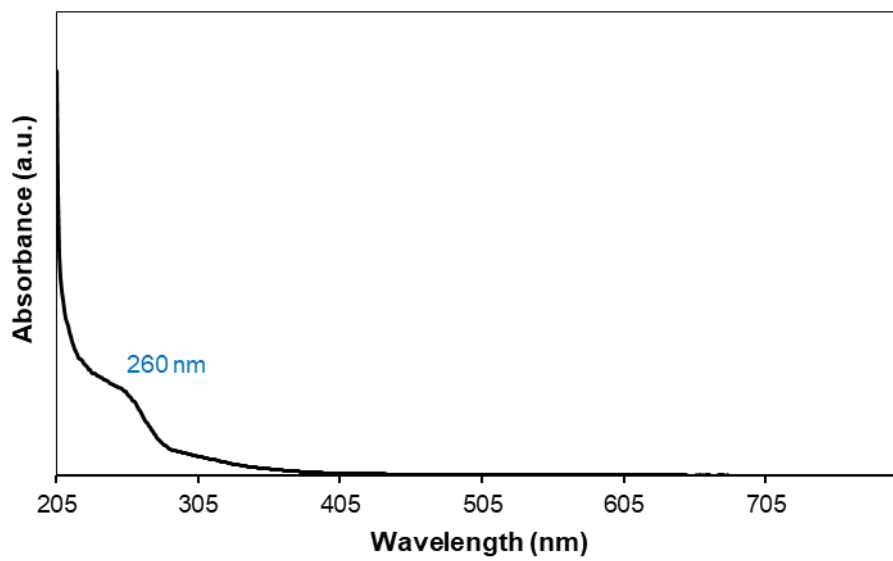


**Figure 4.15** UV-vis absorption spectra of **C9**.

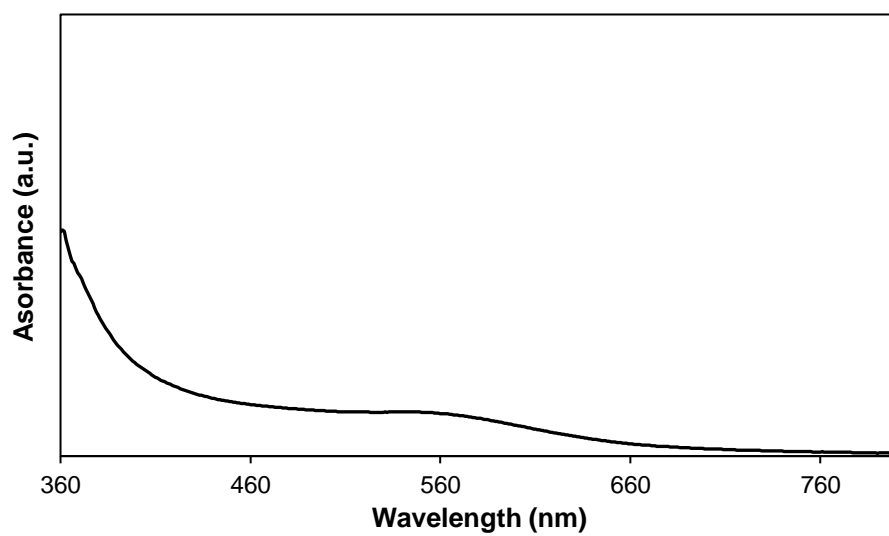


**Figure 4.16** UV-vis absorption spectra of **C10**.

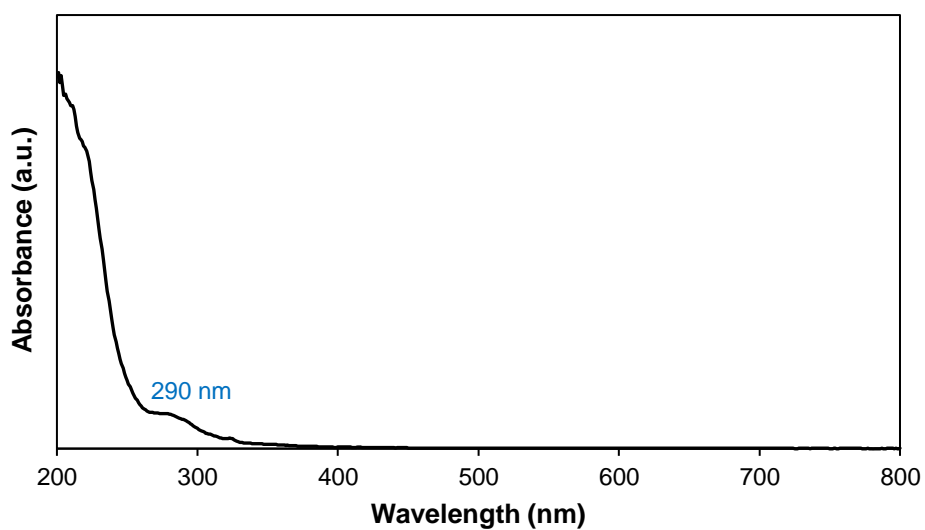


**Figure 4.17** UV-vis absorption spectra of **C11**.

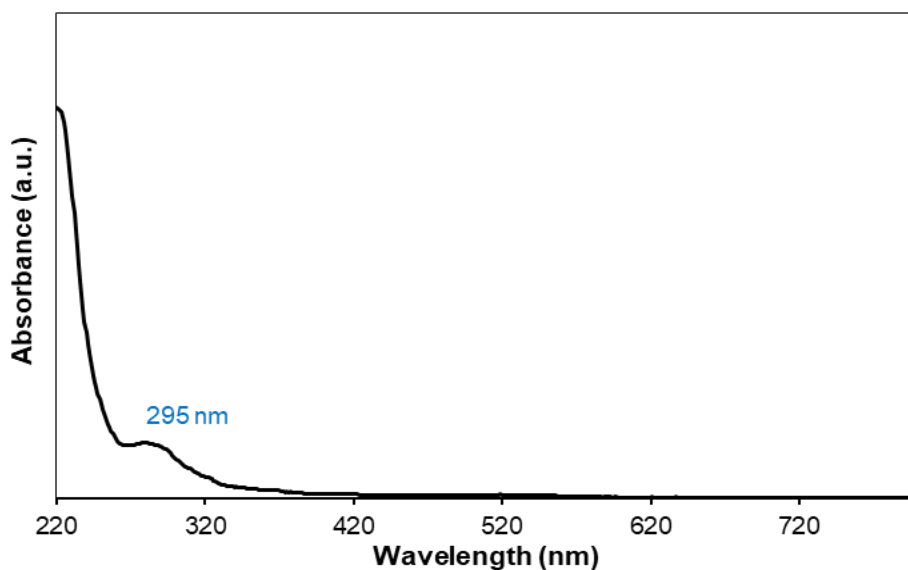


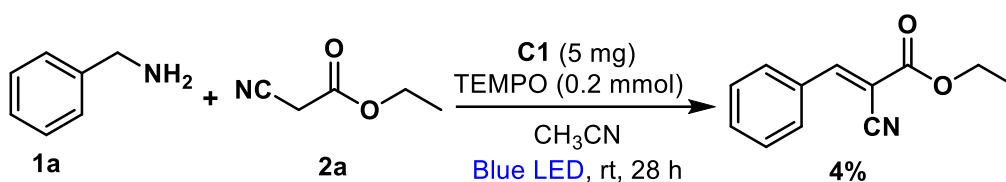
**Figure 4.18** UV-vis absorption spectra of **C12**.

#### 4.4.4 ESR measurement technique

The mixture of benzylamine **1a** (0.2 mmol), ethyl cyanoacetate **2a** (0.3 mmol), **C1** (5 mg), and DMPO (0.2 mmol) was stirred at room temperature for 5 minutes. After 5 minutes, the reaction mixture was taken in a quartz capillary tube and irradiated blue LED light at room temperature for 28 h. After every 7 h intervals, ESR analysis was performed.

#### 4.4.5 The reaction with radical scavenger

The mixture of benzylamine **1a** (0.2 mmol), ethyl cyanoacetate **2a** (0.3 mmol), **C1** (5 mg), 2,2,6,6-tetramethylpiperidine 1-oxyl (0.2 mmol), and CH<sub>3</sub>CN (1.0 mL) was stirred with irradiating blue LED light under an air atmosphere at room temperature for 28 h. After the reaction, the reaction mixture was analyzed by GC using n-dodecane as an internal standard.



#### 4.4.6 Identification of benzaldehyde via imine formation

The mixture of benzylamine **1a** (0.2 mmol), H<sub>2</sub>O (0.02 mmol), **C1** (5 mg), and CH<sub>3</sub>CN (1.0 mL) was stirred with irradiating blue LED light under an air atmosphere at room temperature for 28 h to give benzaldehyde **3x**. After the reaction, the reaction mixture was analyzed by GC-MS and confirmed the formation of benzaldehyde via an imine intermediate.

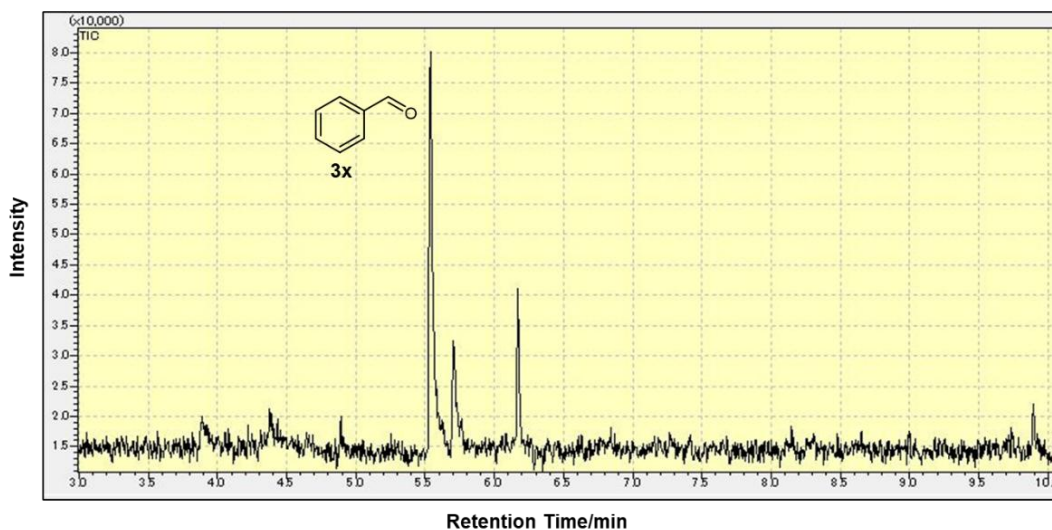
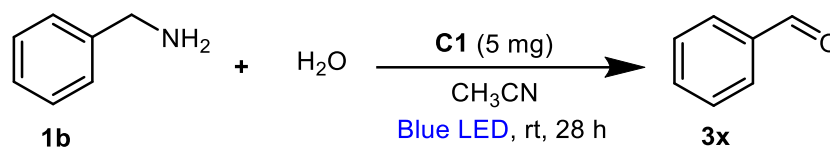


Figure 4.19 GC spectra of **3x**.

---

#### 4.4.7 ICP-MS

**Table 4.5** ICP-MS Analysis

Elements	Concentration (ppb)		
	C1	H <sub>2</sub> O	Background
Li	0.033	1.000	0.043
Be	<0.004	0.005	<0.003
B	62.104	10.535	3.921
Na	361.381	1.442	4.638
Mg	6.179	0.557	0.754
Al	39.198	20.138	0.661
Si	2001.850	15.773	36.535
P	5.436	<0.014	5.436
S	3914.516	151.020	799.096
Cl	665.725	25.197	180.374
Ca	19.572	6.389	2.618
Sc	0.686	<0.001	0.080
Ti	0.513	0.046	0.015
V	0.085	0.007	0.001
Cr	0.267	0.019	0.011
Mn	7.061	0.025	0.030
Fe	4.237	1.500	6.275
Co	0.007	1.000	0.001
Ni	0.184	0.063	0.010

---

Cu	0.417	1.029	0.024
Zn	0.522	7.174	0.038
Ga	0.080	<0.001	0.002
Ge	0.017	0.003	0.014
As	0.022	0.010	0.005
Br	5.850	0.194	0.772
Se	0.268	<0.048	0.583
Rb	0.175	<0.001	0.045
Sr	0.211	0.074	0.008
Y	0.000	1.000	0.002
Zr	0.094	<0.001	<0.001
Nb	0.004	<0.001	0.000
Mo	0.208	<0.003	<0.002
Ru	<0.003	<0.003	<0.002
Rh	0.000	0.000	0.000
Pd	0.123	0.018	<0.002
Ag	0.520	0.008	<0.001
Cd	<0.005	<0.005	<0.004
In	0.001	0.001	0.000
Sn	0.171	0.021	0.028
Sb	0.454	0.002	0.003
Te	<0.029	<0.029	<0.022
I	0.777	0.036	0.628
Cs	0.022	0.001	0.001

---

Ba	0.019	0.025	0.013
La	0.001	0.030	0.001
Ce	0.002	1.000	0.002
Pr	0.000	0.001	0.000
Nd	<0.002	<0.002	<0.002
Sm	<0.002	<0.002	<0.002
Eu	<0.001	0.002	<0.001
Gd	0.002	0.006	0.002
Tb	0.000	0.000	0.000
Dy	<0.001	<0.001	<0.001
Ho	0.000	0.000	0.000
Er	<0.001	<0.001	<0.001
Tm	0.000	0.000	0.000
Yb	<0.002	<0.002	<0.001
Lu	0.000	0.000	0.000
Hf	<0.001	<0.001	<0.001
Ta	0.00	0.00	0.00
W	0.044	<0.002	<0.001
Re	<0.001	<0.001	<0.001
Os	<0.002	<0.002	<0.002
Ir	<0.001	<0.001	<0.001
Pt	0.008	0.018	<0.002
Au	0.036	<0.001	<0.001
Hg	0.008	<0.005	<0.005

Tl	<0.001	1.000	0.003
Pb	0.017	0.085	0.002
Bi	0.017	0.001	<0.001
Th	<0.001	<0.001	<0.001
U	<0.001	0.001	<0.001

**Sample dissolution method:** The samples were completely acid-digested in a closed polytetrafluoroethylene (PTFE) vessel. An accurately weighed portion of the powdered sample 250 mg was weighed into PTFE vessel with the subsequent addition of 6 ml of concentrate HNO<sub>3</sub> (60%) and 2 ml of H<sub>2</sub>O<sub>2</sub> (30%). The vessel was closed, placed into a steel pressurized bomb, and heated in an oven up to 130 °C for 2 h. The obtained digest sample was cooled down naturally to room temperature. The final digest was diluted to 30 ml in a volumetric flask with milli-Q water and centrifuged at 6000 rpm for 30 min. Finally filtered by filter paper and collected a liquid sample.

#### 4.4.8 GC and mass spectra of product 3a

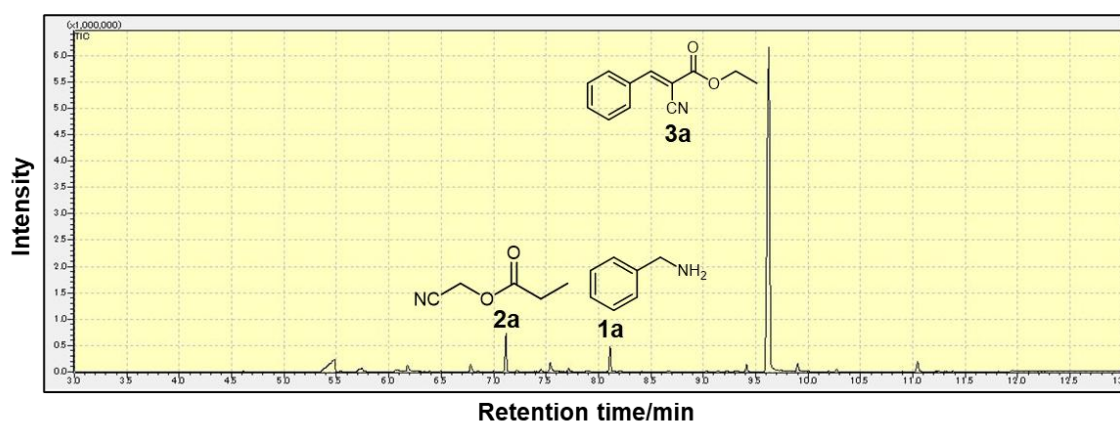


**Figure 4.20** GC spectra of product 3a.

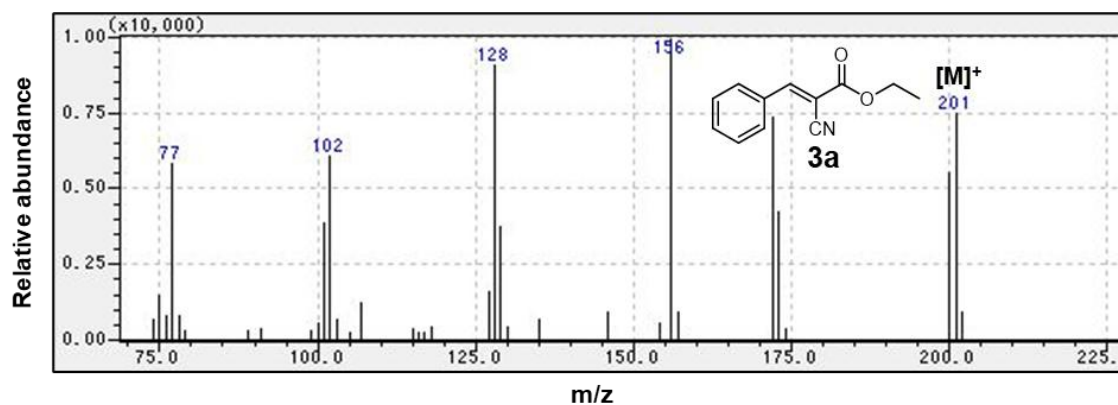


**Figure 4.21** Mass spectra of product **3a**.

#### 4.4.9 NMR spectra of product 3a-f

##### Ethyl-2-cyano-3-phenyl acrylate (**3a**)

<sup>1</sup>H NMR (CDCl<sub>3</sub>) δ ppm: 8.23 (s, 1H), 7.98-7.96 (m, 2H), 7.55-7.48 (m, 3H), 4.37 (q, 2H), 1.38 (t, 3H).

<sup>13</sup>C NMR (CDCl<sub>3</sub>) δ ppm: 62.39, 153.51, 133.61, 133.62, 127.81, 116.64, 115.45, 102.52, 82.79, 14.14.

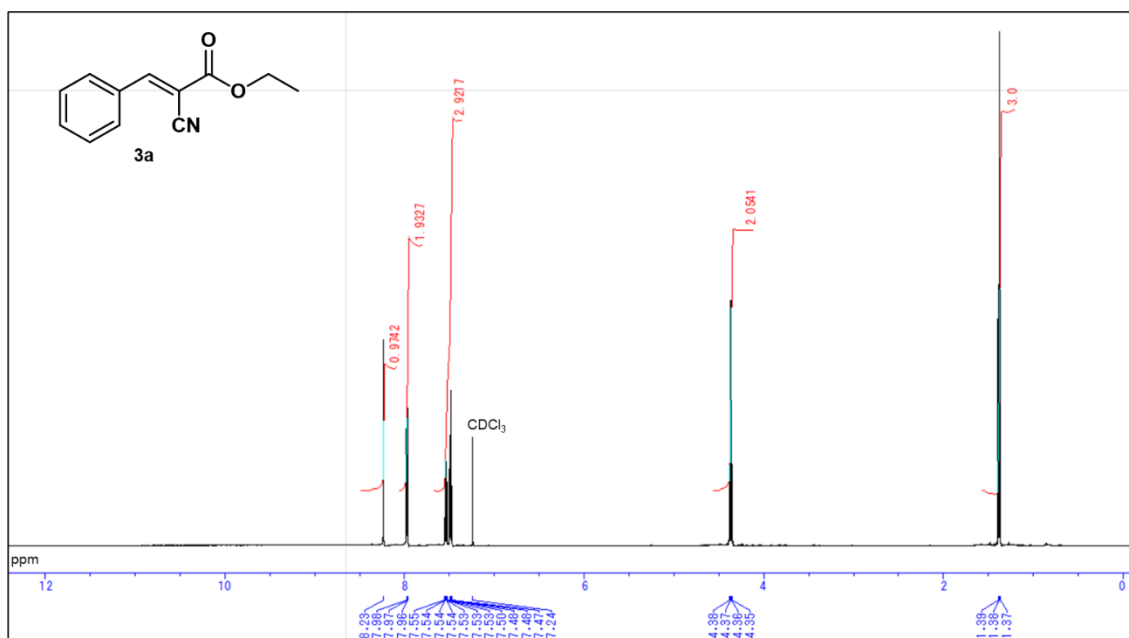


**Figure 4.22** <sup>1</sup>H NMR spectra of product **3a**.

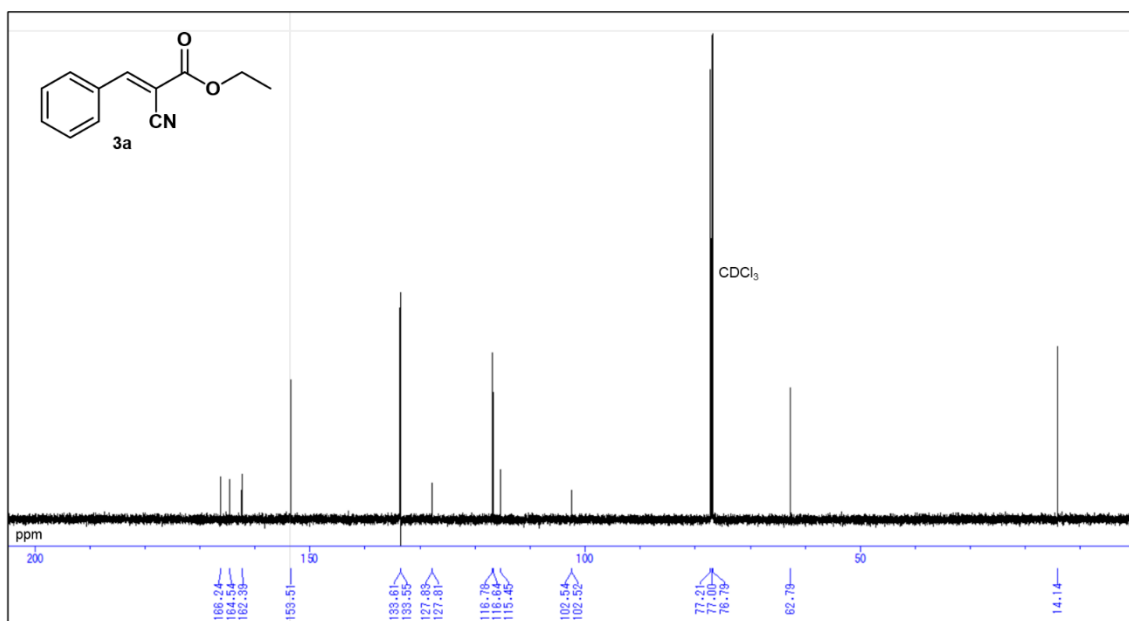


**Figure 4.23** <sup>13</sup>C NMR spectra of product **3a**.

**Ethyl-2-cyano-3-(4-methylphenyl) acrylate (3b)**

<sup>1</sup>H NMR (CDCl<sub>3</sub>) δ ppm: 8.20 (s, 1H), 7.88 (d, 2H), 7.28 (m, 2H), 4.35 (q, 2H), 2.41 (s, 3H) 1.38 (t, 3H).

<sup>13</sup>C NMR (CDCl<sub>3</sub>) δ ppm: 162.77, 155.01, 144.65, 131.25, 130.03, 128.85, 115.79, 101.54, 62.59, 21.87, 14.17.

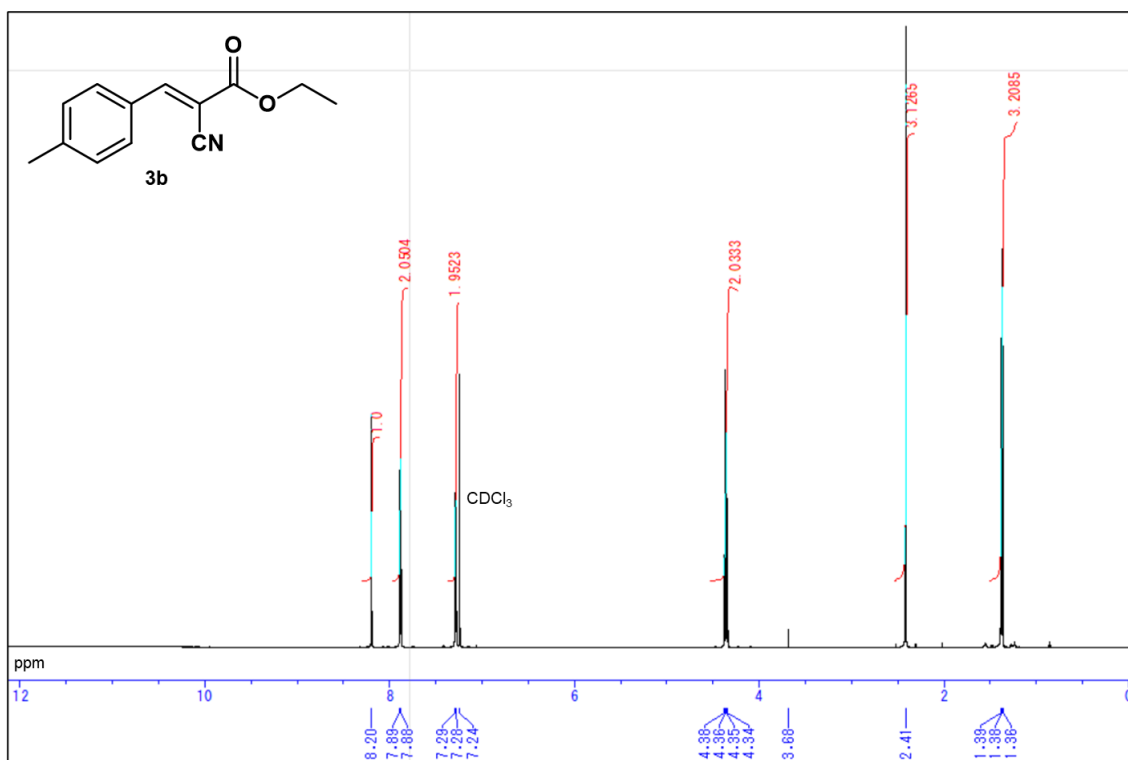


Figure 4.24 <sup>1</sup>H NMR spectra of product **3b**.

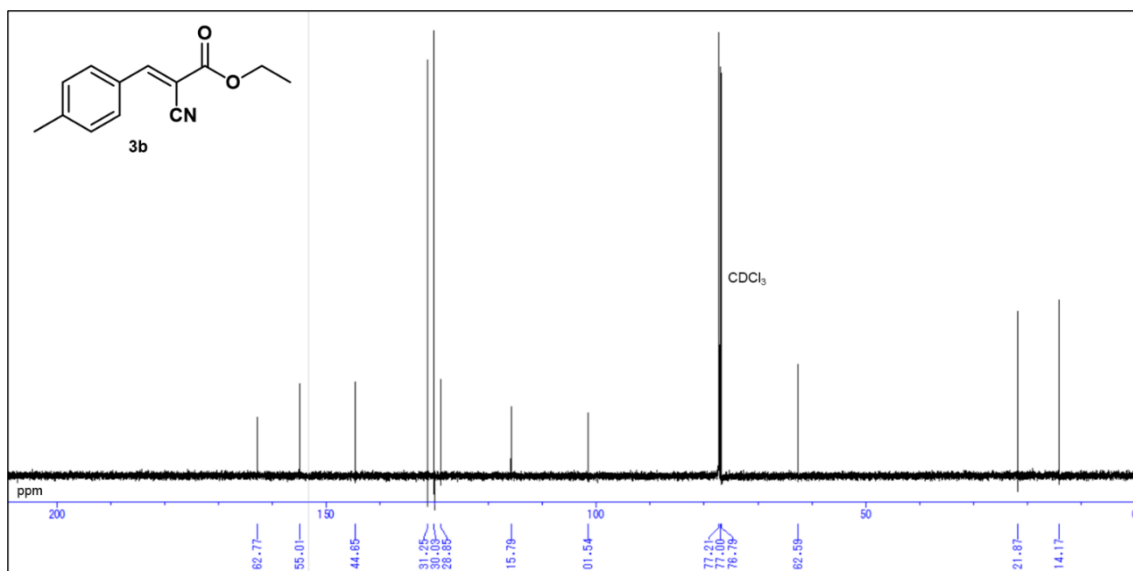


Figure 4.25 <sup>13</sup>C NMR spectra of product **3b**.

### Ethyl-2-cyano-3-(4-methoxyphenyl) acrylate (**3c**)

<sup>1</sup>H NMR (CDCl<sub>3</sub>) δ ppm: 8.15 (s, 1H), 7.98 (m, 2H), 6.97 (m, 2H), 4.34 (q, 2H), 3.8 (s,

3H), 1.36 (t, 3H).

$^{13}\text{C}$  NMR ( $\text{CDCl}_3$ )  $\delta$  ppm: 163.10, 154.38, 154.36, 133.61, 124.32, 116.21, 114.73, 99.30, 62.41, 55.59, 14.18.

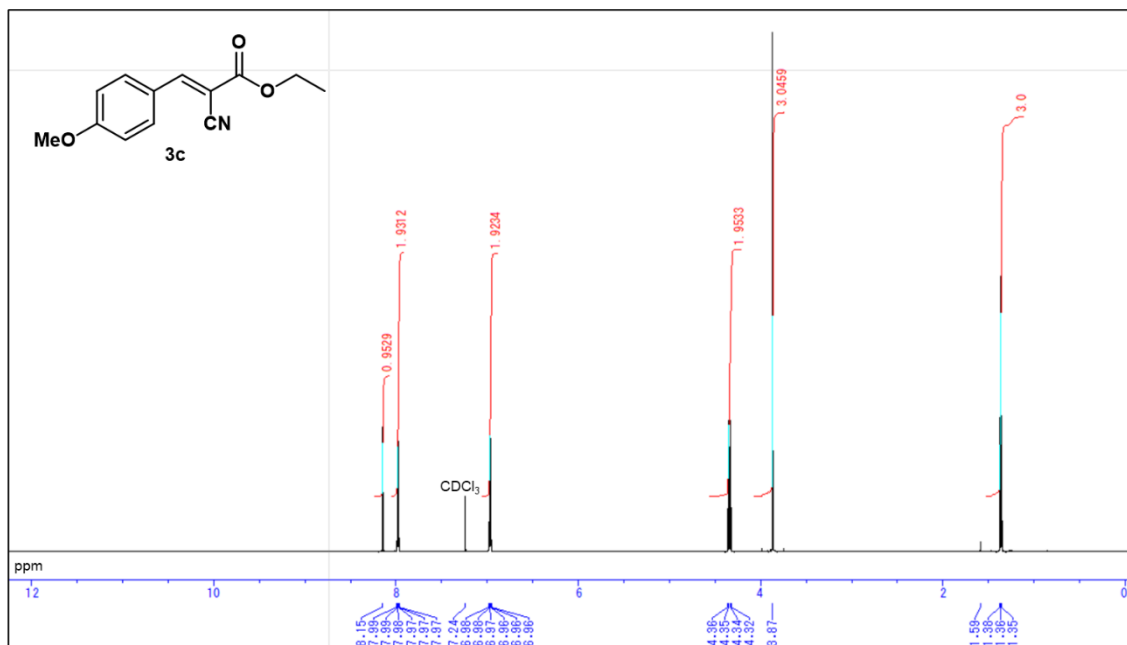


**Figure 4.26**  $^1\text{H}$  NMR spectra of product **3c**.

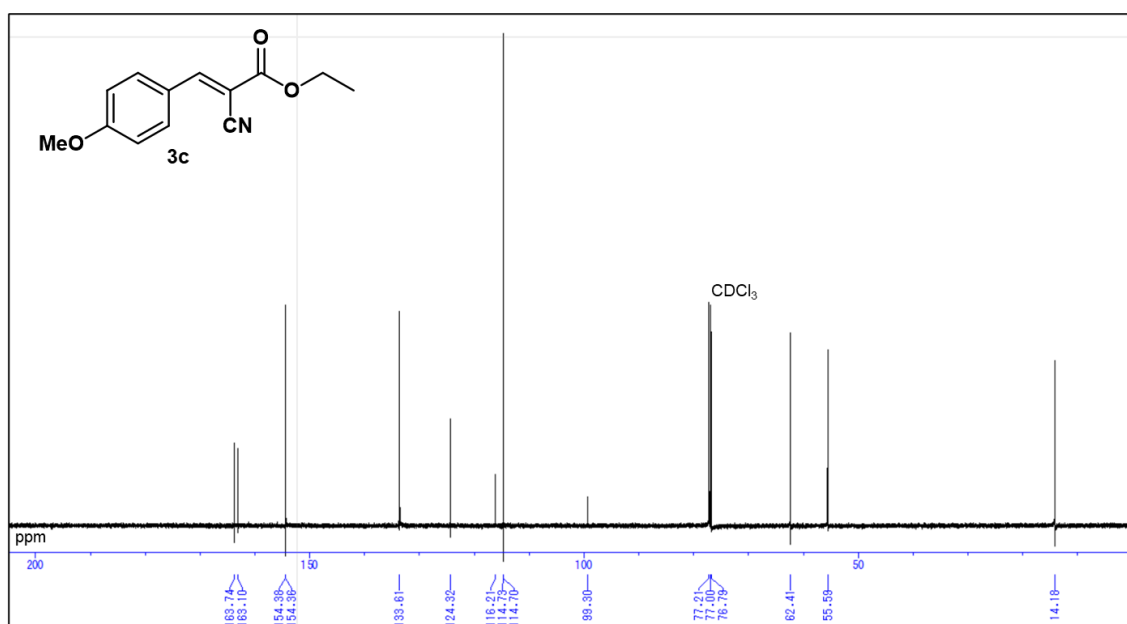


**Figure 4.27**  $^{13}\text{C}$  NMR spectra of product **3c**.

**Ethyl-2-cyano-3-(4-chlorophenyl) acrylate (3d)**

$^1\text{H}$  NMR ( $\text{CDCl}_3$ )  $\delta$  ppm: 8.19 (s, 1H), 8.01 (m, 2H), 7.20-7.16 (m, 2H), 4.36 (q, 2H), 1.38 (t, 3H).

$^{13}\text{C}$  NMR ( $\text{CDCl}_3$ )  $\delta$  ppm: 162.1, 153.4, 132.6, 132.2, 130.2, 128.2, 115.2, 103.6, 62.8, 14.1.

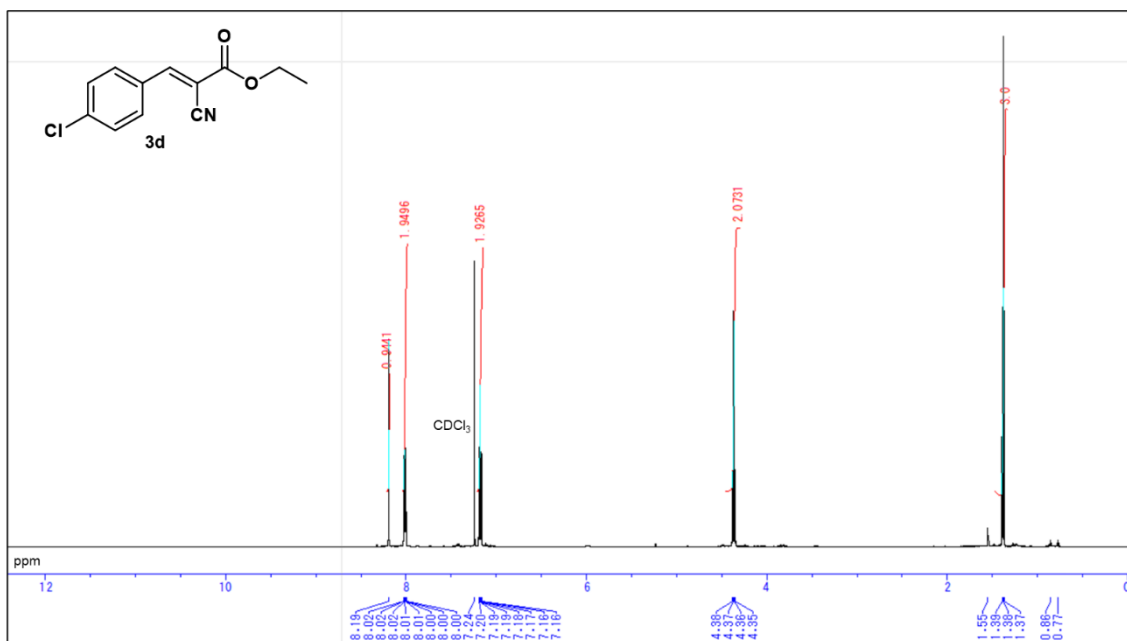


**Figure 4.28**  $^1\text{H}$  NMR spectra of product **3d**.

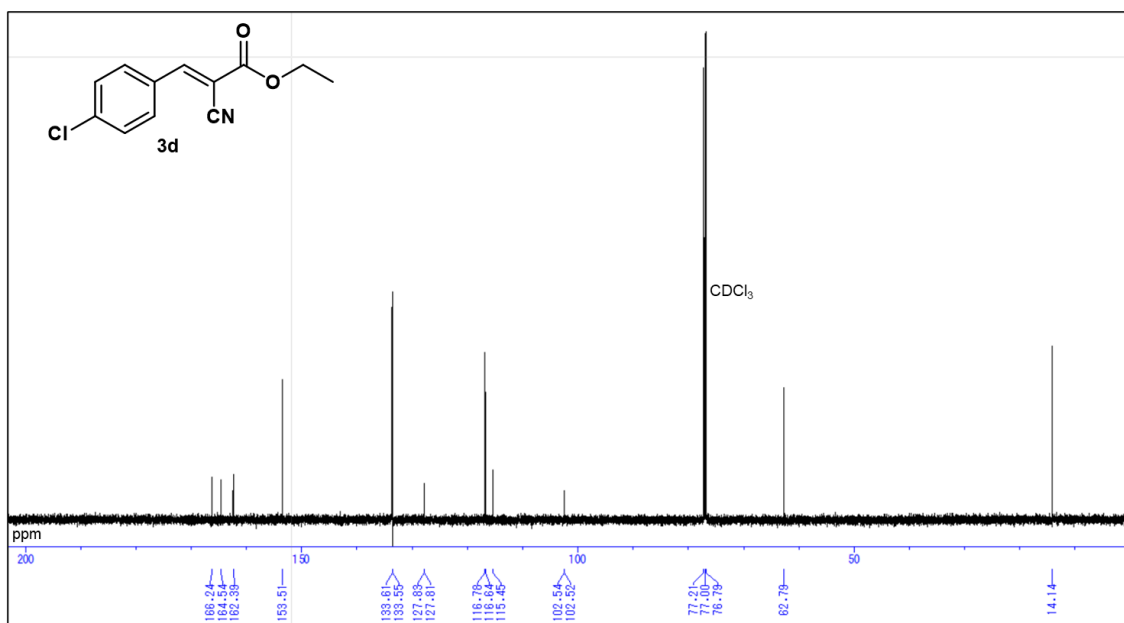


Figure 4.29 <sup>13</sup>C NMR spectra of product **3d**.

### Ethyl-2-cyano-3-(4-bromophenyl) acrylate (**3e**)

<sup>1</sup>H NMR (CDCl<sub>3</sub>) δ ppm: 8.16 (s, 1H), 7.83 (m, 2H), 7.62 (m, 2H), 4.37(q, 2H), 1.38 (t, 3H).

<sup>13</sup>C NMR (CDCl<sub>3</sub>) δ ppm: 162.92, 153.31, 132.37, 132.02, 129.88, 127.93, 115.04, 103.40, 62.68, 13.92.

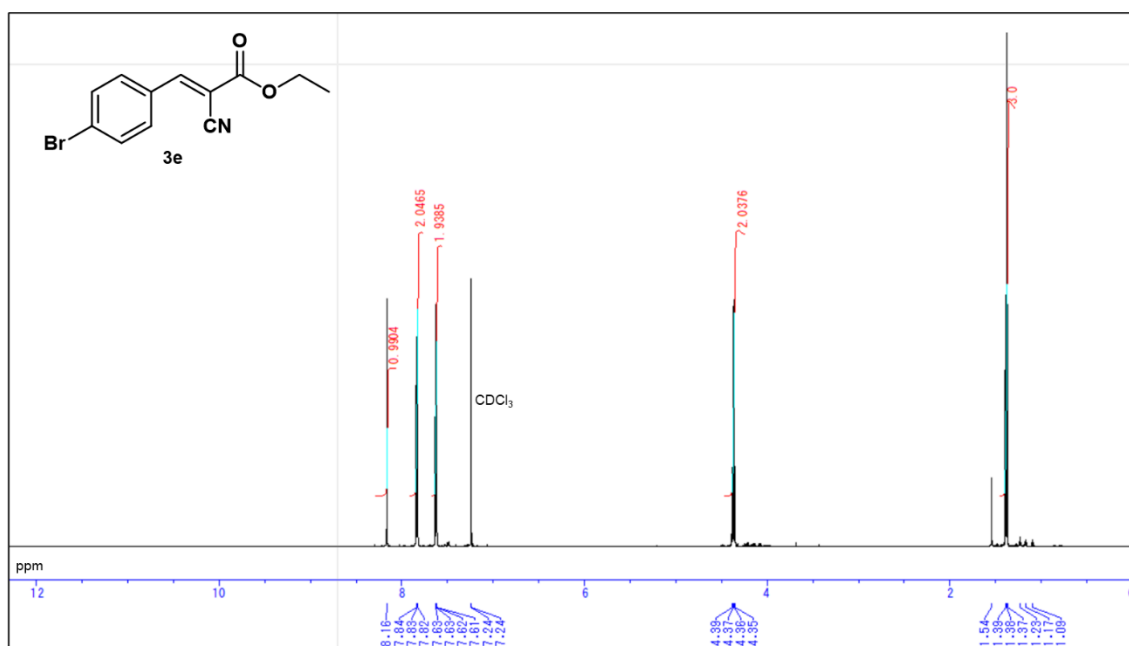
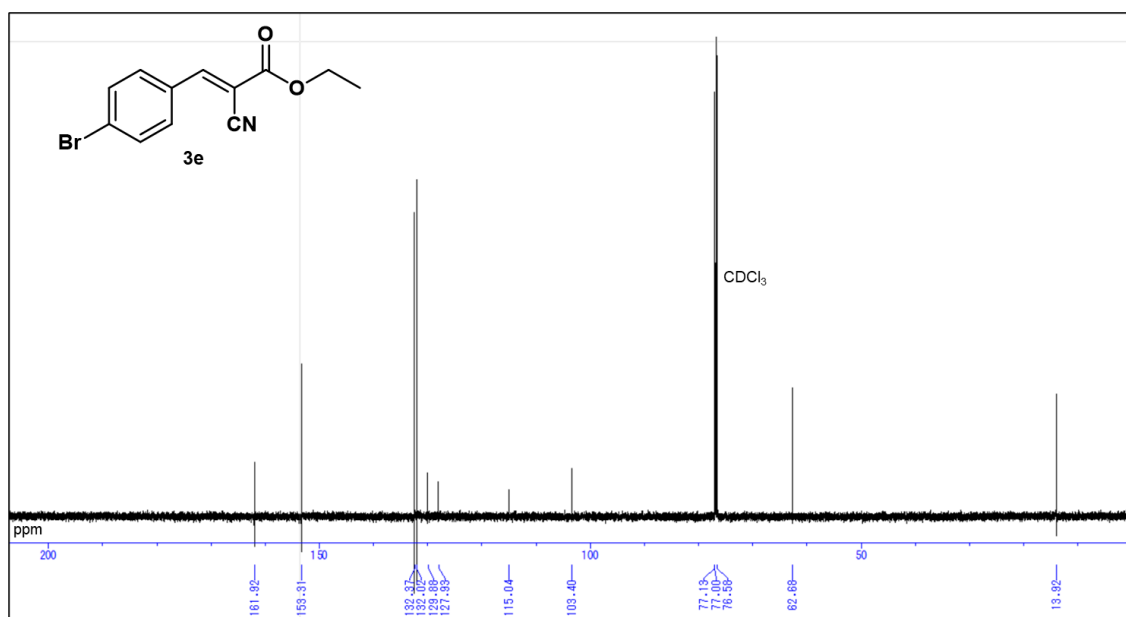


Figure 4.30 <sup>1</sup>H NMR spectra of product **3e**.



**Figure 4.31**  $^{13}\text{C}$  NMR spectra of product **3e**.

**Ethyl-2-cyano-3-(4-nitrophenyl) acrylate (3f)**

$^1\text{H}$  NMR ( $\text{CDCl}_3$ )  $\delta$  ppm: 8.19 (s, 1H), 8.02 (m, 2H), 7.20-7.16 (m, 2H), 4.36 (q, 2H), 1.38 (t, 3H).

$^{13}\text{C}$  NMR ( $\text{CDCl}_3$ )  $\delta$  ppm: 162.39, 153.50, 133.61, 133.55, 127.81, 116.78, 116.63, 115.44, 62.79, 14.14.

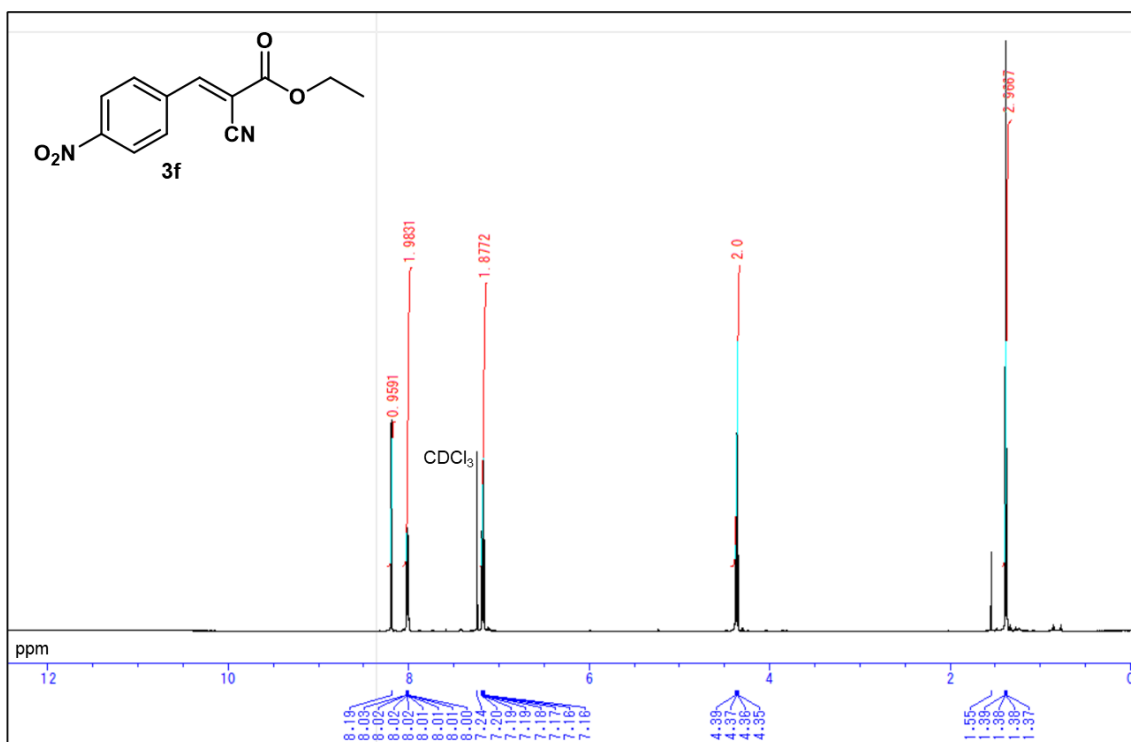


**Figure 4.32**  $^1\text{H}$  NMR spectra of product **3f**.

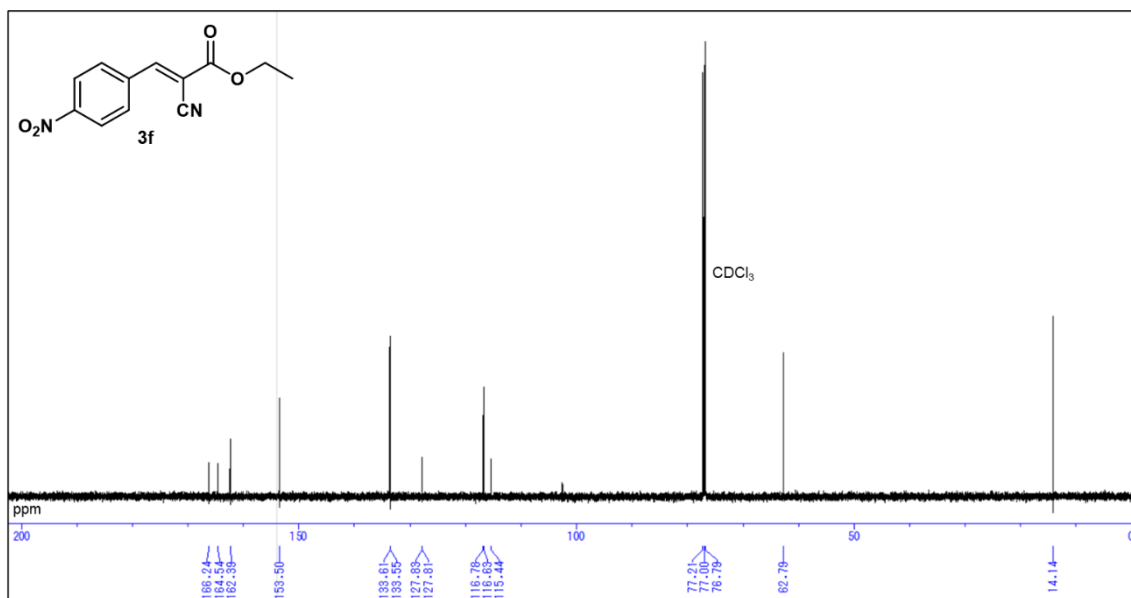


**Figure 4.33**  $^{13}\text{C}$  NMR spectra of product **3f**.

All the  $^1\text{H}$  and  $^{13}\text{C}$  NMR spectra are matched with the literature data.<sup>42-45</sup>

---

## 4.5 References

1. Yoon, T. P.; Ischay, M. A.; Du, J. Visible-Light Photocatalysis as a Greener Approach to Photochemical Synthesis. *Nat. Chem.* **2010**, *2*, 527–532.
2. Schultz, D. M.; Yoon, T. P. Solar Synthesis: Prospects in Visible Light Photocatalysis. *Science* **2014**, *343*, 6174.
3. Kalyani, D.; McMurtrey, K. B.; Neufeldt, S. R.; Sanford, M. S. Room-Temperature C-H Arylation: Merger of Pd-Catalyzed C-H Functionalization and Visible-Light Photocatalysis. *J. Am. Chem. Soc.* **2011**, *133*, 18566–18569.
4. Ischay, M. A.; Anzovino, M. E.; Du, J.; Yoon, T. P. Efficient Visible Light Photocatalysis of [2+2] Enone Cycloadditions. *J. Am. Chem. Soc.* **2008**, *130*, 12886–12887.
5. Narayanam, J. M. R.; Tucker, J. W.; Stephenson, C. R. J. Electron-Transfer Photoredox Catalysis: Development of a Tin-Free Reductive Dehalogenation Reaction. *J. Am. Chem. Soc.* **2009**, *131*, 8756–8757.
6. Le, C. C.; MacMillan, D. W. C. Fragment Couplings via CO<sub>2</sub> Extrusion-Recombination: Expansion of a Classic Bond-Forming Strategy via Metallaphotoredox. *J. Am. Chem. Soc.* **2015**, *137*, 11938–11941.
7. Joe, C. L.; Doyle, A. G. Direct Acylation of C(sp<sup>3</sup>)-H Bonds Enabled by Nickel and Photoredox Catalysis. *Angew. Chem., Int. Ed.* **2016**, *128*, 4108–4111.
8. Jouffroy, M.; Kelly, C. B.; Molander, G. A. Thioetherification via Photoredox/Nickel Dual Catalysis. *Org. Lett.* **2016**, *18*, 876–879.
9. Till, N. A.; Tian, L.; Dong, Z.; Scholes, G. D.; MacMillan, D. W. C. Mechanistic Analysis of Metallaphotoredox C-N Coupling: Photocatalysis Initiates and Perpetuates Ni(I)/Ni(III) Coupling Activity. *J. Am. Chem. Soc.* **2020**, *142*, 15830–15841.
10. Bieszczad, B.; Perego, L. A.; Korsgren, P.; Melchiorre, P. Photochemical C-H Hydroxyalkylation of Quinolines and Isoquinolines. *Angew. Chem. Int. Ed.* **2019**, *58*, 16878–16883.

- 
11. Velasco-Rubio, Á.; Martínez-Balart, P.; Álvarez-Constantino, A. M.; Fañanás-Mastral, M. C-C Bond Formation via Photocatalytic Direct Functionalization of Simple Alkanes. *Chem. Commun.* **2023**, *59*, 9424–9444.
  12. Bai, P.; Tong, X.; Gao, Y.; Xue, S. Visible Light-Driven Selective Carbon-Carbon Bond Formation for the Production of Vicinal Diols. *Sus. Energy Fuels.* **2020**, *4*, 5488–5492.
  13. Daniel, M.; Fensterbank, L.; Goddard, J. P.; Ollivier, C. Visible-Light Photocatalytic Oxidation of 1,3-Dicarbonyl Compounds and Carbon-Carbon Bond Formation. *Org. Chem. Front.* **2014**, *1*, 551–555.
  14. Chen, Y.; Ho, D. M.; Lee, C. Ruthenium-Catalyzed Hydrative Cyclization of 1,5-Enynes. *J. Am. Chem. Soc.* **2005**, *127*, 12184–12185.
  15. Ackermann, L.; Kaspar, L. T. TiCl<sub>4</sub>-Catalyzed Indirect Anti-Markovnikov Hydration of Alkynes: Application to the Synthesis of Benzo[b]Furans. *J. Org. Chem.* **2007**, *72*, 6149–6153.
  16. Pitre, S. P.; McTiernan, C. D.; Ismaili, H.; Scaiano, J. C. Mechanistic Insights and Kinetic Analysis for the Oxidative Hydroxylation of Arylboronic Acids by Visible Light Photoredox Catalysis: A Metal-Free Alternative. *J. Am. Chem. Soc.* **2013**, *135*, 13286–13289.
  17. Hari, D. P.; Schroll, P.; König, B. Metal-Free, Visible-Light-Mediated Direct C-H Arylation of Heteroarenes with Aryl Diazonium Salts. *J. Am. Chem. Soc.* **2012**, *134*, 2958–2961.
  18. Luo, K.; Chen, Y. Z.; Yang, W. C.; Zhu, J.; Wu, L. Cross-Coupling Hydrogen Evolution by Visible Light Photocatalysis toward C(Sp<sup>2</sup>)-P Formation: Metal-Free C-H Functionalization of Thiazole Derivatives with Diarylphosphine Oxides. *Org. Lett.* **2016**, *18*, 452–455.
  19. Pan, Y.; Kee, C. W.; Chen, L.; Tan, C. H. Dehydrogenative Coupling Reactions Catalysed by Rose Bengal Using Visible Light Irradiation. *Green Chem.* **2011**, *13*, 2682–2685.
  20. Yoshioka, E.; Kohtani, S.; Jichu, T.; Fukazawa, T.; Nagai, T.; Kawashima, A.; Takemoto, Y.; Miyabe, H. Aqueous-Medium Carbon-Carbon Bond-Forming

- 
- Radical Reactions Catalyzed by Excited Rhodamine B as a Metal-Free Organic Dye under Visible Light Irradiation. *J. Org. Chem.* **2016**, *81*, 7217–7229.
21. Nicewicz, D. A.; Nguyen, T. M. Recent Applications of Organic Dyes as Photoredox Catalysts in Organic Synthesis. *ACS Catal.* **2014**, *4*, 355–360.
  22. Miyabe, H. Organic Reactions Promoted by Metal-Free Organic Dyes Under Visible Light Irradiation. *Intech.* **2018**.
  23. Ahmed, M. R.; Nishina, Y. Photocatalytic Dehydrogenation of N-Heterocycles Promoted by Radicals from Graphene Oxide. *Bull. Chem. Soc. Ja.* **2023**, *96*, 568–571.
  24. Bai, J.; Yan, S.; Zhang, Z.; Guo, Z.; Zhou, C. Y. Visible-Light Carbon Nitride-Catalyzed Aerobic Cyclization of Thiobenzanilides under Ambient Air Conditions. *Org. Lett.* **2021**, *23*, 4843–4848.
  25. Su, C.; Acik, M.; Takai, K.; Lu, J.; Hao, S. J.; Zheng, Y.; Wu, P.; Bao, Q.; Enoki, T.; Chabal, Y. J.; Loh, K. P. Probing the Catalytic Activity of Porous Graphene Oxide and the Origin of This Behaviour. *Nat. Commun.* **2012**, *3*, 1298.
  26. Li, H.; Liu, R.; Lian, S.; Liu, Y.; Huang, H.; Kang, Z. Near-Infrared Light Controlled Photocatalytic Activity of Carbon Quantum Dots for Highly Selective Oxidation Reaction. *Nanoscale* **2013**, *5*, 3289–3297.
  27. Li, H.; Liu, R.; Kong, W.; Liu, J.; Liu, Y.; Zhou, L.; Zhang, X.; Lee, S. T.; Kang, Z. Carbon Quantum Dots with Photo-Generated Proton Property as Efficient Visible Light Controlled Acid Catalyst. *Nanoscale* **2014**, *6*, 867–873.
  28. Hasani, M.; Kalhor, H. R. Enzyme-Inspired Lysine-Modified Carbon Quantum Dots Performing Carbonylation Using Urea and a Cascade Reaction for Synthesizing 2-Benzoxazolinone. *ACS Catal.* **2021**, *11*, 10778–10788.
  29. Cailotto, S.; Negrato, M.; Daniele, S.; Luque, R.; Selva, M.; Amadio, E.; Perosa, A. Carbon Dots as Photocatalysts for Organic Synthesis: Metal-Free Methylene-Oxygen-Bond Photocleavage. *Green Chem.* **2020**, *22*, 1145–1149.
  30. Qu, D.; Zheng, M.; Du, P.; Zhou, Y.; Zhang, L.; Li, D.; Tan, H.; Zhao, Z.; Xie, Z.; Sun, Z. Highly Luminescent S, N Co-Doped Graphene Quantum Dots with Broad Visible Absorption Bands for Visible Light Photocatalysts. *Nanoscale* **2013**, *5*, 12272–12277.

- 
31. Liu, S.; He, Y.; Liu, Y.; Wang, S.; Jian, Y.; Li, B.; Xu, C. One-Step Hydrothermal Synthesis of Chiral Carbon Dots with High Asymmetric Catalytic Activity for an Enantioselective Direct Aldol Reaction. *Chem. Commun.* **2021**, *57*, 3680–3683.
  32. Wang, H.; Sun, P.; Cong, S.; Wu, J.; Gao, L.; Wang, Y.; Dai, X.; Yi, Q.; Zou, G. Nitrogen-Doped Carbon Dots for “Green” Quantum Dot Solar Cells. *Nanoscale Res. Lett.* **2016**, *11*, 27.
  33. Feng, X.; Ashley, J.; Zhou, T.; Sun, Y. Fluorometric Determination of Doxycycline Based on the Use of Carbon Quantum Dots Incorporated into a Molecularly Imprinted Polymer. *Micr. Act.* **2018**, *185*, 500.
  34. Jiao, X.; Qiu, Y.; Zhang, L.; Zhang, X. Comparison of the Characteristic Properties of Reduced Graphene Oxides Synthesized from Natural Graphites with Different Graphitization Degrees. *RSC Adv.* **2017**, *7*, 52337–52344.
  35. Gedda, G.; Lee, C. Y.; Lin, Y. C.; Wu, H. F. Green Synthesis of Carbon Dots from Prawn Shells for Highly Selective and Sensitive Detection of Copper Ions. *Sen. Act. B: Chem.* **2016**, *224*, 396–403.
  36. Wu, J.; Zhang, Q.; Li, M.; Yan, J.; Zhang, Y.; Liu, J.; Wu, Y. Nitrogen, Sulfur-Codoped Micro-Mesoporous Carbon Derived from Boat-Fruited Sterculia Seed for Robust Lithium-Sulfur Batteries. *RSC Adv.* **2019**, *9*, 15715–15726.
  37. Yan, Y.; Yin, Y. X.; Xin, S.; Guo, Y. G.; Wan, L. J. Ionothermal Synthesis of Sulfur-Doped Porous Carbons Hybridized with Graphene as Superior Anode Materials for Lithium-Ion Batteries. *Chem. Commun.* **2012**, *48*, 10663–10665.
  38. Munir, A.; Haq, T.; Qurashi, A.; Rehman, H.; Hamid, A.; Hussain, I. Ultrasmall Ni/NiO Nanoclusters on Thiol Functionalized and Exfoliated Graphene Oxide Nanosheets for Durable Oxygen Evolution Reaction. *ACS Appl. Energy Mater.* **2019**, *2*, 363–371.
  39. Dychalska, A.; Popielarski, P.; Franków, W.; Fabisiak, K.; Paprocki, K.; Szybowicz, M. Study of CVD Diamond Layers with Amorphous Carbon Admixture by Raman Scattering Spectroscopy. *Mat. Sci.* **2015**, *33*, 799–805.
  40. Karoui, H.; Hogg, N.; Fréjaville, C.; Tordo, P.; Kalyanaraman, B. Characterization of Sulfur-Centered Radical Intermediates Formed during the Oxidation of Thiols

- 
- and Sulfite by Peroxynitrite: ESR-Spin Trapping and Oxygen Uptake Studies. *J. Bio. Chem.* **1996**, *271*, 6000–6009.
41. Van Bergen, L. A. H.; Roos, G.; De Proft, F. From Thiol to Sulfonic Acid: Modeling the Oxidation Pathway of Protein Thiols by Hydrogen Peroxide. *J. Phy. Chem. A* **2014**, *118*, 6078–6084.
42. Bai, P.; Yang, G.; Sun, H.; Tong, X. Highly Efficient Photocatalytic Dehydrogenative Coupling of Amines with Supported Platinum Catalyst under the Oxidant-Free Conditions. *Green Chem. Eng.* **2022**, *3*, 313–320.
43. Lin, M.; Wang, Z.; Fang, H.; Liu, L.; Yin, H.; Yan, C. H.; Fu, X. Metal-Free Aerobic Oxidative Coupling of Amines in Dimethyl Sulfoxide via a Radical Pathway. *RSC Adv.* **2016**, *6*, 10861–10864.
44. Yang, X. J.; Chen, B.; Li, X. B.; Zheng, L. Q.; Wu, L. Z.; Tung, C. H. Photocatalytic Organic Transformation by Layered Double Hydroxides: Highly Efficient and Selective Oxidation of Primary Aromatic Amines to Their Imines under Ambient Aerobic Conditions. *Chem. Commun.* **2014**, *50*, 6664–6667.
45. Rupanawar, B. D.; Veetil, S. M.; Suryavanshi, G. Oxidative Olefination of Benzylamine with an Active Methylene Compound Mediated by Hypervalent Iodine (III). *Eur. J. Org. Chem.* **2019**, *2019*, 6232–6239.
46. Hyodo, K.; Kondo, M.; Funahashi, Y.; Nakamura, S. Catalytic Enantioselective Decarboxylative Cyanoalkylation of Imines by Using Palladium Pincer Complexes with C<sub>2</sub>-Symmetric Chiral Bis(Imidazoline)s. *Chem. A Eur. J.* **2013**, *19*, 4128–4134.

---

## Chapter V

### Conclusion and Future Perspectives

Carbon-based catalysts have emerged as versatile and sustainable tools in organic synthesis due to their unique properties and structural diversity. In chapter I, the active site and reactivity of carbon-based catalyst (**Figure 5.1a-e**) were reviewed and summarized for thermal and photochemical reactions. Thermal reaction requires high temperatures, which consume significant amounts of energy, while photocatalysis uses light energy, making the process energy-efficient and environmentally friendly. My research aim is to design and develop a visible-light-responsive carbon catalyst for organic transformations. As to continuing research aim this thesis presents the development and exploration of visible-light-responsive nanocarbon catalysts for organic transformations, focusing on elucidating the mechanistic pathways and the role of radical intermediates. The study demonstrates the efficiency of nanocarbon materials in harnessing visible light for catalytic processes, offering a sustainable approach to organic synthesis. The research also underscores the versatility of nanocarbon materials, particularly their tunable electronic properties, and light absorption capabilities, which make them promising candidates for diverse photocatalytic applications.

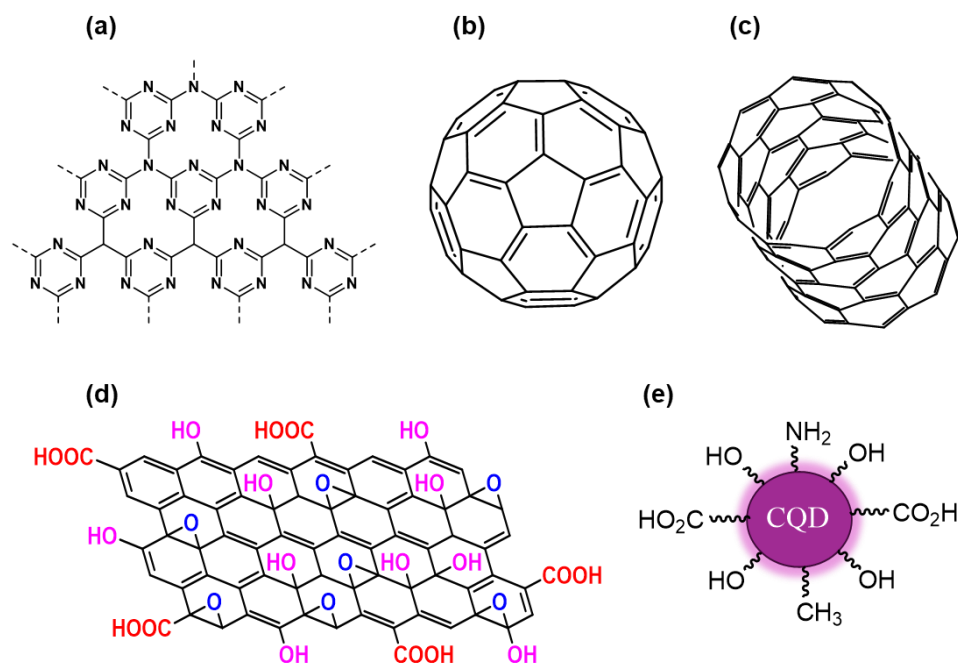
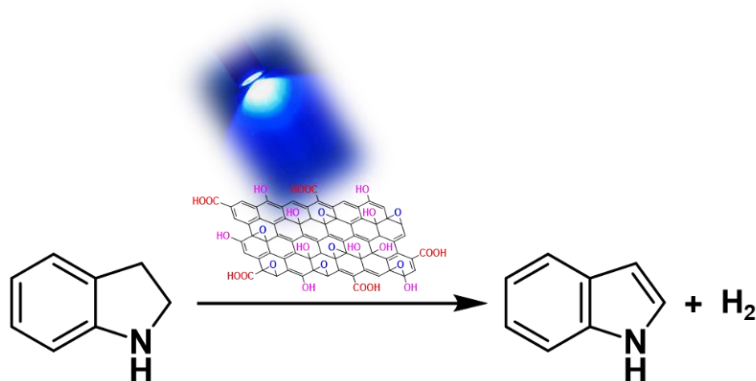


**Figure 5.1** Carbon-based catalyst (a) g-C<sub>3</sub>N<sub>4</sub>, (b) fullerene, (c) CNT, (d) GO, and (e) CQD.

Firstly, a visible-light-driven metal-free carbon-based system was developed for the dehydrogenation of N-heterocycles that proceed via a radical pathway (**Scheme 5.1**) mentioned in Chapter II. Reactivity was compared with various carbon materials such as GO, rGO, N-rGO, activated carbon, graphite, and CQD, while GO showed the highest catalytic activity. GO was recycled and reused at least five times without significant structural change. The mechanistic study revealed that the reaction proceeded with the formation of carbon radicals from GO under irradiation of blue LED light (**Figure 5.2a**). Both GO and light synergistically worked for the dehydrogenation reactions. This is the first example of the detection of molecular hydrogen for dehydrogenation of N-heterocycles using GO photocatalyst (**Figure 5.2b**). Based on the proposed reaction mechanism, the scope of the photocatalytic reaction would be expanded by tuning the band gap and functional group of carbon materials.



**Scheme 5.1** Dehydrogenation of indoline by GO under photo-irradiation, generating molecular hydrogen.

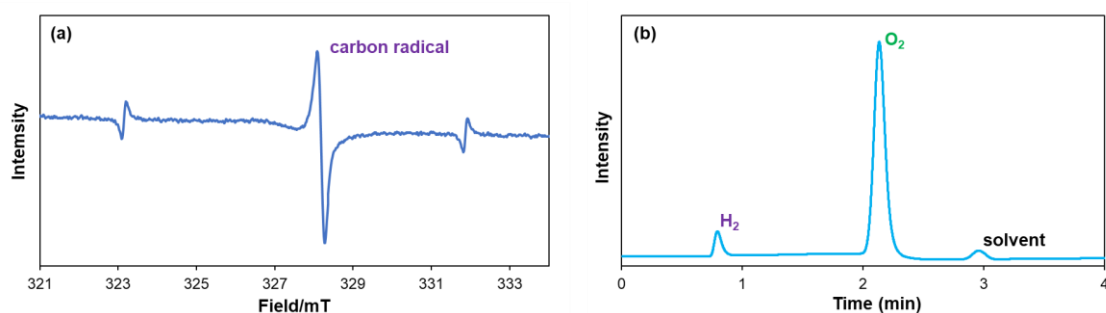


**Figure 5.2** (a) ESR spectrum of the reaction mixture with GO under irradiation of light, (b) GC spectrum of the gas phase of the reaction mixture for detection of H<sub>2</sub> gas. The

---

standard  $\text{Mn}^{2+}$  peaks are observed at 323 and 332 mT.

The results were quite encouraging as carbon was found to be active in the dehydrogenation reaction. Further investigation was carried out to scrutinize the role of radicals and oxidized surface functional groups for other important organic transformations. In chapter III, explored the radical properties of oxidized carbon materials under visible light irradiation. Oxidized carbon materials are a consequence of their unique structure, functional groups, and chemical reactivity, allowing them to generate radicals for organic transformations. Various carbon materials such as graphite, activated carbon, carbon black, carbon nanotube, and nanodiamonds were oxidized and investigated their properties for generating carbon radicals under visible light irradiation (**Figure 5.3**). The number of radicals differs in the types of oxidized carbons; GO showed a higher number of radicals under blue LED irradiation. The photoexcitation of GO under blue LED light irradiation offers a progression of oxidation benzylamine by radical pathway (**Scheme 5.2**). These properties make oxidized carbon materials versatile for potential applications in catalysis, as well as environmental remediation, energy storage, and biomedical engineering.

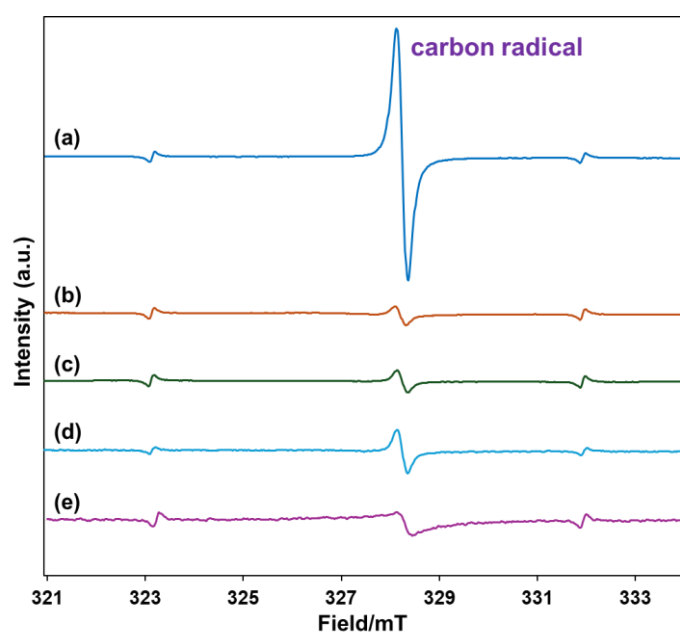
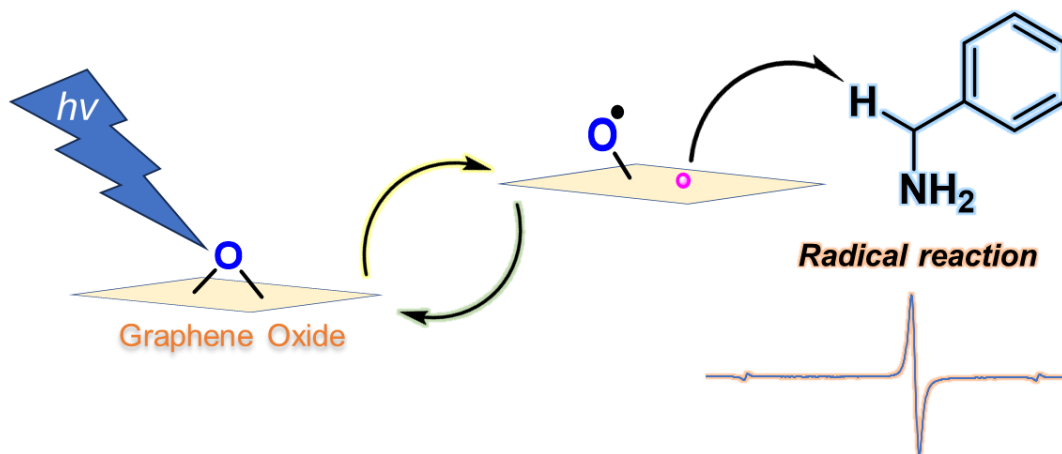


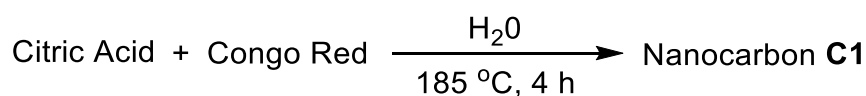
**Figure 5.3** ESR spectra of (a) GO, (b) oxidized activated carbon, (c) oxidized carbon

black, (d) oxidized carbon nanotube, and (e) oxidized nanodiamond under irradiation of blue LED light. The standard  $\text{Mn}^{2+}$  peaks are observed at 323 and 332 mT.



**Scheme 5.2** Mechanistic outline of GO-catalyzed oxidation of benzylamine under irradiation of light.

To understand the radical properties of the surface functional carbon, in Chapter IV, a visible-light-absorbing amorphous nanocarbon was synthesized by hydrothermal treatment of citric acid and Congo Red (**Scheme 5.3**). Among the synthesized carbon materials, this nanocarbon **C1** composed of citric acid and Congo Red, showed only visible-light absorption (**Figure 5.4a**); therefore, this material was extensively characterized. More interestingly, **C1** exhibited high catalytic performance under irradiation of blue LED for the C-C bond formation reaction of benzylamine with ethyl cyanoacetate. The mechanistic studies suggested that the reaction proceeded with forming sulfur radicals from nanocarbon under irradiation of blue LED light (**Figure 5.4b**). This report on the synthesis of visible-light-responsive nanocarbon photocatalysts for carbon-carbon bond-forming reactions will enhance the opportunity for future photocatalytic applications.



**Scheme 5.3** Synthesis reaction route of nanocarbon **C1**.

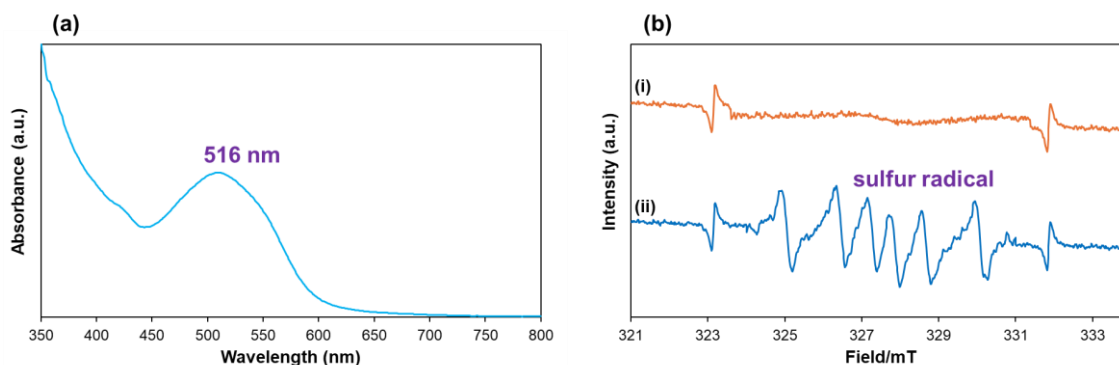


**Figure 5.4** (a) UV-vis spectra of nanocarbon **C1**, (b) ESR spectra of the reaction mixture with DMPO (i) in the absence of light, and (ii) under irradiation of blue LED. 323 and 332 mT are the standard  $\text{Mn}^{2+}$  peaks.

Through detailed mechanistic investigations, the critical functions of photogenerated radicals were identified, providing insights into reaction pathways and facilitating the design of more effective photocatalysts. These findings highlight the potential of nanocarbon-based systems to address challenges in green chemistry and pave the way for future advancements in photocatalysis. Future challenges need to address the following points.

- i. Developing advanced nanocarbon catalysts with improved light absorption, enhanced radical generation efficiency, and better stability under reaction conditions.
- ii. Exploring new classes of radical-mediated transformations and extending the applicability of nanocarbon catalysts to more complex organic reactions.
- iii. Scaling up catalytic processes for industrial applications, particularly in pharmaceuticals, fine chemicals, and sustainable chemical manufacturing.
- iv. Investigating the use of nanocarbon catalysts in photochemical processes for environmental remediation and renewable energy conversion.

---

## Acknowledgment

I would like to express my deepest gratitude to my supervisor Prof. Yuta Nishina for providing me with the opportunity to study Ph.D. at the Graduate School of Natural Science and Technology in Okayama University. I thank Prof. Nishina for his regular guidance and patience throughout my study, and the cookies provided over many discussions. Besides, I thank you for painstakingly going through the draft of this thesis.

I would also like to thank those who have ensured the smooth running of the Nishina lab and equipment. These are Dr. Obata, Komoda, and Nakano; they arranged chemicals, and gases like argon, hydrogen, carbon dioxide, etc. The lab is a much safer and more efficient environment because of these gentlemen, and their importance cannot be overstated.

I am always would like to thank my lab members Mr. Israel, Cheng, Zho, Takahashi, Rubel, Ohkura, Hiramatsu, and Ms. Nusrat, Maram for their kind help, all the fun we shared and for being remarkable friends.

I would also like to thank Okayama University for the financial support for me through the MEXT scholarship, which was extremely helpful in carrying out my research work and for my pleasant stay in Japan.

Finally, I especially thank my family to whom I owe everything. They have provided me with love and support whenever needed and a sense of humor, which has often been employed to take the best from a bad situation. This thesis is for you.